

# Light-front Hamiltonian field theory

*towards a relativistic description of bound  
states*

Nico Schoonderwoerd

Lichtfront Hamiltoniaanse veldentheorie

*Naar een relativistische beschrijving van gebonden toestanden*

<http://xxx.lanl.gov/abs/hep-ph/9811xxx>

Leescommissie: prof.dr. J.F.J. van den Brand  
dr. A.E.L. Dieperink  
prof.dr. G. McCartor  
prof.dr. P.J.G. Mulders  
prof.dr. H.-C. Pauli

Grafisch ontwerp: Alex Henneman  
Nico Schoonderwoerd



Dit werk maakt deel uit van het onderzoekprogramma van de Stichting voor Fundamenteel Onderzoek der Materie (FOM) die financieel wordt gesteund door de Nederlandse Organisatie voor Wetenschappelijk Onderzoek (NWO).

©1998, Nico Schoonderwoerd

VRIJE UNIVERSITEIT

**Light-front Hamiltonian field theory**  
*towards a relativistic description of bound states*

ACADEMISCH PROEFSCHRIFT

ter verkrijging van de graad van doctor aan  
de Vrije Universiteit te Amsterdam,  
op gezag van de rector magnificus  
prof.dr. T. Sminia,  
in het openbaar te verdedigen  
ten overstaan van de promotiecommissie  
natuurkunde en sterrenkunde  
van de faculteit der exacte wetenschappen  
op donderdag 14 januari 1999 om 13.45 uur  
in het hoofdgebouw van de universiteit,  
De Boelelaan 1105

door

**Nicolaas Cornelis Johannes Schoonderwoerd**  
geboren te Breukelen

Promotor: prof.dr. P.J.G. Mulders  
Copromotor: dr. B.L.G. Bakker

*Aan Joop, Bea en Cosander*

# Contents

<b>I</b>	<b>Introduction to light-front Hamiltonian dynamics</b>	<b>1</b>
§1	Forms of relativistic dynamics . . . . .	3
§1.1	The Poincaré group . . . . .	4
§1.2	Light-front coordinates . . . . .	6
§1.3	The initial surface . . . . .	7
§2	Light-front quantization . . . . .	8
§2.1	The scalar propagator . . . . .	8
§2.2	The fermion propagator . . . . .	9
§2.3	The spectrum condition . . . . .	10
§2.4	The energy denominator . . . . .	10
§2.5	Light-front time-ordering . . . . .	11
§2.6	Loop diagrams . . . . .	13
<b>II</b>	<b>The Yukawa model</b>	<b>17</b>
§1	Feynman rules . . . . .	17
§2	Divergences in the Yukawa model . . . . .	18
§2.1	Longitudinal divergences . . . . .	18
§2.2	Transverse divergences . . . . .	19
§3	Instantaneous terms and blinks . . . . .	19
§4	Pair contributions in the Breit-frame . . . . .	20
§4.1	Construction of the blink . . . . .	22
§4.2	The Breit-frame . . . . .	23
<b>III</b>	<b>Longitudinal divergences in the Yukawa model</b>	<b>24</b>
§1	Introduction . . . . .	25
§1.1	Minus regularization . . . . .	25
§1.2	Proof of equivalence for the Yukawa model . . . . .	26
§2	Example: the one-boson exchange correction . . . . .	28
§3	Equivalence of the fermion self-energy . . . . .	32
§3.1	Covariant calculation . . . . .	32
§3.2	Residue calculation . . . . .	32
§3.3	Equivalence . . . . .	34
§3.4	Conclusions . . . . .	36
§4	Equivalence of the boson self-energy . . . . .	38
§4.1	Minus regularization . . . . .	39
§4.2	Equivalence . . . . .	40
§5	Conclusions . . . . .	41

<b>IV</b>	<b>Transverse divergences in the Yukawa model</b>	<b>42</b>
§1	Formulation of the problem . . . . .	42
	§1.1 Ultraviolet and transverse divergences . . . . .	43
	§1.2 Light-front structure functions . . . . .	45
§2	Minus regularization . . . . .	46
	§2.1 One external momentum . . . . .	46
	§2.2 Two external momenta . . . . .	47
	§2.3 Several external momenta . . . . .	49
	§2.4 Summary . . . . .	49
§3	Equivalence for the fermion triangle . . . . .	50
	§3.1 Covariant calculation . . . . .	50
	§3.2 BPHZ regularization . . . . .	51
	§3.3 Light-front calculation . . . . .	51
	§3.4 Equivalence . . . . .	53
§4	Equivalence for the one-boson exchange diagram . . . . .	57
	§4.1 Covariant calculation . . . . .	57
	§4.2 BPHZ regularization . . . . .	58
	§4.3 Light-front calculation . . . . .	59
	§4.4 Equivalence . . . . .	60
§5	Conclusions . . . . .	62
<b>V</b>	<b>Entanglement of Fock-space expansion and covariance</b>	<b>65</b>
§1	Formulation of the problem . . . . .	65
	§1.1 Suppression of higher Fock states . . . . .	66
	§1.2 Setup . . . . .	67
§2	The Lippmann-Schwinger formalism . . . . .	68
§3	The box diagram . . . . .	72
	§3.1 The covariant box diagram . . . . .	72
	§3.2 The LF time-ordered diagrams . . . . .	73
§4	A numerical experiment . . . . .	74
§5	Light-front versus instant-form dynamics . . . . .	75
§6	Numerical results above threshold . . . . .	77
	§6.1 Evaluation method . . . . .	77
	§6.2 Results as a function of $\alpha$ . . . . .	79
	§6.3 Results as a function of $v$ . . . . .	80
§7	Numerical results off energy-shell . . . . .	80
	§7.1 Determination of the momenta . . . . .	81
	§7.2 Calculation of the amplitude . . . . .	83
§8	Analysis of the on energy-shell results . . . . .	85
	§8.1 Trapezium . . . . .	87
	§8.2 Diamond . . . . .	93
	§8.3 Stretched box . . . . .	93
§9	Analysis of the off energy-shell results . . . . .	95

---

§10 Conclusions . . . . .	97
<b>VI Summary and conclusions</b>	<b>99</b>
<b>A Relations between Euclidian integrals</b>	<b>102</b>
<b>B The fermion self-energy in closed form</b>	<b>103</b>
<b>C Internal and external variables</b>	<b>105</b>
<b>Samenvatting</b>	<b>107</b>
<b>Scientific publications</b>	<b>111</b>
<b>Bibliography</b>	<b>112</b>



## Introduction to light-front Hamiltonian dynamics

*Einstein's great achievements, the principle of relativity, imposes conditions which all physical laws have to satisfy. It profoundly influences the whole of physical science, from cosmology, which deals with the very large, to the study of the atom, which deals with the very small.*

Paul Dirac

This quote reflects the work that I have done in physics so far, which began with an investigation of new black hole solutions to the Einstein equation [1] when I was a student in Groningen, and which now ends with the research presented in this Ph.D.-thesis on models to describe bound states of elementary particles [2, 3, 4, 5, 6, 7].

The above quote contains the first two lines of an important article that Dirac [8] wrote in 1949, in the middle of a century that has produced enormous progress in the understanding of the properties of matter. Not only the development of relativity, but also the rise of Quantum Mechanics was instrumental for this progress. At the end of this century, these and many other advances have resulted in a model that ambitiously is called the Standard Model. It describes all elementary particles that have been discovered until now; the leptons and the quarks, and their interactions.

However, this does not imply we have to call it the end of the day for high-energy physics. A number of problems of a fundamental nature remain in the Standard Model. As an example we mention the question of the neutrino mass, that may or may not point to physics not included in the Standard Model.

There are many practical problems when one wants to calculate a physical amplitude. If the interactions are sufficiently weak, perturbation theory is usually applied and gives in many cases extremely accurate results. However, in the case of strong interactions, or when bound states are considered, nonperturbative methods must be developed.

We have to ensure that in such methods covariance is maintained. We mean by this that measured quantities, like cross sections and masses, are relativistic invariants. When the equations are written down in covariant form it is clear that the outcome will satisfy relativistic invariance and we refer to such methods as manifestly covariant.

For example, the Bethe-Salpeter equation is manifestly covariant, but suffers from numerical intractability beyond the ladder approximation. Great progress is made by Lattice Field Theory, which is now able to give quantitative predictions. However, it depends on the choice of a specific frame of reference and the advances in its application rely strongly on a continued increase of the speed of computers.

A very intuitive picture of a bound state is provided by Hamiltonian methods. However, the “classical” method of setting up a relativistic Hamiltonian theory by quantization on the equal-time plane, so-called instant-form (IF) quantization, suffers from problems such as a square root in the energy operator, which results in the existence of both positive and negative energy eigenstates, and the complexity of the boost operators, which keeps us away from determining the wavefunctions in an arbitrary reference frame. Weinberg [9] proposed to use the Infinite Momentum Frame (IMF), because in this limit time-ordered diagrams containing vacuum creation or annihilation vertices vanish, and therefore the total number of contributing diagrams is significantly reduced. It is found that it provides a picture which connects to the one of the constituent quark model. However, its big disadvantage is that the IMF is connected to the rest frame by a boost for which one takes the limit of the boost parameter to infinity. It is dubitable whether this limit commutes with others that are taken in field theory.

It was only in the seventies that one began to realize that a theory with the same advantages as the IMF, but without the disadvantages, had already been suggested by Dirac some decades before: light-front (LF) quantization, i.e., quantization on a plane tangent to the light-cone. Of the ten Poincaré generators, seven are kinematic, i.e., can be formulated in a simple way and correspond to conserved quantities in perturbation theory. Most important is that these seven operators include one of the boost operators, allowing us to determine the wavefunction in a boosted frame if it is known in the rest frame. This property is not found in IF quantization. As a drawback one finds that not all rotations are kinematic, and therefore rotational invariance is not manifest in LF quantization, a problem which is discussed frequently in the literature. In particular, our interest was triggered by an article by Burkardt and Langnau [10] who claimed that rotational invariance is broken for  $S$ -matrix elements in the Yukawa model. Instead of a lack of manifest rotational invariance, we prefer to talk about lack of manifest covariance, as this is a property that all Hamiltonian theories share. Because in each form of quantization dynamical operators that involve creation or annihilation of particles are present, in any relativistic Hamiltonian theory particle number is not conserved, implying that each eigenstate has to be represented as a sum over Fock states of arbitrary particle number. However, light-front dynamics (LFD) is the only Hamiltonian dynamical theory which has the property that the perturbative vacuum is an eigenstate of the (light-front) Hamiltonian, provided that zero-modes are neglected (in this thesis zero-modes will not explicitly be discussed). Bound states are also eigenstates and are distinct from the LF vacuum, which simplifies their analysis.

In this thesis we shall not solve the eigenvalue problem, an interacting Hamiltonian will not even be written down! The goal of this thesis will not be to calculate a spectrum, but to illuminate two important properties of LF Hamiltonian dynamics. The first is:

1. *Light-front dynamics provides a covariant framework for the treatment of bound states.*

Although the calculation of bound states requires nonperturbative methods, these usually involve ingredients encountered in perturbation theory, e.g., the driving term in a Lippmann-Schwinger or Bethe-Salpeter approach. We prove that LF perturbation theory is equivalent to covariant perturbation theory. By equivalent we mean that physical observables in LF perturbation theory are the same as those obtained in covariant perturbation theory. This can be done by showing that the rules for constructing LF time-ordered diagrams can be obtained algebraically from covariant diagrams by integration over the LF energy  $k^-$ . Two technical difficulties, namely that the integration over  $k^-$  can be ill-defined, and that divergences in the transverse directions may remain, are solved in Chapters III and IV respectively, for the Yukawa model, which is introduced in Chapter II.

In Chapter V we discuss the entanglement of covariance and the Fock-space expansion, and show another important property of LF Hamiltonian dynamics:

2. *Higher Fock state contributions in LF Hamiltonian field theory are typically small, in particular much smaller than in IF Hamiltonian field theory, and therefore the ladder approximation gives accurate results for the spectrum.*

It has been known for a long time that on the light-front one has to take into account fewer diagrams than in the instant-form of Hamiltonian dynamics. On top of this, diagrams involving higher Fock states are numerically smaller, as we will show. We look at two nucleons interacting via boson exchange, and we compare the contributions of the diagrams with one boson in the air, to diagrams where two bosons are simultaneously exchanged. The latter are ignored if we use the ladder approximation. We show in numerical calculations involving scalar particles that this approximation is viable for both scattering amplitudes and off energy-shell states, if masses and momenta are chosen in such a way that they are relevant for the deuteron.

## §1 Forms of relativistic dynamics

An important first step on the path to a Hamiltonian description of a dynamical system was taken by Dirac in 1949, in his famous article 'Forms of Relativistic Dynamics' [8]. One foot of this work is in special relativity, when Dirac writes:

... *physical laws shall be invariant under transformations from one such coordinate system to another.*

The other foot of his method is in Quantum Mechanics because Dirac writes:

... *the equations of motion shall be expressible in the Hamiltonian form.*

In more technical terms, this condition tells us that any two dynamical variables have a Poisson bracket, later to be associated with (anti-)commutation relations. We restrict the transformations further to continuous ones, therefore excluding space inversion and time reversal. In the forthcoming subsections we are going to work out these two principles and construct the generators of the Poincaré group.

### §1.1 The Poincaré group

The transformations mentioned in the first quote are the four translations  $P^\mu$ , the three rotations  $J^i = \frac{1}{2}\epsilon^{ijk}M_{jk}$ , and the three boosts  $K^i = M^{0i}$ , where  $M$  is an anti-symmetric tensor. These transformations should satisfy

$$[P^\mu, P^\nu] = 0, \quad (\text{I-1})$$

$$[M^{\mu\nu}, P^\rho] = -g^{\mu\rho}P^\nu + g^{\nu\rho}P^\mu, \quad (\text{I-2})$$

$$[M^{\mu\nu}, M^{\rho\sigma}] = -g^{\mu\rho}M^{\nu\sigma} + g^{\nu\rho}M^{\mu\sigma} - g^{\mu\sigma}M^{\rho\nu} + g^{\nu\sigma}M^{\rho\mu}. \quad (\text{I-3})$$

Setting up a dynamical system is equivalent to finding a solution to these equations. The solution of the ten generators is generally such that some of them are simple, and correspond to conserved quantities. These are labeled as *kinematical*, indicating that they do not contain any interaction. Others are more complicated and describe the dynamical evolution of the system as the Hamiltonian does in nonrelativistic dynamics. Therefore these are called *dynamical*, which means that they do contain interaction. It seems obvious that one should want to setup the framework in such a way that the number of dynamical operators is small. A simple solution of the Eqs. (I-1)-(I-3) can be found if we define a point in space-time to be given by the dynamical variable  $x^\mu$  and its conjugate momentum by  $p^\nu$ . Using

$$[x^\mu, x^\nu] = 0, \quad [p^\mu, p^\nu] = 0, \quad [x^\mu, p^\nu] = ig^{\mu\nu}, \quad (\text{I-4})$$

a solution is now given by

$$P^\mu = p^\mu, \quad M^{\mu\nu} = x^\mu p^\nu - x^\nu p^\mu. \quad (\text{I-5})$$

As already mentioned by Dirac, this solution may not be of practical importance, however, it can serve as a building block for future solutions.

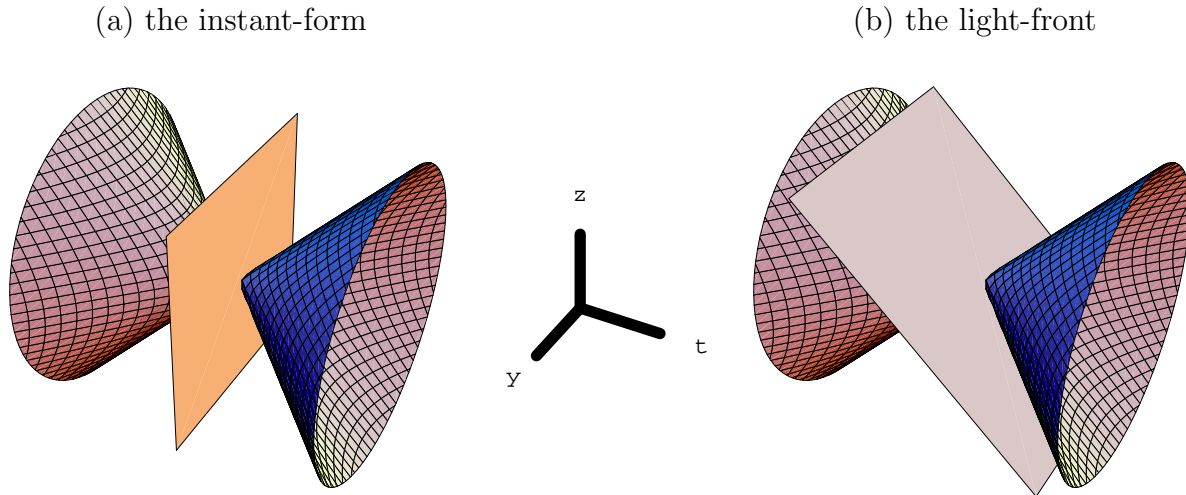


Figure I-1: Projection of two initial surfaces onto  $y$ - $z$ - $t$ -space. In (a) the initial surface is at  $t = 0$ , and in (b) it is tangent to the light-cone.

Another important ingredient for the dynamical theory is that we have to specify boundary conditions. We do this by taking a three-dimensional surface  $\Sigma$  in space-time not containing time-like directions, at which we specify the initial conditions of the dynamical system. The ten generators then split into two groups, namely those that leave  $\Sigma$  invariant and those that do not. The first group is called the stability group. The larger the stability group of  $\Sigma$ , the smaller the dynamical part of the problem. We can ensure a large stability group by demanding that it acts transitively on  $\Sigma$ : every point on  $\Sigma$  may be mapped on any other point of  $\Sigma$  by applying a suitable element of the stability group. This ensures that all points on the initial surface are equivalent.

The restriction of relativistic causality reduces the number of world lines, and therefore increases the number of surfaces that one can choose for  $\Sigma$ . Dirac found three independent choices for the initial surface that fulfill these conditions. In total there are five, as was pointed out by Leutwyler and Stern [11]. We, however, only discuss the two most important ones. They are listed in Fig. I-1. In IF Hamiltonian dynamics one quantizes on the equal-time plane, given by

$$x^0 = 0. \quad (\text{I-6})$$

This is the form of dynamics closest to nonrelativistic Quantum Mechanics. Another important possibility for quantization is offered by a plane tangent to the light-cone. The light-front is given by the equation

$$cx^0 + x^3 = 0. \quad (\text{I-7})$$

Notice that this plane contains light-like directions. It is common to use the  $z$ -direction to define the light-front. The different status of the other space-like

directions  $x$  and  $y$  leads to the fact that the symmetry of rotational invariance becomes nonmanifest on the light-front. In explicitly covariant LFD [12], one defines the light-front by its normal vector  $\vec{\omega}$ , which is not fixed. This method will be encountered in Chapter V.

Note that in the nonrelativistic limit ( $c \rightarrow \infty$ ) the planes (I-6) and (I-7) coincide. This degeneracy is a feature of Hamiltonian relativistic dynamics. In this limit only one operator remains dynamical, namely the Hamiltonian, the operator that generates time translations.

## §1.2 Light-front coordinates

In the remainder of this chapter, we show some of the advantages of LF quantization. We define so-called longitudinal coordinates

$$A^- = \frac{cA^0 - A^3}{\sqrt{2}}, \quad (\text{I-8})$$

$$A^+ = \frac{cA^0 + A^3}{\sqrt{2}}, \quad (\text{I-9})$$

and transverse coordinates

$$A^\perp = (A^1, A^2), \quad (\text{I-10})$$

such that the spatial coordinates  $x^\perp$  and  $x^-$  define a coordinate system on the light-front, and  $x^+$  plays the role of time. From now on we will put the velocity of light equal to unity:  $c = 1$ . The indices of the four-vectors can be lowered and raised using the following LF metric  $g^{\mu\nu}$ :

$$g^{\mu\nu} = \begin{pmatrix} 0 & 1 & 0 & 0 \\ 1 & 0 & 0 & 0 \\ 0 & 0 & -1 & 0 \\ 0 & 0 & 0 & -1 \end{pmatrix}, \quad (\text{I-11})$$

where the first and second row/column refer to the longitudinal components, and the third and fourth to the transverse components. Unfortunately, a number of conventions are frequently used for LF coordinates. We will stick to the one given above, commonly referred to as the Kogut-Soper convention [13]. The stability group on the light-front has seven elements, as can be verified by writing out the commutation relations between these operators and  $x^+$ :

$$\begin{aligned} [x^+, P^\perp] &= [x^+, P^+] = [x^+, M^{12}] = [x^+, M^{+\perp}] = 0, \\ [x^+, M^{+-}] &= -2ix^+ = 0. \end{aligned} \quad (\text{I-12})$$

The other three operators are dynamical, as can be seen by the fact that they do not commute with  $x^+$ ,

$$\begin{aligned} [x^+, P^-] &= -i \\ [x^+, M^{-\perp}] &= -ix^\perp. \end{aligned} \quad (\text{I-13})$$

If we look at Fig. I-1b, we see that we can describe the operation of  $P^-$  as a translation perpendicular to the light-front. The operators  $M^{-\perp}$  correspond to rotations of the light-front about the light-cone. Using these two words in one sentence clearly indicates why the common expression “light-cone quantization” is badly chosen. We prefer to use the phrase “light-front quantization”.

### §1.3 The initial surface

In LF quantization, we first solve the Poincaré algebra on the surface  $x^+ = 0$ . The stability group is the group generated by transformations of this surface into itself. We already met these operators in Eq. (I-12). As  $x^+$  is fixed, the dynamical variable  $p^-$  has lost its meaning and, according to Dirac, it should be eliminated. We can add to the generators in Eq. (I-5) multiples of  $(p_\sigma p^\sigma - m^2)$ :

$$\begin{aligned} P^\mu &= p^\mu + \lambda^\mu (p_\sigma p^\sigma - m^2), \\ M^{\mu\nu} &= x^\mu p^\nu - x^\nu p^\mu + \beta^{\mu\nu} (p_\sigma p^\sigma - m^2). \end{aligned} \quad (\text{I-14})$$

We then construct the  $\lambda^\mu$  and  $\beta^{\mu\nu}$  in such a way that on the light-front the  $p^-$ -dependence drops from these equations. For the elements of the stability group we find:

$$\begin{aligned} P^\perp &= p^\perp, & P^+ &= p^+, \\ M^{+\perp} &= -x^\perp p^+, & M^{+-} &= -x^- p^+, & M^{12} &= x^1 p^2 - x^2 p^1, \end{aligned} \quad (\text{I-15})$$

and for the three dynamical operators we find:

$$P^- = \frac{p^{\perp 2} + m^2}{2p^+}, \quad (\text{I-16})$$

$$M^{-1} = x^- p^1 + x^1 \frac{p^{\perp 2} + m^2}{2p^+}, \quad M^{-2} = x^- p^2 + x^2 \frac{p^{\perp 2} + m^2}{2p^+}. \quad (\text{I-17})$$

When one quantizes in the instant-form, one finds four operators to be dynamical, which is one more than in LF quantization. However, more important is the form of the energy operator. In the instant-form, it is

$$P^0 = \sqrt{\vec{p}^2 + m^2}. \quad (\text{I-18})$$

The presence of the square root causes the degeneracy of positive and negative energy solutions in IF dynamics, whereas on the light-front they are kinematically separated, as can be seen from Eq. (I-16): positive longitudinal momentum  $p^+$  corresponds to positive LF energy  $P^-$ , and vice versa. This effect leads to the spectrum condition, which is explained in the next section.

The dynamical operators (I-16) and (I-17) reveal a little of the problems encountered on the light-front: the infrared problem for  $p^+ = 0$ , which can be

associated with the so-called zero-modes. As the path of quantization on the light-front is beset by problems, such as the nonuniqueness of the solution of the Cauchy problem, attempts have been made to find another path. Inspiration may be found in Quantum Field Theory, which leads to expressions for propagators of particles, and finally for  $S$ -matrix elements. They may serve as a starting point to derive rules for time-ordered diagrams.

## §2 Light-front quantization

The first to set foot on the new path towards a LF perturbation theory were Chang and Ma [14], and Kogut and Soper [13]. Their work relies on the Feynman rules that are constructed in Quantum Field Theory. To determine the LF time-ordered propagator we take the Feynman propagator and integrate out the energy component.

For the types of theories that are discussed in this thesis, two are of importance: the scalar propagator and the fermion propagator.

### §2.1 The scalar propagator

The Klein-Gordon propagator for a particle of mass  $m$  is well-known:

$$\Delta_{\text{F}}(x) = \frac{1}{(2\pi)^4} \int_{\text{Min}} d^4k \frac{e^{-ik_\mu x^\mu}}{k^2 - m^2 + i\epsilon}, \quad (\text{I-19})$$

where the subscript ‘‘Min’’ denotes that the integral is over Minkowski space. The inner products of the Lorentz vectors can be written in LF coordinates:

$$k^2 = k_\mu k^\mu = 2k^+ k^- - k^\perp{}^2, \quad (\text{I-20})$$

$$k_\mu x^\mu = k^- x^+ + k^+ x^- - k^\perp \cdot x^\perp. \quad (\text{I-21})$$

Following Kogut and Soper [13], we separate the energy integral from the integral over the kinematical components of  $k$ , indicated by  $\vec{k}$ :

$$\vec{k} = (k^+, k^\perp), \quad (\text{I-22})$$

We then find for the propagator of Eq. (I-19):

$$\Delta_{\text{F}}(x) = \frac{1}{(2\pi)^4} \int \frac{d^3\vec{k}}{2k^+} e^{-i\vec{k}\vec{x}} \int dk^- \frac{e^{-ik^- x^+}}{k^- - k_{\text{on}}^-}, \quad (\text{I-23})$$

in which we use the definition

$$\vec{k}\vec{x} = k^+ x^- - k^\perp \cdot x^\perp, \quad (\text{I-24})$$



and where  $k_{\text{on}}^-$  is the on mass-shell value, or, in other words, the pole in the complex  $k^-$ -plane:

$$k_{\text{on}}^- = \frac{k^\perp{}^2 + m^2 - i\epsilon}{2k^+}. \quad (\text{I-25})$$

Forward propagation in LF time requires  $x^+ \geq 0$ . Then, we can only evaluate the integral over  $k^-$  by closing the contour in the lower complex half-plane, because of the presence of the factor  $e^{-ik^-x^+}$  in the integrand. For  $k^+ > 0$  the pole is below the real axis. Therefore application of Cauchy's theorem gives a nonvanishing result only in this region:

$$\Delta_{\text{F}}(x) = \frac{-i}{(2\pi)^3} \int \frac{d^3\vec{k} \theta(k^+)}{2k^+} e^{-ik_{\text{on}}^\mu x_\mu}, \quad (\text{I-26})$$

where the on mass-shell four-vector  $k$  is given by

$$k_{\text{on}}^\mu = (k_{\text{on}}^-, k^+, k^\perp). \quad (\text{I-27})$$

## §2.2 The fermion propagator

The well-known propagator for a spin-1/2 particle is related to the Klein-Gordon propagator by the following relation:

$$S_{\text{F}}(x) = (i\partial_\mu \gamma^\mu + m)\Delta_{\text{F}}(x), \quad (\text{I-28})$$

where  $\partial_\mu$  is short for  $\partial/(\partial x^\mu)$ . We interchange differentiation and integration. Differentiation of the integrand in Eq. (I-19) gives:

$$S_{\text{F}}(x) = \frac{1}{(2\pi)^4} \int_{\text{Min}} d^4k \frac{\not{k} + m}{k^2 - m^2 + i\epsilon} e^{-ik_\mu x^\mu}, \quad (\text{I-29})$$

where the Feynman slash for an arbitrary four-vector  $p$  is defined by

$$\not{p} = p_\mu \gamma^\mu. \quad (\text{I-30})$$

An important difference with Eq. (I-23) is that the numerator contains the LF energy  $k^-$ . We can remove it by rewriting the numerator,

$$\not{k} + m = (k^- - k_{\text{on}}^-)\gamma^+ + (\not{k}_{\text{on}} + m). \quad (\text{I-31})$$

Upon substitution of this expansion into Eq. (I-29) we see that the first term of Eq. (I-31) cancels against a similar factor in the denominator. Integration over the LF energy gives the LF time-ordered fermion propagator:

$$\begin{aligned} S_{\text{F}}(x) &= \frac{-i}{(2\pi)^3} \int \frac{d^3\vec{k} \theta(k^+)}{2k^+} (\not{k}_{\text{on}} + m) e^{-ik_{\text{on}}^\mu x_\mu} \\ &+ \frac{-i}{(2\pi)^3} \int \frac{d^3\vec{k}}{2k^+} \gamma^+ \delta(x^+). \end{aligned} \quad (\text{I-32})$$



where  $P$  is the total momentum, and  $p$  is the momentum of the intermediate particle. Because of momentum conservation, they are the same. However, we make this distinction, to be able to write it in the following form:

$$\begin{array}{c} \diagup \\ \diagdown \end{array} \text{---} \text{---} \begin{array}{c} \diagdown \\ \diagup \end{array} = \frac{1}{2p^+} \frac{1}{P^- - p_{\text{on}}^-} = \begin{array}{c} \diagup \\ \diagdown \end{array} \text{---} \text{---} \begin{array}{c} \diagdown \\ \diagup \end{array} , \quad (\text{I-34})$$

where  $p_{\text{on}}^-$  is the on mass-shell value of  $p^-$ , conform Eq. (I-25). To stress that the diagram on the right-hand side is a time-ordered diagram, we draw a vertical thin line, indicating an energy denominator. The first denominator in Eq. (I-34) is the phase-space factor, constructed by taking for each intermediate particle the plus-momentum and a factor 2 because of the Kogut-Soper convention [13, 15]. The direction of the momenta should be chosen forward in time, such that the plus-component, satisfying the spectrum condition, is positive. The energy denominator is constructed by taking the total energy  $P^-$  and subtracting from it the on mass-shell values of the minus-momentum of the particles in the corresponding intermediate state. Thus, it is proportional to the energy that is “borrowed” from the vacuum. This explains why highly off energy-shell intermediate states are suppressed. In the next subsection we present examples where the energy denominators are more complicated because different time-orderings of the vertices are involved.

### §2.5 Light-front time-ordering

The most trivial example of time-ordering of vertices was already discussed in the previous subsection. In Compton-like scattering there are two time-orderings, however, one, the so-called Z-graph, is excluded because of the spectrum condition.

#### The one-boson exchange

If we look at a similar amplitude as Eq. (I-33), now with the exchanged particle in the  $t$ -channel, both time-orderings can contribute.

$$\begin{array}{c} q \text{---} \\ p \text{---} \end{array} \begin{array}{c} \text{---} \\ | \\ \text{---} \end{array} \begin{array}{c} q' \\ p' \end{array} = \frac{1}{k^2 - m^2 - i\epsilon} = \frac{1}{2k^+ \left( p^- - p'^- - \frac{m^2 + k^{\perp 2} + i\epsilon}{2k^+} \right)}, \quad (\text{I-35})$$

where the momentum of the intermediate particle  $k = p' - p = q - q'$ . The sign of  $k^+$  determines the time-ordering of the vertices:

$$\begin{array}{c} \text{---} \\ | \\ \text{---} \end{array} = \begin{array}{c} \text{---} \\ \diagdown \\ \text{---} \end{array} + \begin{array}{c} \text{---} \\ \diagup \\ \text{---} \end{array}, \quad (\text{I-36})$$

with

$$\begin{array}{c} \text{---} \\ \diagdown \\ \text{---} \\ \diagup \\ \text{---} \end{array} = \theta(k^+) \frac{1}{2k^+} \frac{1}{P^- - p'^- - \frac{m^2 + k^{\perp 2} + i\epsilon}{2k^+} - q^-}, \quad (\text{I-37})$$

$$\begin{array}{c} \text{---} \\ \diagup \\ \text{---} \\ \diagdown \\ \text{---} \end{array} = \theta(-k^+) \frac{1}{2(-k^+)} \frac{1}{P^- - p^- - \frac{m^2 + k^{\perp 2} + i\epsilon}{2(-k^+)} - q'^-}, \quad (\text{I-38})$$

where  $P^- = p^- + q^-$ , which, if the external states are on energy-shell, coincides with the energy of the system. Again we see that the energy denominators are constructed by subtracting from the total energy  $P^-$  the on mass-shell values of the minus-momentum of the particles in the intermediate state. Because of our choice of momenta, for the diagram (I-38) the momentum flow of the intermediate particle is backward in time. If we substitute  $k'^+ = -k^+$ , then the plus-momentum becomes positive, and the particle can be reinterpreted as going forward in LF time. In Chapter V we will again encounter these two time-orderings when we describe the interaction of two nucleons by the exchange of bosons.

### The scalar shower

The next example is used to illustrate that some algebraic manipulations are needed to construct all LF time-ordered diagrams. We look at the decay of a particle into four scalars, again in  $\phi^3$  theory.

$$\begin{array}{c} p_4 \\ \diagdown \\ P \text{---} \\ \diagup \\ p_3 \\ \diagdown \\ p_2 \\ \diagup \\ p_1 \end{array} = \frac{1}{(p_{12}^2 - m^2 - i\epsilon)(p_{34}^2 - m^2 - i\epsilon)} = \frac{1}{p_{12}^+ p_{34}^+} \frac{1}{(p_{12}^- - p_{12\text{on}}^-)(p_{34}^- - p_{34\text{on}}^-)}, \quad (\text{I-39})$$

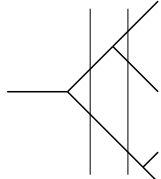
where the two intermediate scalars have momentum  $p_{12} = p_1 + p_2$  and  $p_{34} = p_3 + p_4$  respectively. We now use the algebraic identity

$$\frac{1}{(a-b)(c-d)} = \frac{1}{a+c-b-d} \left( \frac{1}{a-b} + \frac{1}{c-d} \right), \quad (\text{I-40})$$

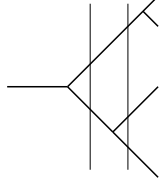
This splitting can be used for the covariant amplitude in Eq. (I-39). We find:

$$\begin{array}{c} \diagup \\ \diagdown \\ \text{---} \\ \diagup \\ \diagdown \end{array} = \begin{array}{c} \diagup \\ \diagdown \\ \text{---} \\ \diagup \\ \diagdown \\ \text{---} \\ \diagup \\ \diagdown \end{array} + \begin{array}{c} \diagup \\ \diagdown \\ \text{---} \\ \diagup \\ \diagdown \\ \text{---} \\ \diagdown \\ \diagup \end{array}, \quad (\text{I-41})$$

with



$$= \frac{1}{4p_{12}^+ p_{34}^+} \frac{1}{(P^- - p_{12 \text{ on}}^- - p_{34 \text{ on}}^-)(P^- - p_{12 \text{ on}}^- - p_3^- - p_4^-)} \quad (\text{I-42})$$



$$= \frac{1}{4p_{12}^+ p_{34}^+} \frac{1}{(P^- - p_{12 \text{ on}}^- - p_{34 \text{ on}}^-)(P^- - p_1^- - p_2^- - p_{34 \text{ on}}^-)} \quad (\text{I-43})$$

which again are energy denominators as defined above. This way to split the covariant denominator using the trick of (I-40) is the simplest example of a complicated recombination scheme for denominators which can be found in the article of Ligterink and Bakker [16].

### §2.6 Loop diagrams

In the case of a loop diagram, covariant Feynman rules require an integration over the internal four-momentum  $k$ . Time-ordered diagrams have an integration over the three kinematical components. As was found by Kogut and Soper [13], a relation between these types of diagrams can be established if we integrate out the energy component  $k^-$  from the covariant diagram. Upon doing this integration one finds all LF time-ordered diagrams with the vertices time-ordered in all possible ways, however, respecting the spectrum condition. For an arbitrary number of particles in a loop, the proof was only recently given by Ligterink and Bakker [16]. As an example, which also shows some of the problems encountered in LF Hamiltonian dynamics, we discuss the electromagnetic form factor in  $\phi^3$  theory, given earlier by Sawicki [17]:

$$J^\mu(0) = \int_{\text{Min}} d^4k \frac{1}{(k-q)^2 - m^2 + i\epsilon} (2k^\mu - q^\mu) \frac{1}{k^2 - m^2 + i\epsilon} \frac{1}{(P-k)^2 - m^2 + i\epsilon}, \quad (\text{I-44})$$

where the kinematics are given in Fig. I-3a. All time-orderings corresponding to this diagram are given in Fig. I-3b.

An essential difference between the instant-form and the light-front occurs if we write the Feynman propagator in terms of the poles in the energy plane. In terms of IF coordinates we find:

$$k^2 - m^2 + i\epsilon = \left( k^0 - \sqrt{\vec{k}^2 + m^2 - i\epsilon} \right) \left( k^0 + \sqrt{\vec{k}^2 + m^2 - i\epsilon} \right), \quad (\text{I-45})$$

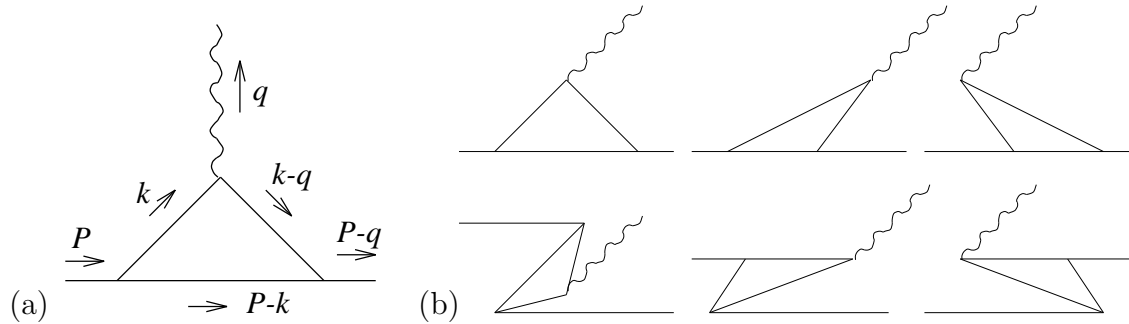


Figure I-3: (a) Kinematics for the current. (b) The six time-orderings contributing to the electro-magnetic form factor in  $\phi^3$  theory. The vertical lines denoting energy denominators have been omitted.

and on the light-front we have:

$$k^2 - m^2 + i\epsilon = 2k^+ \left( k^- - \frac{k^{\perp 2} + m^2 - i\epsilon}{2k^+} \right). \quad (\text{I-46})$$

We see that the Feynman propagator is quadratic in the IF energy  $k^0$  but only linear in the LF energy  $k^-$ . In the former case it leads to the presence of both positive and negative energy eigenstates, whereas on the light-front only positive energy states occur. In the instant-form, half of the poles occur above the real axis, and the other half below. Therefore contour integration will always give a nonvanishing result. In contrast to this, on the light-front the poles can cross the real axis. If all poles are on the same side of the real axis, the contour can be closed in the other half of the complex plane, and contour integration gives a vanishing result. Because of this effect, four of the six time-ordering in Fig. I-3 disappear. Only the first two remain. This is another manifestation of the spectrum condition. If we then turn to the Breit-frame  $(q^-, q^+, q^\perp) = (0, 0, q^\perp)$ , also the second diagram of Fig. I-3 vanishes, as will follow from the analysis we present below.

Most important in our analysis is the sign of the imaginary part of the poles. Because of our choice of the Breit-frame, these are identical for the first and the second Feynman propagator in Eq. (I-44), namely  $-\epsilon/2k^+$ . The imaginary part of the third Feynman propagator is  $\epsilon/2(P^+ - k^+)$ . In Fig. I-4 we show the location of these poles for different  $k^+$  intervals.

We see in (a) and (c) of Fig. I-4 that the contour can be closed in such a way that no poles are inside the contour, and therefore contour integration leads to a vanishing result. In case that we calculate the component  $J^-$  of the current, application of Cauchy's theorem is not valid because there is a contribution to the integral from a pole at infinity, i.e., for large absolute values of  $k^-$  the integrand

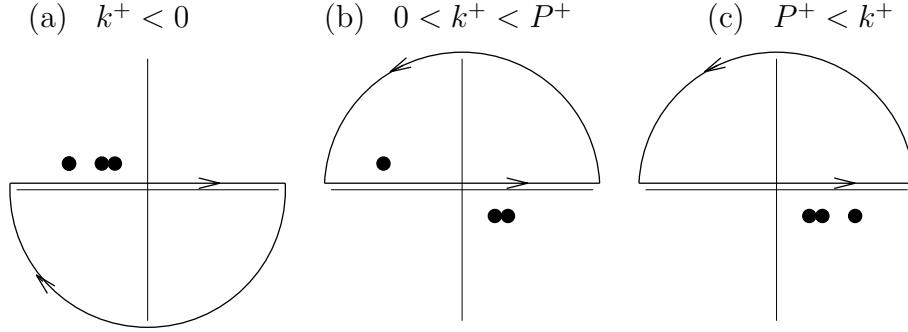


Figure I-4: The position of the double dot (first and second propagator in Eq. (I-44)) and the dot (third propagator in Eq. (I-44)) indicate in which quadrant of the complex  $k^-$ -plane the corresponding poles are located.

goes as  $1/k^-$ . Therefore we restrict ourselves in this example to the components  $J^+$  and  $J^\perp$ . Only one LF time-ordered diagram contributes to the current:

$$\begin{aligned}
 J^\mu(0) &= \text{[Diagram: A triangle with a wavy photon line on top and two vertical lines on the sides, representing a time-ordered diagram]} \\
 &= 2\pi i \int d^2 k^\perp \int_0^{P^+} \frac{dk^+}{8k^{+2}(P^+ - k^+)} (2k^\mu - q^\mu) \quad (\text{I-47}) \\
 &\times \frac{1}{P^- - \frac{k^\perp{}^2 + m^2}{2k^+} - \frac{(P^\perp - k^\perp)^2 + m^2}{2(P^+ - k^+)}} \frac{1}{P^- - \frac{(k^\perp - q^\perp)^2 + m^2}{2k^+} - \frac{(P^\perp - k^\perp)^2 + m^2}{2(P^+ - k^+)}}
 \end{aligned}$$

where we have drawn vertical lines in the LF time-ordered diagram to indicate the energy denominators and to avoid confusion with the covariant diagram. The kinematics are given in Fig. I-3a. The photon line is vertical to indicate that we are in the Breit-frame. The imaginary parts have been omitted.

For the result above to be correct three assumptions are essential:

1. Interchange of the limit  $q^+ \rightarrow 0$  and  $k^-$ -integration is valid,
2. There is no contribution of poles at infinity upon doing the  $k^-$ -integration,
3. The amplitude is well-defined and finite.

All three assumptions can be justified in this case. De Melo *et al.* [18] have shown that the interchange mentioned under assumption 1 may cause pair creation or annihilation contributions to become nonvanishing. In §4 of Chapter II we show that this effect may also occur in the Yukawa model. However, it is not a violation of the spectrum condition.

The second assumption can be justified by looking at Eq. (I-44). As  $k^2$  is linear in  $k^-$ , we see that the integration over the minus component is well-defined for each component of the current. In a theory with fermions, this integration

can be ill-defined, leading to longitudinal divergences and the occurrence of so-called forced instantaneous loops (FILs). Divergences for the Yukawa model are classified in §2 of Chapter II and the longitudinal ones are dealt with in Chapter III, where it is shown that the FILs vanish upon using an appropriate regularization method: “minus regularization” [19].

The third assumption is also satisfied, since the superficial degree of divergence for integration over the perpendicular components is smaller than zero for all components of the current. If any transverse divergences occur, they can be attacked with the method of extended minus regularization presented in Chapter IV. The phase space factor contains endpoint singularities in  $k^+$ . However, these are canceled by identical factors in the energy denominators.



## The Yukawa model

In particle physics several models are used to describe existing elementary particles, interactions and bound states. Many of these models are just used to highlight certain properties, or to make exact or numerical calculation possible. Although the latter are referred to as toy models, they are helpful because they are stripped from those properties that are of no concern to the investigation that is done. In this thesis we are going to “play around” with two models. One of them we already met in the introductory chapter:  $\phi^3$  theory. In this model one can very nicely demonstrate that higher Fock states are much more suppressed on the light-front than in instant-form Hamiltonian dynamics, as will be done in Chapter V. This model only contains scalar particles. The simplest model including fermions is the Yukawa model, which has the following Lagrangian:

$$\mathcal{L} = \bar{\psi}(i\partial_\mu\gamma^\mu - m)\psi + \phi(\partial_\mu\partial^\mu + \mu^2)\phi + g\bar{\psi}\psi\phi. \quad (\text{II-1})$$

The field  $\psi$  describes the fermions and the field  $\phi$  describes the scalar particles, from now on referred to as bosons. The last term is the interaction between the fermion–anti-fermion field and the boson field. Yukawa introduced this model to describe the interaction of nucleons (fermions) via pions (bosons). The strength of the interaction is given by  $g$ . In our calculations we limit ourselves to a scalar coupling.

### §1 Feynman rules

Using perturbation theory one can deduce from the Lagrangian the well-known rules for Feynman diagrams. Summing over these diagrams one then finds the  $S$ -matrix.

The first term of the Lagrangian (II-1) leads to the following propagator:

$$\text{---} \underset{k}{\text{---}} \text{---} = \frac{i(\not{k} + m)}{k^2 - m^2 + i\epsilon}, \quad (\text{II-2})$$

for a fermion with momentum  $k^\mu$  and mass  $m$ . For a (scalar) boson with momentum  $k^\mu$  and mass  $\mu$  we have the following Feynman rule:

$$\text{---} \underset{k}{\text{---}} \text{---} = \frac{i}{k^2 - \mu^2 + i\epsilon}. \quad (\text{II-3})$$

The full set of Feynman rules to compute the scattering amplitude in the Yukawa model can be found in many text books such as Itzykson and Zuber [20]. Our goal is to translate these rules to rules for diagrams that one uses in LFD.

In Chapter I we introduced the  $k^-$ -integration to obtain the rules for the LF time-ordered diagrams. A complication in this procedure was already mentioned there: the integration over  $k^-$  may be ill-defined, and the resulting integral may be divergent. Before solving these problems, we first classify the divergences.

## §2 Divergences in the Yukawa model

In the previous subsection we described how to construct each covariant Feynman diagram. Covariant diagrams may contain infrared and ultraviolet divergences. Therefore we are not surprised that both in the process of constructing the LF time-ordered diagrams as in the diagrams themselves divergences can be encountered. The first type can be classified as longitudinal divergences, and the second as transverse divergences.

### §2.1 Longitudinal divergences

We can deduce what (superficial) divergences we are going to encounter upon integration over  $k^-$ . We denote the longitudinal degree of divergence by  $D^-$ . Suppose we have a truncated one-loop diagram containing  $b$  bosons and  $f$  fermions. In the fermion propagator Eq. (II-2) the factor  $k^-$  occurs both in the numerator and in the denominator, and therefore it does not contribute to  $D^-$ . Each boson will, according to Eq. (II-3) contribute  $-1$  to the degree of divergence, and the measure  $d^4k$  of the loop contributes 1, resulting in

$$D^- = 1 - b. \quad (\text{II-4})$$

Longitudinally divergent diagrams, i.e.,  $D^- \geq 0$ , contain one boson in the loop, or none. Since every loop contains at least two lines, a longitudinally divergent diagram contains at least one fermion. For the model we discuss, the Yukawa model with a scalar coupling, the degree of divergence is reduced. For scalar coupling  $g$  it turns out that  $\gamma^+ g \gamma^+ = 0$  and therefore two instantaneous parts cannot be neighbors. The longitudinal degree of divergence for the Yukawa model with scalar coupling is

$$D_{\text{Yuk}}^- = 1 - b - \left[ \frac{1+f-b}{2} \right]_{\text{entier}} = 1 - \left[ \frac{1+f+b}{2} \right]_{\text{entier}}, \quad (\text{II-5})$$

where the subscript “entier” denotes that we take the largest integer not greater than the value between square brackets.

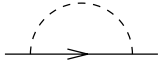
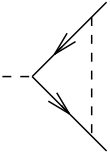
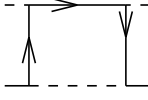
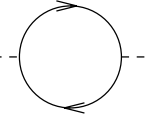
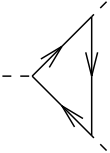
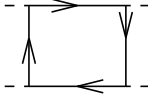
	$D_{\text{Yuk}}^- = 0$	$D_{\text{Yuk}}^- = -1$	$D_{\text{Yuk}}^- = -1$
$b = 1$			
	$D^\perp = 1$	$D^\perp = 0$	$D^\perp = -1$
	$D_{\text{Yuk}}^- = 0$	$D_{\text{Yuk}}^- = -1$	$D_{\text{Yuk}}^- = -1$
$b = 0$			
	$D^\perp = 2$	$D^\perp = 1$	$D^\perp = 0$

 Table II-1: Longitudinal ( $D^-$ ) and transverse ( $D^\perp$ ) degrees of divergence in the Yukawa model.

## §2.2 Transverse divergences

The transverse degree of divergence  $D^\perp$  of a LF time-ordered diagram is the divergence one encounters upon integrating over the perpendicular components. In most cases this degree of divergence is the same as what is known in covariant perturbation theory as the superficial degree of divergence  $D$  of a diagram. In that case it is the divergence one finds if in the covariant amplitude odd terms are removed and Wick rotation is applied. For a one-loop Feynman diagram in four space-time dimensions with  $f$  internal fermion lines and  $b$  internal boson lines the transverse degree of divergence is

$$D^\perp = 4 - f - 2b. \quad (\text{II-6})$$

In case of  $d$  space-time dimensions we have to replace the term 4 by  $d$ .

In Table II-1 all one-loop diagrams up to order  $g^4$  that are candidates to be divergent have been listed with their longitudinal and transverse degree of divergence.

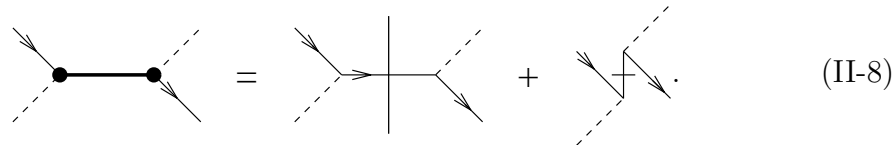
## §3 Instantaneous terms and blinks

As was already illustrated in the introduction, in the case of fermions we have to differentiate between propagating and instantaneous parts. Therefore this distinction plays an important role in the Yukawa model. The covariant propagator in momentum representation for an off-shell spin-1/2 particle can be written analogously to Eq. (I-32):

$$\frac{i(\not{k} + m)}{k^2 - m^2 + i\epsilon} = \frac{i(\not{k}_{\text{on}} + m)}{k^2 - m^2 + i\epsilon} + \frac{i\gamma^+}{2k^+}. \quad (\text{II-7})$$

The first term on the right-hand side is the propagating part. The second one is the instantaneous part. The splitting of the covariant propagator corresponds to a similar splitting of LF time-ordered diagrams. For any fermion line in a covariant diagram two LF time-ordered diagrams occur, one containing the propagating part of the covariant propagator, the other containing the instantaneous part. For obvious reasons we call the corresponding lines in the LF time-ordered diagrams propagating and instantaneous respectively. For a general covariant diagram the  $1/k^+$ -singularity in the propagating part cancels a similar singularity in the instantaneous part. Therefore the LF time-ordered diagrams with instantaneous lines are necessary; they are usually well-defined.

If the  $1/k^+$ -singularities are inside the area of integration we may find it necessary to combine the propagating and the instantaneous contribution again into the so-called blink, introduced by Ligterink and Bakker [16], such that there is a cancellation of the singularities:



$$\text{Blink} = \text{Propagating} + \text{Instantaneous} \quad (\text{II-8})$$

The thick straight line between fat dots is a blink. The bar in the internal line of the third diagram is the common way to denote an instantaneous fermion. When a LF time-ordered diagram resembles a covariant diagram, we draw a vertical line as in the second diagram of Eq. (II-8). If no confusion is possible, we omit it in the remainder of this thesis. The difference between Eqs. (II-7) and (II-8) lies in the fact that the former uses covariant propagators, and the latter has energy denominators. In this case the difference is only formal. However, in more complicated diagrams there is a big difference, as we will see later. Examples of blinks are discussed in the next section, and in §2 of Chapter III where we discuss the one-boson exchange correction to the vertex.

## §4 Pair contributions in the Breit-frame

In Chapter I we found that for massive particles the spectrum condition applies: there can be no creation from or annihilation into the vacuum. This gives a significant reduction of the number of diagrams that one has to incorporate in a light-front calculation. In any frame where the particles have positive plus-momentum this is valid. In Leutwyler and Stern [11] it was already noted that on the light-front the regions  $p^+ < 0$ ,  $p^+ = 0$  and  $p^+ > 0$  are kinematically separated, another manifestation of the spectrum condition. This fact should

already make us aware that the Breit-frame, where one takes the limit of the plus-momentum of the incoming virtual photon going to zero, is dangerous.

Indeed one finds that pair creation or annihilation contributions play a role in this limit. This was first found by De Melo *et al.* [18] and later by Choi and Ji [21]. They discuss as an example the electro-magnetic current in  $\phi^3$  theory, and find a pair creation contribution for the component  $J^-$  of the current. We have shown in Chapter I that for the other components  $J^+$  and  $J^\perp$  pair creation contributions vanish. Because De Melo *et al.* discuss a scalar theory, we infer that this effect is not related to the presence of fermions in the theory.

In a theory with fermions, such as the Yukawa model, we now show that the pair creation/annihilation term is also nonvanishing, and that its omission leads to a breaking of covariance and rotational invariance.

In the presence of fermions, the individual time-ordered diagrams may contain  $1/k^+$  singularities that cancel in the full sum. Because this cancellation has nothing to do with the time-ordering of the diagrams, we combine the LF time-ordered diagrams into blink diagrams. After that, we have a clear view on the point we want to discuss.

Again, we use kinematics as in Fig. I-3a. Two blinks contribute to the current, provided we have chosen the plus-component of the momentum of the outgoing boson  $q^+ \geq 0$ .

$$\text{Diagram} = \text{Blink}_1 + \text{Blink}_2, \quad (\text{II-9})$$

where the diagrams containing blinks are given by:

$$\begin{aligned} &= -2\pi i \int d^2 k^\perp \int_{q^+}^{P^+} \frac{dk^+}{8k^+(k^+ - q^+)(P^+ - k^+)} \\ &\times \frac{-(\not{P} - \not{k})_{\text{on}} + \not{P} + m}{P^- - \frac{k^\perp{}^2 + m^2}{2k^+} - \frac{(P^\perp - k^\perp)^2 + m^2}{2(P^+ - k^+)}} \frac{-(\not{P} - \not{k})_{\text{on}} + \not{P} - \not{q} + m}{P^- - \frac{(k^\perp - q^\perp)^2 + m^2}{2(k^+ - q^+)} - \frac{(P^\perp - k^\perp)^2 + m^2}{2(P^+ - k^+)}} - q^-, \end{aligned} \quad (\text{II-10})$$

$$\begin{aligned} &= -2\pi i \int d^2 k^\perp \int_0^{q^+} \frac{dk^+}{8k^+(q^+ - k^+)(P^+ - k^+)} \\ &\times \frac{\not{k}_{\text{on}} + m}{P^- - \frac{k^\perp{}^2 + m^2}{2k^+} - \frac{(P^\perp - k^\perp)^2 + m^2}{2(P^+ - k^+)}} \frac{\not{k}_{\text{on}} - \not{q} + m}{q^- - \frac{k^\perp{}^2 + m^2}{2k^+} - \frac{(k^\perp - q^\perp)^2 + m^2}{2(q^+ - k^+)}}. \end{aligned} \quad (\text{II-11})$$

The diagram (II-10) is an example of a “double” blink. The total blink is the thick line between the two fat dots. For both blinks we see that the energy denominators are the same as for usual LF time-ordered diagrams. However, the numerators are different. In the next subsection we show how the numerator of the blink is constructed.

### §4.1 Construction of the blink

As an example, we show how we can construct the blink (II-11). For the fat line we have to substitute the propagating and instantaneous part.

(II-12)

The propagating contribution is

(II-13)

and the instantaneous contribution, denoted by the perpendicular tag, is

(II-14)

We see that both have a singularity at the upper boundary  $q^+$  of the integration interval over  $k^+$ . These cancel in the sum: the blink Eq. (II-11). It is obtained by making the denominators common for the two diagrams. We can verify, using the relation  $\gamma^+\gamma^+ = 0$ , that the lower boundary at  $k^+ = 0$  does not cause any problems, neither for the LF time-ordered diagrams, nor for the blink.

In an analogous way the double blink is constructed. It consists out of the following LF time-ordered diagrams:

(II-15)

We see that one diagram is missing: the diagram with two instantaneous fermions. Because it contains two neighboring  $\gamma^+$  matrices, it vanishes. It is an example of a forced instantaneous loop (FIL), which is related to longitudinal divergences and will be discussed in the next chapter. The LF time-ordered diagrams have the same integration interval as the double blink (II-10). The last diagram on the right-hand side is the same as the diagram in Eq. (II-14), the only difference being the integration range. The instantaneous fermions have been 'tilted' a little

in these two diagrams, to indicate that the integration interval is such that the instantaneous fermions carry positive plus-momentum. The second diagram on the right-hand side of Eq. (II-15) has no tilted instantaneous fermion, because the integration range has not been split as in the previous case. We will not give the formulas for the LF time-ordered diagrams in Eq. (II-15), but we have verified that their end-point singularities are removed when the diagrams are combined into the double blink.

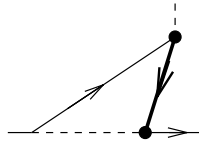
### §4.2 The Breit-frame

What happens to the current in Eq. (II-9) in the limit of  $q^+ \downarrow 0$ ? Relying on the spectrum condition, one may expect that diagrams like (II-11) disappear, and that only the double blink (II-10) contributes. This is confirmed by the fact that the integration area of the single blink (II-11) goes to zero. However, it could be that the integrand obtains singularities in the limit  $q^+ \downarrow 0$  that cause a nonzero result. We denote this limit in the diagrams by drawing the line of the outgoing boson vertically.

For the numerator of the blink (II-11) we use the relation

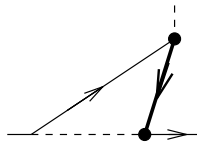
$$(\not{k}_{\text{on}} + m)(\not{k}_{\text{on}} - \not{q} + m) = 2m^2 + \not{k}_{\text{on}}(2m - \not{q}). \quad (\text{II-16})$$

The integral is dominated by factors  $k^+$  and  $(k^+ - q^+)$ . Identifying these factors in (II-11) we find:



$$= -2\pi i \int d^2k^\perp \int_0^{q^+} \frac{dk^+}{8k^+(k^+ - q^+)P^+} \frac{\gamma^+(2m - \not{q})}{q^- - \frac{k^\perp{}^2 + m^2}{2k^+} - \frac{(k^\perp - q^\perp)^2 + m^2}{2(q^+ - k^+)}}. \quad (\text{II-17})$$

We write Eq. (II-17) in internal coordinates  $x = k^+/q^+$ , and find that the  $q^+$  dependence on the integration range drops. Moreover, the integration contains no singularities in the internal variable  $x$ .



$$= -\pi i \int d^2k^\perp \int_0^1 dx \frac{\gamma^+}{2P^+} \frac{2m - \not{q}}{(k^\perp - xq^\perp)^2 + m^2 - x(1-x)q^2}. \quad (\text{II-18})$$

If we disregard for a moment the transverse integration, we see that in the Breit-frame there is a finite contribution of pair-creation/annihilation to the current. This agrees with the result of De Melo *et al.* [18]. Furthermore, we see that it is not covariant, and therefore its omission will not only lead to the wrong amplitude, but also to breaking of Lorentz covariance and rotational invariance.



## Longitudinal divergences in the Yukawa model

*If the doors of perception were cleansed everything would appear as it is, infinite.*

William Blake, The marriage of heaven and hell [22]

For a number of reasons mentioned in the previous chapters, quantization on the light-front is nontrivial. Subtleties arise that have no counterpart in ordinary time-ordered theories. We will encounter some of them in this chapter and show how to deal with them in such a way that covariance of the perturbation series is maintained.

In LFD, or any other Hamiltonian theory, covariance is not manifest. Burkardt and Langnau [10] claimed that, even for scattering amplitudes, rotational invariance is broken in naive light-cone quantization (NLCQ). In the case they studied, two types of infinities occur: longitudinal and transverse divergences. They regulate the longitudinal divergences by introducing noncovariant counterterms. In doing so, they restore at the same time rotational invariance. The transverse divergences are dealt with by dimensional regularization.

We would like to maintain the covariant structure of the Lagrangian and take the path of Ligterink and Bakker [16]. Following Kogut and Soper [13] they derive rules for LFD by integrating covariant Feynman diagrams over the LF energy  $k^-$ . For covariant diagrams where the  $k^-$ -integration is well-defined this procedure is straightforward and the rules constructed are, in essence, equal to the ones of NLCQ. However, when the  $k^-$ -integration diverges the integral over  $k^-$  must be regulated first. We stress that it is important to do this in such a way that covariance is maintained.

In this chapter, we will show that the occurrence of longitudinal divergences is related to the so-called forced instantaneous loops (FILs). If these diagrams are included and renormalized in a proper way we can give an analytic proof of covariance. FILs were discussed before by Mustaki *et al.* [23], in the context of QED. They refer to them as *seagulls*. There are, however, some subtle differences between their treatment of longitudinal divergences and ours, which are explained in §3.

Transverse divergences have a different origin. However, they can be treated with the same renormalization method as longitudinal divergences. We shall



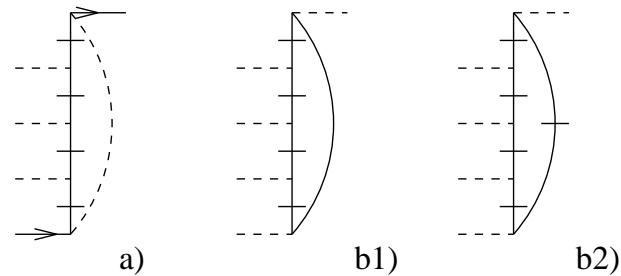


Figure III-1: Examples of FILs. In (a) a boson in the loop is forced to be instantaneous. In (b1) a fermion is obstructed in its propagation. In (b2) all fermions are instantaneous.

present an analytic proof of the equivalence of the renormalized covariant amplitude and the sum of renormalized LF time-ordered amplitudes in two cases, the fermion and the boson self-energy. In the other cases we have to use numerical techniques. They will be dealt with in Chapter IV.

## §1 Introduction

In the previous chapters we already introduced instantaneous fermions. For a discussion on longitudinal divergences they play an important role. Without fermions there are no longitudinal divergences! The longitudinal divergences can be both seen from a “pictorial” and a mathematical point of view.

The pictorial view is the following. When a diagram contains a loop where all particles but one are instantaneous, a conceptual problem occurs. Should the remaining boson or fermion be interpreted as propagating or as instantaneous? Loops with this property are referred to as forced instantaneous loops (FILs). Loops where all fermions are instantaneous are also considered as FILs. However, they do not occur in the Yukawa model with (pseudo-)scalar coupling. Examples of these three types of FILs are given in Fig. III-1.

Mathematically this problem also shows up. The FILs correspond to the part of the covariant amplitude where the  $k^-$ -integration is ill-defined. The problem is solved in the following way. First we do not count FILs as LF time-ordered diagrams. Second we find that this special type of diagram disappears upon regularization if we use the method of Ligterink and Bakker [19]: minus regularization.

### §1.1 Minus regularization

The minus-regularization scheme was developed for the purpose of maintaining the symmetries of the theory such that the amplitude is covariant order by order. It can be applied to Feynman diagrams as well as to ordinary time-ordered or

to LF time-ordered diagrams. Owing to the fact that minus regularization is a linear operation, it commutes with the splitting of Feynman diagrams into LF time-ordered diagrams.

We explain very briefly how the method works. Consider a diagram defined by a divergent integral. Then the integrand is differentiated with respect to the external energy, say  $q^-$ , until the integral is well defined. Next the integration over the internal momenta is performed. Finally the result is integrated over  $q^-$  as many times as it was differentiated before. This operation is the same as removing the lowest orders in the Taylor expansion in  $q^-$ . For example, if the two lowest orders of the Taylor expansion with respect to the external momentum  $q$  of a LF time-ordered diagram  $\int d^3k \mathcal{F}(q, k)$  are divergent, minus regularization is the following operation:

$$\int_{\frac{q_+^2}{2q^+}}^{q^-} dq' \int_{\frac{q_+^2}{2q^+}}^{q'^-} dq'' \int d^2k^\perp dk^+ \left( \frac{\partial}{\partial q''^-} \right)^2 \mathcal{F}(k, q''). \quad (\text{III-1})$$

The point  $q^2 = 0$  is chosen in this example as the renormalization point. This regularization method of subtracting the lowest order terms in the Taylor expansion is similar to what is known in covariant perturbation theory as BPHZ (Bogoliubov-Parasiuk-Hepp-Zimmermann) [24]. Some advantages of the minus-regularization scheme are preservation of covariance and local counterterms. Another advantage is that longitudinal as well as transverse divergences are treated in the same way. A more thorough discussion on minus regularization can be found in the next chapter.

## §1.2 Proof of equivalence for the Yukawa model

The proof of equivalence will not only hold order by order in the perturbation series, but also for every covariant diagram separately. In order to allow for a meaningful comparison with the method of Burkardt and Langnau we apply our method to the same model as they discuss, the Yukawa model, as introduced in Chapter II.

In this model we have to distinguish four types of diagrams, according to their longitudinal ( $D^-$ ) and transverse degrees ( $D^\perp$ ) of divergence. These divergences were classified also in Table II-1 on page 19. The proof of equivalence is illustrated in Fig. III-2.

We integrate an arbitrary covariant diagram over LF energy. For longitudinally divergent diagrams this integration is ill-defined and results in FILs. A regulator  $\alpha$  is introduced which formally restores equivalence. Upon minus regularization the  $\alpha$ -dependence is lost and the transverse divergences are removed. We can distinguish

- *Longitudinally and transversely convergent diagrams* ( $D^- < 0, D^\perp < 0$ ). No FILs will be generated. No regularization is needed. The LF time-ordered diagrams may contain  $1/k^+$ -poles, but these can be removed using

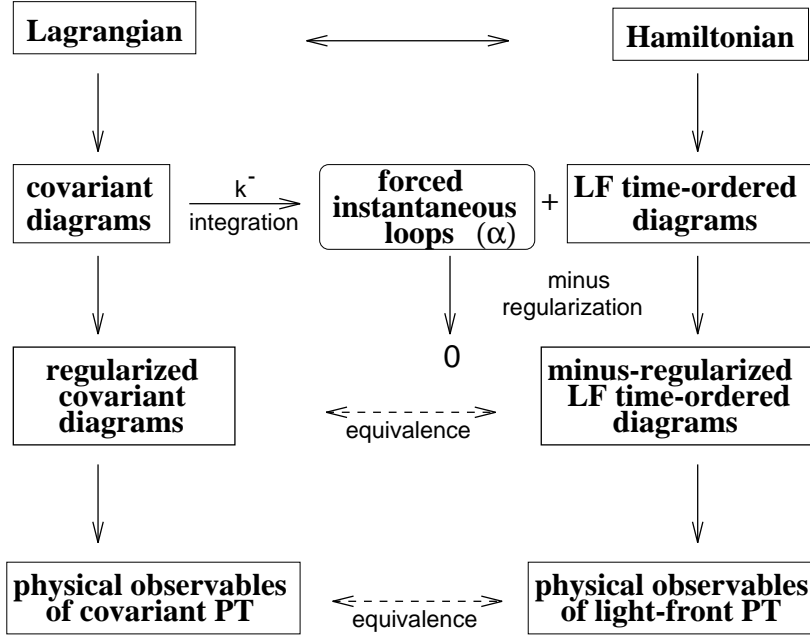


Figure III-2: Outline of the proof of equivalence for diagrams with longitudinal divergences.

blinks. A rigorous proof of equivalence for this class of diagrams is given by Ligterink and Bakker [16].

- *Longitudinally convergent diagrams* ( $D^- < 0$ ) with a transverse divergence ( $D^\perp \geq 0$ ). In the Yukawa model there are three such diagrams: the four fermion box, the fermion triangle and the one-boson exchange correction. Again, no FILs occur. Their transverse divergences and therefore the proof of equivalence will be postponed until Chapter IV. However, because the one-boson exchange correction illustrates the concept of  $k^-$ -integration, the occurrence of instantaneous fermions and the construction of blinks, it will be discussed as an example in §2. In Chapter I we gave an example for a longitudinally convergent diagram in  $\phi^3$  theory: the electro-magnetic current.
- *Longitudinally divergent diagrams* ( $D^- = 0$ ) with a logarithmic transverse divergence ( $D^\perp = 0$ ). In the Yukawa model with a scalar coupling there is one such diagram: the fermion self-energy. Upon splitting the fermion propagator two diagrams are found. The troublesome one is the diagram containing the instantaneous part of the fermion propagator. According to our definition it is a FIL and needs a regulator. In §3 we show how to determine the regulator  $\alpha$  that restores covariance formally. Since  $\alpha$  can be chosen such that it does not depend on the LF energy, the FIL will vanish upon minus regularization.



We now show how the LF time-ordered diagrams, including those containing instantaneous terms, can be constructed. The LF time-ordered diagrams contain on-shell spin projections in the numerator. They are

$$\not{k}_{\text{on}} = k_{i\text{on}}^- \gamma^+ + k_i^+ \gamma^- - k_i^\perp \gamma^\perp. \quad (\text{III-8})$$

We also use the following relation:

$$k^- - H_i^- = k_i^- - k_{i\text{on}}^-. \quad (\text{III-9})$$

We rewrite the numerator

$$\begin{aligned} (\not{k}_1 + m)(\not{k}_2 + m) &= ((k^- - H_1^-) \gamma^+ + (\not{k}_{1\text{on}} + m)) \\ &\times ((k^- - H_2^-) \gamma^+ + (\not{k}_{2\text{on}} + m)). \end{aligned} \quad (\text{III-10})$$

This separation allows us to write Eq. (III-4) as

$$\begin{aligned} \text{---} \langle \text{---} \rangle &= \int \frac{d^2 k^\perp dk^+ dk^-}{8k_1^+ k_2^+ k^+} \left\{ \frac{\gamma^+ \gamma^+}{(k^- - H^-)} + \frac{(\not{k}_{1\text{on}} + m)(\not{k}_{2\text{on}} + m)}{(k^- - H_1^-)(k^- - H_2^-)(k^- - H^-)} \right. \\ &\quad \left. + \frac{\gamma^+(\not{k}_{2\text{on}} + m)}{(k^- - H_2^-)(k^- - H^-)} + \frac{(\not{k}_{1\text{on}} + m)\gamma^+}{(k^- - H_1^-)(k^- - H^-)} \right\} \quad (\text{III-11}) \end{aligned}$$

The splitting corresponds to the splitting of the covariant amplitude into LF time-ordered diagrams. The numerators are written in such a form that Cauchy's formula can be applied easily to the  $k^-$ -integration. Only for the first term of Eq. (III-11) can  $k^-$  contour integration not be applied because the semi-circle at infinity gives a nonvanishing contribution. Such a singularity corresponds to a pole at infinity. However, we are saved by the fact that  $\gamma^+ \gamma^+ = 0$ . Therefore we obtain for the first term of Eq. (III-11)

$$\text{---} \langle \text{---} \rangle = 0. \quad (\text{III-12})$$

Here the bars in the two internal fermion lines again denote instantaneous terms. This forces the boson line to be instantaneous too. We see that this diagram is a FIL according to the definition we gave in the previous section. The longitudinal divergences which occur due to such diagrams are discussed in the next sections. Since FILs are not LF time-ordered diagrams, the rules given by NLCQ do not apply.

The second term of Eq. (III-11) contains only propagating parts. It has three poles (III-5)-(III-7). We are free to close the contour either in the lower or in the upper half plane. The poles do not always lie on the same side of the real

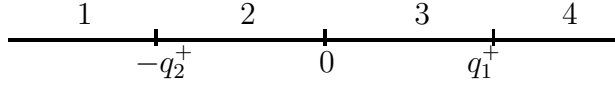


Figure III-3: Regions for the  $k^+$ -integration. At the boundaries a pole crosses the real  $k^-$ -axis.

$k^-$ -axis. For example, the pole given in Eq. (III-5) is in the upper half plane for  $k^+ < 0$ . At  $k^+ = 0$  it changes side. In Fig. III-3 we show the four intervals that can be distinguished.

In region 1 all poles lie above the real  $k^-$ -axis. By closing the contour in the lower half plane we see that the integral vanishes. At  $k^+ = -q^+$  the pole (III-7) crosses the real axis. In interval 2 the integral is proportional to its residue:

$$= -2\pi i \int d^2 k^\perp \int_{-q_2^+}^0 \frac{dk^+}{8k_1^+ k_2^+ k^+} \frac{(k_{1\text{on}} + m)(k_{2\text{on}} + m)}{(H_1^- - H_2^-)(H^- - H_2^-)}. \quad (\text{III-13})$$

No vertical lines are drawn since this is clearly a LF time-ordered diagram. The factor  $(H_1^- - H_2^-)^{-1}$  is the energy denominator corresponding to the fermion-anti-fermion state between the moment in LF time that the boson decays and the moment that the exchanged boson is emitted.  $(H^- - H_2^-)^{-1}$  is the energy denominator corresponding to the state in the period that the exchanged boson exists.

At  $k^+ = 0$  a second pole crosses the real axis. For positive  $k^+$  we close the contour in the upper half plane. Here only one pole (III-6) is present. The result is

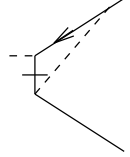
$$= 2\pi i \int d^2 k^\perp \int_0^{q_1^+} \frac{dk^+}{8k_1^+ k_2^+ k^+} \frac{(k_{1\text{on}} + m)(k_{2\text{on}} + m)}{(H_1^- - H_2^-)(H_1^- - H^-)}. \quad (\text{III-14})$$

Only the second energy denominator differs from the one in Eq. (III-13).

The terms of Eq. (III-11) with one instantaneous term are easier to determine. There are two poles and a contribution only occurs if the poles are on different sides of the real  $k^-$ -axis. The third term of Eq. (III-11) is

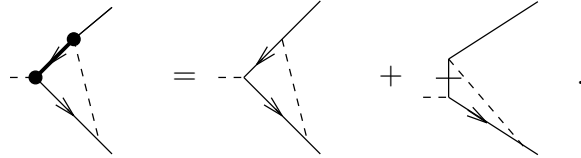
$$= -2\pi i \int d^2 k^\perp \int_{-q_2^+}^0 \frac{dk^+}{8k_1^+ k_2^+ k^+} \frac{\gamma^+(k_{2\text{on}} + m)}{H^- - H_2^-}. \quad (\text{III-15})$$

For the fourth and last term of Eq. (III-11) we have



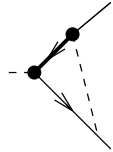
$$= 2\pi i \int d^2 k^\perp \int_0^{q_1^+} \frac{dk^+}{8k_1^+ k_2^+ k^+} \frac{(\not{k}_{1\text{on}} + m)\gamma^+}{H_1^- - H^-}. \quad (\text{III-16})$$

The possible  $1/k^+$  poles inside the integration area can be removed using the blinks.



$$= \dots + \dots. \quad (\text{III-17})$$

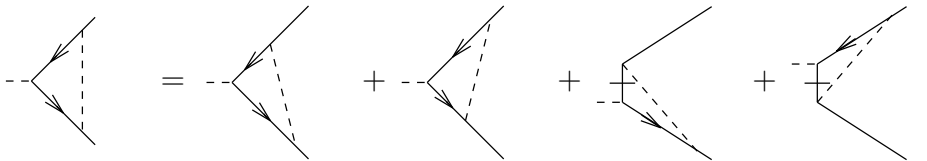
Using Eqs. (III-13) and (III-15) we get



$$= -2\pi i \int d^2 k^\perp \int_{-q_2^+}^0 \frac{dk^+}{8k_1^+ k_2^+ k^+} \frac{(\not{k}_{2\text{on}} - \not{p} + m)(\not{k}_{2\text{on}} + m)}{(H_1^- - H_2^-)(H^- - H_2^-)}. \quad (\text{III-18})$$

The other blink is constructed in the same way.

We have now succeeded in doing the  $k^-$ -integration and have rewritten the covariant expression for the one-boson exchange correction (III-2) in terms of LF time-ordered diagrams. The result is



$$= \dots + \dots + \dots + \dots. \quad (\text{III-19})$$

Diagrams with instantaneous parts are typical for LFD. There is another difference with equal-time PT. Of the six possible time-orderings of the triangle diagram two have survived, which give rise to two diagrams each, upon splitting the fermion propagators into instantaneous and propagating parts. This reduction of the number of LF time-ordered diagrams compared to ordinary time-ordered ones is well known in LFD, and explained in detail in Ref. [16].

All the calculations in this section were purely algebraic. The formulas for the LF time-ordered diagram we derived are the same as those given by NLCQ. The integrals that remain are logarithmically divergent in the transverse direction and must be regularized. This calculation will be done in Chapter IV in which we discuss transverse divergences.

### §3 Equivalence of the fermion self-energy

There are two longitudinally divergent diagrams in the Yukawa model. We first discuss the fermion self-energy. For our discussion the location of the poles is not relevant and therefore we ignore the  $i\epsilon$  term. For a fermion momentum  $q$  we have the following self-energy amplitude:

$$\text{Diagram: a fermion line with momentum } q \text{ entering from the left, a dashed loop with momentum } k \text{ and } q-k, \text{ and a fermion line exiting to the right.} = \int_{\text{Min}} \frac{d^4k}{(k^2 - m^2)((q-k)^2 - \mu^2)} (\not{k} + m). \quad (\text{III-20})$$

#### §3.1 Covariant calculation

We introduce a Feynman parameter  $x$  and change the integration variable to  $k'$  given by  $k = k' + xq$  in order to complete the square in the denominator. This gives

$$\text{Diagram: same as III-20} = \int_0^1 dx \int_{\text{Min}} \frac{d^4k'}{(k'^2 - (1-x)m^2 - x\mu^2 + x(1-x)q^2)^2} (\not{k}' + x\not{q} + m). \quad (\text{III-21})$$

The integral (III-21) is ill-defined. The appearance of  $\not{k}'$  in the numerator causes the integral to be divergent in the minus-direction and obstructs the Wick rotation. However, this term is odd and is removed in accordance with common practice [24]. Wick rotation gives then

$$\text{Diagram: same as III-20} = i \int_0^1 dx \int \frac{d^4k'}{(k'^2 + (1-x)m^2 + x\mu^2 - x(1-x)q^2)^2} (x\not{q} + m). \quad (\text{III-22})$$

The subscript Min is dropped denoting that the integration is over Euclidean space. From Eq. (III-22) we can immediately infer that the fermion self-energy has the covariant structure

$$\text{Diagram: same as III-20} = \not{q} F_1(q^2) + m F_2(q^2). \quad (\text{III-23})$$

#### §3.2 Residue calculation

To obtain the LF time-ordered diagram and the FIL corresponding to the fermion self-energy we perform the  $k^-$ -integration by doing the contour integration:

$$\text{Diagram: same as III-20} = \int \frac{d^2k^\perp dk^+ dk^-}{4k^+(q^+ - k^+)} \frac{k^- \gamma^+ + k^+ \gamma^- - k^\perp \gamma^\perp + m}{(k^- - H_1^-)(k^- - H_2^-)}, \quad (\text{III-24})$$



with the following poles:

$$H_1^- = \frac{k^\perp{}^2 + m^2}{2k^+}, \quad (\text{III-25})$$

$$H_2^- = q^- - \frac{(q^\perp - k^\perp)^2 + \mu^2}{2(q^+ - k^+)}. \quad (\text{III-26})$$

We rewrite Eq. (III-24) as

$$\begin{aligned} \text{---} \overbrace{\hspace{1.5cm}}^{\text{dashed}} \text{---} &= \int \frac{d^2k^\perp dk^+ dk^-}{4k^+(q^+ - k^+)} \frac{H_1^- \gamma^+ + k^+ \gamma^- - k^\perp \gamma^\perp + m}{(k^- - H_1^-)(k^- - H_2^-)} \\ &+ \int \frac{d^2k^\perp dk^+ dk^-}{4k^+(q^+ - k^+)} \frac{\gamma^+(k^- - H_1^-)}{(k^- - H_1^-)(k^- - H_2^-)}. \end{aligned} \quad (\text{III-27})$$

The first term of Eq. (III-27) is the part that gives a convergent  $k^-$ -integration. The second term contains the divergent part. This separation can also be written in terms of diagrams:

$$\text{---} \overbrace{\hspace{1.5cm}}^{\text{dashed}} \text{---} = \text{---} \overbrace{\hspace{1.5cm}}^{\text{dashed}} \text{---} + \text{---} \overbrace{\hspace{1.5cm}}^{\text{dashed}} \text{---}. \quad (\text{III-28})$$

The propagating diagram is

$$\text{---} \overbrace{\hspace{1.5cm}}^{\text{dashed}} \text{---} = 2\pi i \int d^2k^\perp \int_0^{q^+} \frac{dk^+}{4k^+(q^+ - k^+)} \frac{\frac{m^2 + k^\perp{}^2}{2k^+} \gamma^+ + k^+ \gamma^- - k^\perp \gamma^\perp + m}{H_2^- - H_1^-} \quad (\text{III-29})$$

It has the usual form for a LF time-ordered diagram. It is divergent because of the  $1/k^+$  singularity in the numerator. To shed more light on the structure of this formula we introduce internal variables  $x$  and  $k'^\perp$ :

$$x = \frac{k^+}{q^+}, \quad k'^\perp = k^\perp - xq^\perp. \quad (\text{III-30})$$

The denominator is now a complete square and we drop as usual the terms odd in  $k'^\perp$  in the numerator. Then we find

$$\text{---} \overbrace{\hspace{1.5cm}}^{\text{dashed}} \text{---} = \pi i \int d^2k'^\perp \int_0^1 dx \frac{\frac{m^2 + k'^\perp{}^2 - x^2 q^2}{2xq^+} \gamma^+ + x \not{q} + m}{k'^\perp{}^2 + (1-x)m^2 + x\mu^2 - x(1-x)q^2}. \quad (\text{III-31})$$

The FIL is

$$\overline{\text{---}\text{---}\text{---}} = \int \frac{d^2k^\perp dk^+ dk^-}{4k^+(q^+ - k^+)} \frac{\gamma^+}{k^- - H_2^-}. \quad (\text{III-32})$$

It contains the divergent part of the  $k^-$ -integration and a  $1/k^+$  singularity too. The single bar in Eq. (III-32) stands for an instantaneous part. The diagram is instantaneous because it does not depend on the external energy  $q^-$ . In order to demonstrate this we shift  $k^-$  by  $q^-$ . Then we see that the dependence on  $q^-$  disappears. However, this way of reasoning is dangerous since the integral is divergent. We make the integral well-defined by inserting a function  $\mathcal{R}$  containing a regulator  $\alpha$ :

$$\mathcal{R} = \left( \frac{\alpha(k^+)}{1 - i\delta q^+ k^-} + \frac{1 - \alpha(k^+)}{1 + i\delta q^+ k^-} \right). \quad (\text{III-33})$$

If we choose  $\alpha = 1$  for  $k^+ < 0$  and  $\alpha = 0$  for  $k^+ > q^+$ , the extra pole only contributes for  $0 < k^+ < q^+$ . In other words, then the spectrum condition is also satisfied for all lines in the FIL. This is convenient, but not necessary. Mustaki *et al.* [23] do not require the spectrum condition to be fulfilled for instantaneous particles. They have as integration boundaries for the FIL  $0 < k^+ < \infty$ .

We perform the  $k^-$ -integration and take the limit  $\delta \rightarrow 0$ . This gives

$$\overline{\text{---}\text{---}\text{---}} = 2\pi i \int d^2k^\perp \int_0^{q^+} dk^+ \frac{\gamma^+ \alpha(k^+)}{4k^+(q^+ - k^+)}. \quad (\text{III-34})$$

Using internal variables (III-30) we obtain

$$\overline{\text{---}\text{---}\text{---}} = \pi i \frac{\gamma^+}{2q^+} \int d^2k'^\perp \int_0^1 dx \frac{\alpha(x)}{x(1-x)}. \quad (\text{III-35})$$

### §3.3 Equivalence

The FIL is not a LF time-ordered diagram. We think it is a remnant of the problems encountered in quantization on the light-front. We require it to satisfy two conditions:

1. the FIL has to restore covariance and equivalence of the full series of LF time-ordered diagrams;
2. the FIL has to be a polynomial in  $q^-$ .

The first condition will also ensure that the FIL contains a  $1/k^+$  singularity that cancels a similar singularity in the propagating diagram. The second condition is that the FIL is truly instantaneous; i.e., it does not contain  $q^-$  in the denominator like a propagating diagram. To find the form of the FIL that satisfies these conditions we calculate

$$\text{---}\overbrace{\text{---}}^{\text{---}}\text{---} - \text{---}\overbrace{\text{---}}^{\text{---}}\text{---} \quad (III-36)$$

where we take for the covariant diagram Eq. (III-22). This is a strictly formal operation. The covariant diagram is a 4-dimensional integral, whereas the propagating diagram has only 2 dimensions (not counting the  $x$ -integration). We can calculate Eq. (III-36) without evaluation of the integrals. In Appendix A useful relations are derived between  $d$ - and  $(d-2)$ -dimensional integrals. Upon using them we obtain

$$\begin{aligned} \text{---}\overbrace{\text{---}}^{\text{---}}\text{---} - \text{---}\overbrace{\text{---}}^{\text{---}}\text{---} &= -\pi i \frac{\gamma^+}{2q^+} \int d^2 k'^{\perp} \int_0^1 dx \\ &\times \frac{m^2 + k'^{\perp 2} - x^2 q^2}{x(k'^{\perp 2} + (1-x)m^2 + x\mu^2 - x(1-x)q^2)}. \end{aligned} \quad (III-37)$$

This can be rewritten as

$$\begin{aligned} \text{---}\overbrace{\text{---}}^{\text{---}}\text{---} - \text{---}\overbrace{\text{---}}^{\text{---}}\text{---} &= -\pi i \frac{\gamma^+}{2q^+} \int d^2 k'^{\perp} \int_0^1 dx \\ &\times \left( \frac{1}{x} + \frac{m^2 - \mu^2 + (1-2x)q^2}{k'^{\perp 2} + (1-x)m^2 + x\mu^2 - x(1-x)q^2} \right). \end{aligned} \quad (III-38)$$

The dependence on  $q^2$  is limited to the second term. The integral over  $x$  of the latter can be done explicitly, whence one finds that the integral is independent of  $q^2$ . Therefore we can take  $q^2 = 0$  in Eq. (III-38).

$$\begin{aligned} \text{---}\overbrace{\text{---}}^{\text{---}}\text{---} - \text{---}\overbrace{\text{---}}^{\text{---}}\text{---} &= -\pi i \frac{\gamma^+}{2q^+} \int d^2 k'^{\perp} \int_0^1 dx \\ &\times \left( \frac{1}{x} + \frac{m^2 - \mu^2}{k'^{\perp 2} + (1-x)m^2 + x\mu^2} \right). \end{aligned} \quad (III-39)$$

This is a good moment to see if we can satisfy the two conditions we put forward in the beginning of this subsection.

The first condition is satisfied if the right-hand sides of Eqs. (III-39) and (III-35) are equal. We can verify that there is an infinite number of solutions for  $\alpha$  to make this happen. We are free to choose  $\alpha$  to be  $q^-$ -independent. This will make formula (III-35) also independent of  $q^-$ . Then the second condition is trivially satisfied.

$$\begin{array}{c}
 \text{---} \overbrace{\text{---}}^{\text{---}} \text{---} = \text{---} \overbrace{\text{---}}^{\text{---}} \text{---} + \text{---} \overbrace{\text{---}}^{\text{---}} \text{---} \\
 \frac{\delta m}{\times} \quad \frac{\delta h}{\times} = \frac{\delta m}{\times} + \frac{\delta h}{\times} + \frac{\delta i}{\times} + \frac{-\delta i}{\times} \\
 \text{---} \overbrace{\text{---}}^{\text{---}} \text{---} = \text{---} \overbrace{\text{---}}^{\text{---}} \text{---} + \text{---} \overbrace{\text{---}}^{\text{---}} \text{---}
 \end{array}$$

Figure III-4: Addition of the counterterms. The result is the minus-regularized fermion self-energy.

### §3.4 Conclusions

Our renormalization method is visualized in Fig. III-4.

There are two noncovariant counterterms ( $\delta i$ ). One of them occurs in the LF time-ordered part; the other one is associated with a self-induced inertia. Minus regularization guarantees that they cancel provided the regulator  $\alpha$  is chosen appropriately. The other counterterms  $\delta m$  and  $\delta h$  are covariant. After the (infinite) counterterms have been added the renormalized amplitude (denoted by the superscript  $r$ ) remains. An illustration of the full procedure of minus regularization is given in the next section.

We take another look at Fig. III-4. The first line contains three ill-defined objects. The covariant amplitude (III-20) has a Minkowskian measure and contains odd terms. Divergent odd terms are dropped as part of the regularization procedure. To calculate the LF time-ordered diagram (III-29) we also dropped surface terms. Can these assumptions be justified? Would another set of assumptions give different physical amplitudes? We conjecture that any set of assumptions corresponds to a certain class of choices for  $\alpha$ . The  $\alpha$ -dependence is only present in the FILs. In the process of minus regularization the  $\alpha$ -dependence is lost, as we see for the fermion self-energy in Fig. III-4. Therefore the physical observables do not depend on the assumptions we started out with.

Finally we give the result for the fermion self-energy.

$$\text{---} \overbrace{\text{---}}^{\text{---}} \text{---} = -\pi^2 i \int_0^1 dx (x \not{q} + m) \log \left( 1 - \frac{x(1-x)q^2}{(1-x)m^2 + x\mu^2} \right). \quad (\text{III-40})$$

This integral can be done analytically, but the result is a rather long formula, which we give in Appendix B. Here we display the result in pictorial form. Fig. III-5 shows  $F_1$  and  $F_2$  for values of the fermion momentum squared in the

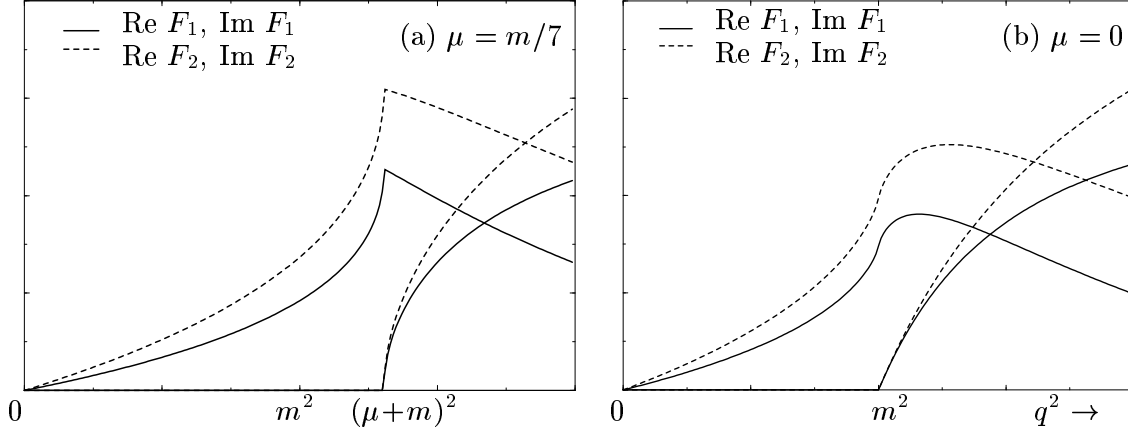


Figure III-5: The renormalized fermion self-energy. The left-hand panel (a) shows the case  $\mu = m/7$ ; the right-hand panel (b) is for  $\mu = 0$ .

range  $q^2 \in [0, 2m^2]$  for the case of a massless boson and the case where  $\mu = m/7$ , corresponding to the self-energy correction for a nucleon due to a scalar pion. The case  $\mu = 0$  is included because it was calculated before by Ligterink and Bakker [19].

The threshold behavior in the two cases is clearly seen in this figure. Above threshold,  $q^2 > (m + \mu)^2$ , the self-energy becomes complex.

We have verified that our result is in agreement with the result given by dimensional regularization and the result given by Bjorken and Drell [25], using Pauli-Villars regularization.

For the following reasons our analysis differs essentially from the analysis of Mustaki *et al.* [23]. First of all, we make an explicit distinction between LF time-ordered diagrams and FILs. Second, we make the integration over the longitudinal coordinates well-defined by introducing a regulator  $\alpha(k^+)$ . Mustaki *et al.* make the  $k^+$ -integration well-defined by using cutoffs. The form of the cutoffs depends on the regularization scheme of the divergences in the transverse directions. In our calculation the form of  $\alpha(k^+)$  is determined by requiring equivalence to the covariant calculation. In our opinion, this is the most important constraint on the FIL. We do not think that the cutoffs can always be determined from an analysis of the transverse divergences. For example, in two dimensions ( $D = 1 + 1$ ) there are no transverse divergences, but longitudinal divergences are still present and  $\alpha(k^+)$  has to ensure that covariance is maintained. Moreover, in  $D = 1 + 1$  the covariant calculation of the fermion self-energy gives a finite result. Our choice of  $\alpha(k^+)$ , independent of  $k^\perp$ , ensures also in this case that the LF time-ordered calculation reproduces the covariant result. The same is true for



### §4.1 Minus regularization

We will now apply the minus regularization scheme to the LF time-ordered boson self-energy. For a self-energy diagram the following ten steps can be used to find the regularized diagram. Some steps are explained in more detail for the boson self-energy.

1. Write the denominator in LF coordinates.
2. Complete the squares in the denominator by introducing internal variables ( $k'^{\perp}$  and  $x$ ).
3. Write the numerator in terms of internal and external LF coordinates.
4. Remove terms odd in  $k'^{\perp}$  in the numerator.

These steps were also taken in our discussion of the fermion self energy. Next we diverge.

5. Subtraction of the lowest order in the Taylor expansion is equivalent to inserting a multiplier  $X$ . Construct the multiplier.
6. Compensate for the subtraction by adding counterterms. Verify that they are infinite. If they are not, the corresponding divergence was only apparent and we should not subtract it. We do not allow for finite renormalizations.

For the boson self-energy all terms have the same denominator. For them we can write the expansion

$$\frac{1}{k'^{\perp 2} + m^2 - x(1-x)q^2} = \frac{1}{k'^{\perp 2} + m^2} \sum_{j=0}^{\infty} X^j, \quad (\text{III-45})$$

where the multiplier  $X$  has the form

$$X = \frac{x(1-x)q^2}{k'^{\perp 2} + m^2}. \quad (\text{III-46})$$

7. Identify, term by term, the degree of divergence and insert the corresponding multiplier. To compensate for this, add a polynomial of the appropriate degree with infinite coefficients.

Steps 1-7 lead to the following result for the boson self-energy:

$$\begin{array}{c} \text{---} \bigcirc \text{---} \\ | \\ \text{---} \end{array} = \pi i \int d^2 k'^{\perp} \int_0^1 dx X \text{Tr} \left[ \left( \frac{X k'^{\perp 2} + x^2 q^{\perp 2} + m^2}{2xq^+} \gamma^+ + x(q^+ \gamma^- - q^{\perp} \gamma^{\perp}) + m \right) \right]$$

$$\left( \frac{Xk'^{\perp 2} + (x-1)^2 q^{\perp 2} + m^2}{2(x-1)q^+} \gamma^+ + (x-1)(q^+ \gamma^- - q^\perp \gamma^\perp) + m \right) + X(k'^{\perp} \gamma^\perp)^2 \left[ (k'^{\perp 2} + m^2 - x(1-x)q^2)^{-1} + A + Bq^2. \right. \quad (\text{III-47})$$

Longitudinal divergences appear as  $1/x$  singularities. Transverse divergences appear as ultraviolet  $k'^{\perp}$  divergences. Since every term in the boson self-energy is at least logarithmically divergent, there is an overall factor  $X$ . Some of the terms are quadratically divergent in  $k'^{\perp}$  and have an extra factor  $X$ . We use the fact that terms containing the factor  $\gamma^+ \gamma^+$  vanish. We are not interested in the exact form of the counterterms  $A$  and  $B$ . We can verify that they are infinite. They are included to allow for comparison with other regularization schemes.

8. Rewrite the numerator in terms of objects having either covariant or  $\gamma^+/q^+$  structure.

For our integral we use the following relation

$$\frac{x^2 q^{\perp 2} + m^2}{2xq^+} \gamma^+ + x(q^+ \gamma^- - q^\perp \gamma^\perp) = \frac{x^2 q^2 + m^2}{2x} \frac{\gamma^+}{q^+} + x \not{q}. \quad (\text{III-48})$$

9. Perform the trace, if present.

10. Do the  $x$  and  $k'^{\perp}$  integrations.

Application of the last two steps gives

$$-\text{---} \left( \text{circle with vertical line} \right) \text{---} = A + Bq^2 - 2\pi^2 i \left( 3q^2 - 8m^2 + 2(4m^2 - q^2) \sqrt{\frac{4m^2 - q^2}{q^2}} \arctan \sqrt{\frac{q^2}{4m^2 - q^2}} \right). \quad (\text{III-49})$$

## §4.2 Equivalence

We will now compare the result of the minus regularization scheme applied to the LF time-ordered boson self-energy with dimensional regularization applied to the covariant diagram. Using the standard rules of dimensional regularization given by Collins [24] we obtain

$$-\text{---} \left( \text{circle with arrows} \right) \text{---} = A' + B'q^2 - 4\pi^2 i (4m^2 - q^2) \sqrt{\frac{4m^2 - q^2}{q^2}} \arctan \sqrt{\frac{q^2}{4m^2 - q^2}} \quad (\text{III-50})$$

The constants  $A'$  and  $B'$  contain  $1/\varepsilon$ , where  $\varepsilon$  is the dimensional regulator. In the limit of  $\varepsilon \rightarrow 0$  they diverge. Of course,  $A'$  and  $B'$  can not be related to the



infinite constants generated by minus regularization. However, this is not necessary. Both schemes are equivalent if the same physical amplitudes are generated. To calculate them we have to construct the counterterms or, equivalently, fix the amplitude and its first derivative at the renormalization point. For the unrenormalized amplitudes (III-49) and (III-50) the coefficients  $A$  or  $A'$  of the constant term are used to determine the physical mass  $\mu_{\text{ph}}$  of the boson. The coefficients  $B$  or  $B'$  determine the fermion wave function renormalization. Only the  $q^4$  and higher order terms can be used to make predictions. These coefficients must be the same for the two methods. We see that Eqs. (III-49) and (III-50) only differ in the first two coefficients of the polynomial in  $q^2$ . Therefore the two methods generate the same physical amplitudes.

## §5 Conclusions

We discussed in this chapter the problem of covariance, which includes the problem of nonmanifest rotational invariance, in LFD.

For diagrams which are both longitudinally and transversely convergent one can give a rigorous demonstration of equivalence, without discussing renormalization explicitly. It is given by Ligterink and Bakker [16].

For longitudinally divergent diagrams such a proof is not possible because the integration over LF energy is ill-defined. Still, LF time-ordered diagrams can be constructed applying the rules of NLCQ. However, FILs have to be included to make the full series add up to the covariant diagram. These FILs contain the ambiguity related to the ill-defined integration, as can be shown by our analysis involving the regulator  $\alpha$ .

We conjecture that the FILs are remnants of the difficulty of quantizing on the light-front. Just like NLCQ, we are not able to provide general rules to construct them. However, we can identify the conditions for their occurrence. We show that it is not necessary to find an explicit expression for the FILs. Upon minus regularization they vanish. Therefore the  $\alpha$ -dependence drops too. The remaining series of regularized LF time-ordered diagrams is again covariant.

The main difficulty we encountered was to show that the FILs are instantaneous indeed. This can be shown by proving that the regulator  $\alpha$  does not depend on the LF energy, as we did for the fermion self-energy. Another way is to show that the regularized covariant amplitude equals the corresponding series of minus-regularized LF time-ordered diagrams. We used this technique for the boson self-energy.

This concludes our proof of equivalence of renormalized covariant and LF perturbation theory for longitudinally divergent diagrams in the Yukawa model. Three diagrams with transverse divergences remain. They require a more elaborate analysis of minus regularization and numerical implementation of the method. This subject is treated in the next chapter.

# IV

## Transverse divergences in the Yukawa model

Light-front quantization has found many applications since it was conceived. Still, some problems of a fundamental nature remained. One that we are particularly interested in is the question of whether full covariance can be maintained in the Hamiltonian formulation, which is of course not manifestly covariant. A partial answer can be obtained in perturbation theory. Then the problem can be reformulated as follows: can one prove that LF perturbation theory produces the same values of the  $S$ -matrix elements as covariant perturbation theory? If the answer to this question is affirmative, then we use the word equivalent to describe the situation.

This chapter is concerned with one aspect of this problem, viz the treatment of transverse divergences in a simple model: the Yukawa model with spin-1/2 fermions, spin-0 bosons and a scalar coupling.

### §1 Formulation of the problem

In the previous chapters, we used the method of Kogut and Soper [13] to define LF perturbation theory. This method defines LF time-ordered ( $x^+$ -ordered) amplitudes by integration of the integrand of a covariant diagram, say

$$F(q) = \int d^4k I(q; k), \quad (\text{IV-1})$$

over the LF energy variable  $k^-$ . In this chapter,  $q$  always denotes the external momenta and  $k$  the loop momentum. We can also write Eq. (IV-1) using LF coordinates:

$$F(q) = \int dk^+ d^2k^\perp \int dk^- I(q^-, q^+, q^\perp; k^-, k^+, k^\perp). \quad (\text{IV-2})$$

Next, one expresses the integral over  $k^-$ , using Cauchy's formula, as a sum of residues. One arrives in this way at an expression that can be interpreted, possibly after recombination of the terms in this sum, as the splitting of the covariant amplitude  $F(q)$  into a sum of noncovariant but LF time-ordered amplitudes.

This procedure, sometimes called naive light-cone quantization, has been in principle known since the early work of Kogut and Soper [13]. For convergent diagrams, it is nicely pictured in Fig. IV-1.

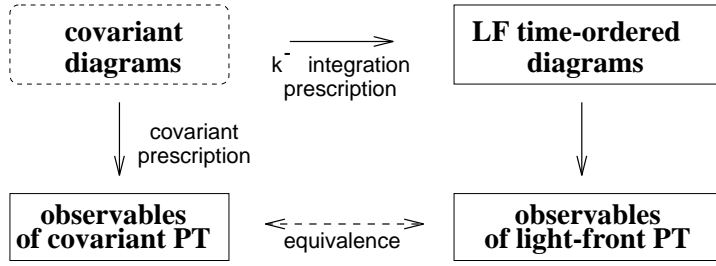


Figure IV-1: The “ideal” case: Outline of our proof of equivalence of LF and covariant perturbation theory (PT) for convergent diagrams. The dashed box indicates an ill-defined object.

The covariant diagram in Fig. IV-1 is an ill-defined object and needs some prescription to give it a definite meaning. For example, the measure of the Minkowski integration is not positive definite. The covariant prescription involves introduction of Feynman parameters to complete the squares in the denominator, the removal of terms odd in the loop momentum  $k$  and the Wick rotation to obtain a Euclidian integral.

It has been the work of Ligterink and Bakker [16] to prove in detail that the rules for constructing LF time-ordered diagrams, explained in many articles [13, 26], are correct upon using the  $k^-$ -integration prescription. They were the first authors to give a systematic derivation of all the different time-ordered diagrams corresponding to a given covariant amplitude, for any number of particles involved. If the  $k^-$ -integral is convergent and the corresponding covariant diagram is also superficially convergent, then what remains can be written in terms of well-defined, convergent Euclidian integrals.

When the  $k^-$ -integration is divergent, the prescription must be altered. Naive light-front quantization fails in this case and one must first find a way to regulate the  $k^-$ -integrals. We proposed in Chapter III a regularization that maintains covariance. There we showed that the longitudinal divergences give rise to so-called forced instantaneous loops (FILs) and we showed how to deal with them such that covariance is maintained. This method was also applied to the Yukawa model containing spin-1/2 and spin-0 particles. We were able to regularize the  $k^-$ -integrals for the diagrams with one loop. However, in order to show full equivalence to the covariant calculation one needs to compute the full integral including the integrations over  $k^+$  and  $k^\perp$ .

### §1.1 Ultraviolet and transverse divergences

Even after the usual procedure has been followed, the covariant integral can still be ultraviolet divergent. Ligterink and Bakker did not only discuss diagrams that are superficially convergent, but also what to do in cases where the covariant diagram is divergent. Their method of regularizing divergent diagrams, minus regularization [19], is also used in this chapter. A scheme for the equivalence of

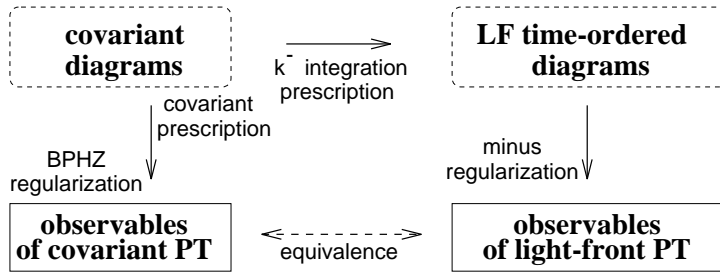


Figure IV-2: Outline of our proof of equivalence for diagrams with ultraviolet divergences. Dashed boxes indicate ambiguously defined objects.

ultraviolet divergent diagrams is given in Fig. IV-2.

Several techniques are available to remove the ultraviolet divergences, not involving the  $k^-$ -integration. They remain in the LF time-ordered diagrams as divergences of the integrals over the transverse momenta. Therefore these diagrams are also ill-defined, as indicated by the dashed box in Fig. IV-2. A problem is that many of the techniques which are used to regularize covariant diagrams have limited use for LF time-ordered diagrams. For example, one cannot use dimensional regularization for the longitudinal divergences. Still, it is common to apply it to the transverse divergences. The strength of the regularization scheme we use, minus regularization, is that it does not discriminate between transverse and longitudinal divergences. Minus regularization is based on the Bogoliubov-Parasiuk-Hepp-Zimmerman method of regularization [27, 28, 29, 30, 31]. In their paper, Ligterink and Bakker applied minus regularization to three self-energy diagrams. Our contribution is to extend their method to more complicated diagrams and prove that there is a one-to-one relation between minus and BPHZ regularization, such that the physical observables found using LF perturbation theory exactly match those found in covariant perturbation theory.

In the Yukawa model there are five covariant diagrams with ultraviolet divergences. The boson and the fermion self-energy were treated in Chapter III in which longitudinal divergences were discussed. Minus regularization was applied and simultaneously removed the longitudinal and the transverse divergences. Equivalence was established.

In two cases we were not able to either find an answer in the literature or produce ourselves full analytic results for the integrals involved; so we had to resort to numerical integration. In this chapter we discuss these two diagrams: the one-boson exchange correction to the boson-fermion-fermion vertex and the fermion loop with three external boson lines. The first one was considered by Burkardt and Langnau [10], who stated that naive light-cone quantization leads to a violation of rotational invariance of the corresponding  $S$ -matrix elements and found that invariant results can be obtained using noncovariant counterterms. Here we show that no violation of rotational invariance occurs if our method of regulariza-

tion is applied. Furthermore, our results for the LF time-ordered diagrams sum up to the covariant amplitude, calculated using conventional methods.

## §1.2 Light-front structure functions

The two triangle diagrams, presented before in Table II-1, can be written in the form of a sum of tensors in the external momenta, multiplied by scalar functions, which we call (covariant) structure functions. After splitting a covariant diagram in LF time-ordered ones, these can be written again in terms of tensors multiplied by functions of the external momenta. The latter are called LF structure functions. They are not invariant as they are not defined by four-dimensional invariant integrals, but rather by three-dimensional integrals. The different structure functions have different divergences and they must be treated according to their types of divergence, which we enumerate.

**Type 1: LF structure functions without transverse divergences.** Neither the covariant nor the LF formulation contains any divergences. Integration over  $k^-$  suffices to prove equivalence. Minus regularization is not allowed.

**Type 2: LF structure functions with cancelling transverse divergences.** The individual LF time-ordered diagrams contain divergences not present in the covariant amplitude. Application of minus regularization to the time-ordered diagrams is not allowed. We show that the divergences cancel if all the time-ordered diagrams are added, and that their sum equals the corresponding covariant amplitude.

**Type 3: LF structure functions with overall transverse divergences.** Divergences appear in the covariant amplitude as well as in the LF time-ordered diagrams. We apply BPHZ regularization to the covariant amplitude and minus regularization to the time-ordered diagrams.

For the first two cases one can prove equivalence using analytic methods alone. This proof is found in Ref. [16] and in Chapter III. For the structure functions with overall transverse divergences we have to use numerical techniques. We show that for the decay of a boson at rest, for both triangle diagrams, one obtains a rotational invariant amplitude, identical to the covariant calculation using BPHZ regularization. The fifth diagram with transverse divergences, the fermion box, will not be discussed.

The setup for this chapter is as follows. In §2 we introduce minus regularization. In §3 and §4 we discuss the equivalence of covariant and LF perturbation theory for the fermion triangle and the one-boson exchange correction. In both cases we start with the covariant calculation and do the BPHZ regularization

if necessary. Then we calculate the LF time-ordered diagrams and apply the method mentioned above. In both cases we conclude by giving a numerical example of rotational invariance.

## §2 Minus regularization

Minus regularization is inspired by the BPHZ method of regularization, which gives finite and covariant results. By construction, we ensure that minus regularization does the same. First we sketch the method in the case of one-loop diagrams with one independent external momentum (self-energies), and next when two independent external momenta (triangle diagrams) are present. We conclude by generalizing this to a one-loop diagram with  $n$  external momenta. For convenience, we shall assume in the latter case that only logarithmic and linear divergences are present, such that only the first term of the Taylor expansion around the renormalization point needs to be subtracted.

Wherever we use the word “amplitude” in this chapter, we refer to an invariant function of the external momenta. It is understood that the integrals defining the invariant functions are formally written down in terms of four-dimensional integrals, which are split into time-ordered pieces by integration over  $k^-$ .

### §2.1 One external momentum

First we discuss the simple case of one external momentum, which can be applied for self-energy diagrams.

#### BPHZ regularization

We start with the BPHZ regularization method, which can be applied to covariant diagrams. The amplitude has the following form

$$F(q^2) = \int d^4k I_{\text{cov}}(q^2; k) = F(0) + q^2 F'(0) + \dots \quad (\text{IV-3})$$

where  $I_{\text{cov}}(q^2; k)$  is the covariant integrand generated by applying standard Feynman rules. BPHZ regularization renders the amplitude finite by subtracting the infinite parts. We choose the point  $q^2 = 0$  as the renormalization point, around which we expand the amplitude in a Taylor series. The higher orders in the expansion (IV-3) are denoted by the ellipsis. The regularized amplitude is then

$$F^{\text{R}}(q^2) = F(q^2) - F(0). \quad (\text{IV-4})$$

However, this is a purely formal operation, since we are subtracting two infinite quantities. It is better to write:

$$F^{\text{R}}(q^2) = \int d^4k \left( I_{\text{cov}}(q^2; k) - I_{\text{cov}}(0; k) \right) = \int_0^{q^2} dq'^2 \int d^4k \frac{\partial}{\partial q'^2} I_{\text{cov}}(q'^2; k) \quad (\text{IV-5})$$

This guarantees that the amplitude becomes finite.

### Minus regularization

Typical for minus regularization is that one writes the amplitude, as well as the renormalization point, in LF coordinates. The covariant choice  $q^2 = 0$  corresponds to  $q^- = q^{\perp 2}/(2q^+)$ . A time-ordered amplitude corresponding to the covariant form (IV-3) can be written in LF coordinates as follows

$$\begin{aligned} F(q^-, q^+, q^\perp) &= \int d^3k I_{\text{lfto}}(q^-, q^+, q^\perp; k) \\ &= F\left(\frac{q^{\perp 2}}{2q^+}, q^+, q^\perp\right) + 2q^+(q^- - \frac{q^{\perp 2}}{2q^+})F'\left(\frac{q^{\perp 2}}{2q^+}, q^+, q^\perp\right) + \dots \end{aligned} \quad (\text{IV-6})$$

where  $I_{\text{lfto}}$  is the integrand of the LF time-ordered diagram, which was generated by integrating the covariant integrand  $I_{\text{cov}}$  over  $k^-$  as is explained in Ref. [16]. The prime denotes differentiation with respect to  $q^-$ . Similar to Eq. (IV-5) we can write the regularized amplitude as

$$F^{\text{MR}}(q^-, q^+, q^\perp) = \int_{\frac{q^{\perp 2}}{2q^+}}^{q^-} dq'^- \int d^3k \frac{\partial}{\partial q'^-} I_{\text{lfto}}(q'^-, q^+, q^\perp; k). \quad (\text{IV-7})$$

So far we have described the minus regularization method introduced by Ligterink and Bakker [19].

### §2.2 Two external momenta

In Ref. [19] three self-energy diagrams were discussed. For the triangle diagram the minus regularization technique needs to be extended. We suggest the name  $\text{MR}^+$ . We will tune the technique by comparing it to BHPZ regularization.

### BPHZ regularization

The amplitude has the following covariant form

$$\begin{aligned} F(q_1^2, q_2^2, q_1 \cdot q_2) &= \int d^4k I_{\text{cov}}(q_1^2, q_2^2, q_1 \cdot q_2; k) \\ &= F(\tilde{0}) + q_1^2 F'_1(\tilde{0}) + q_2^2 F'_2(\tilde{0}) + q_1 \cdot q_2 F'_3(\tilde{0}) + \dots \end{aligned} \quad (\text{IV-8})$$

where  $\tilde{0}$  is the renormalization point  $q_1^2 = q_2^2 = q_1 \cdot q_2 = 0$  and  $F'_i$  is the derivative of  $F$  with respect to the  $i$ th argument.

$$F^{\text{R}}(q_1^2, q_2^2, q_1 \cdot q_2) = F(q_1^2, q_2^2, q_1 \cdot q_2) - F(\tilde{0}). \quad (\text{IV-9})$$

Again, this is a purely formal operation, since we are subtracting two infinite quantities. It is better to write

$$F^{\text{R}}(q_1^2, q_2^2, q_1 \cdot q_2) = \int d^4k \left( I_{\text{cov}}(q_1^2, q_2^2, q_1 \cdot q_2; k) - I_{\text{cov}}(\tilde{0}; k) \right). \quad (\text{IV-10})$$

We cannot, as in the previous section, differentiate with respect to all external momenta. We would then subtract finite parts from the Taylor series, containing physical information. This can be circumvented by introducing a dummy variable  $\lambda$ , which parametrizes a straight line in the space of the invariants between the actual values  $q_1^2, q_2^2, q_1 \cdot q_2$  and the renormalization point:

$$F^{\text{R}}(q_1^2, q_2^2, q_1 \cdot q_2) = \int_0^1 d\lambda \int d^4k \frac{\partial}{\partial \lambda} I_{\text{cov}}(\lambda q_1^2, \lambda q_2^2, \lambda q_1 \cdot q_2; k). \quad (\text{IV-11})$$

We have verified that the  $\lambda$ -method gives the correct result for the case where one independent external momentum occurs.

### Minus regularization

Again, we write the amplitude in the LF time-ordered case as a three-dimensional integral:

$$F(q_i^-, q_i^+, q_i^\perp) = \int d^3k I_{\text{fto}}(q_i^-, q_i^+, q_i^\perp; k). \quad (\text{IV-12})$$

The regularized amplitude is

$$F^{\text{R}}(q_i^-, q_i^+, q_i^\perp) = F(q_i^-, q_i^+, q_i^\perp) - F(r_i^-, r_i^+, r_i^\perp), \quad (\text{IV-13})$$

where the four-vector  $r$  defines the renormalization surface. It is a hypersurface determined by the following conditions:

$$\begin{aligned} r_1^2 &= 2r_1^- r_1^+ - r_1^\perp{}^2 = 0, \\ r_2^2 &= 2r_2^- r_2^+ - r_2^\perp{}^2 = 0, \\ r_1 \cdot r_2 &= r_1^- r_2^+ + r_1^+ r_2^- - r_1^\perp \cdot r_2^\perp = 0. \end{aligned} \quad (\text{IV-14})$$

This set of equations is equivalent to

$$r_1^2 = 0, \quad r_2 = \chi r_1. \quad (\text{IV-15})$$

The  $r_i^+$  enter in the integration boundaries; therefore we would like them to remain unaffected by regularization ( $r_i^+ = q_i^+$ ). This implies that  $\chi$  can be found from

$$\chi = \frac{q_2^+}{q_1^+}. \quad (\text{IV-16})$$

The only freedom that remains is the choice for  $r_1^\perp$ . Two choices come easily to mind:  $r_1^\perp = 0$  (method MR0) and  $r_1^\perp = q_1^\perp$  (method MR1).

$$(\text{MR0}) \quad r_1^\perp = 0^\perp \Rightarrow r_2^\perp = 0^\perp, \quad (\text{IV-17})$$

$$(\text{MR1}) \quad r_1^\perp = q_1^\perp \Rightarrow r_2^\perp = \chi q_1^\perp. \quad (\text{IV-18})$$

The final results are given in Table IV-1. The LF coordinates of the renormalization point are used in the following way to find the regularized LF amplitude:

$$F^{\text{MR}}(q_i^-, q_i^+, q_i^\perp) = \int_0^1 d\lambda \int d^3k \frac{\partial}{\partial \lambda} I_{\text{fto}}(\lambda(q_i^- - r_i^-) + r_i^-, q_i^+, \lambda(q_i^\perp - r_i^\perp) + r_i^\perp; k). \quad (\text{IV-19})$$

In this formula we recognize our choice  $r_i^+ = q_i^+$ .



	MR0	MR1
$(r_1^-, r_1^+, r_1^\perp)$	$(0, q_1^+, 0^\perp)$	$(q_1^{\perp 2}/(2q_1^+), q_1^+, q_1^\perp)$
$(r_2^-, r_2^+, r_2^\perp)$	$\chi (0, q_1^+, 0^\perp)$	$\chi (q_1^{\perp 2}/(2q_1^+), q_1^+, q_1^\perp)$

Table IV-1: The LF parametrization of the renormalization point  $r^\mu$  for two equivalent choices of minus regularization, MR0 and MR1.

### §2.3 Several external momenta

The method just described can be generalized to the case of a loop with an arbitrary number of external lines. The procedure is almost the same as for two external momenta. The renormalization surface is given by

$$r_i^2 = 2r_i^- r_i^+ - r_i^{\perp 2} = 0, \quad (\text{IV-20})$$

$$r_i \cdot r_j = r_i^- r_j^+ + r_i^+ r_j^- - r_i^\perp \cdot r_j^\perp = 0 \quad (i \neq j). \quad (\text{IV-21})$$

These equations are equivalent to

$$r_1^2 = 0, \quad r_i = \chi_i r_1. \quad (\text{IV-22})$$

Again, we make the choice to leave the plus-components of the momenta unaffected by regularization:  $r_i^+ = q_i^+$ . This implies that the  $\chi_i$  are fractional longitudinal LF momenta.

$$\chi_i = \frac{q_i^+}{q_1^+}. \quad (\text{IV-23})$$

Two choices for  $r_1^\perp$  are listed below. This then determines all other  $r_i^\perp$ .

$$(\text{MR0}) \quad r_1^\perp = 0^\perp \Rightarrow r_i^\perp = 0^\perp, \quad (\text{IV-24})$$

$$(\text{MR1}) \quad r_1^\perp = q_1^\perp \Rightarrow r_i^\perp = \chi_i q_1^\perp. \quad (\text{IV-25})$$

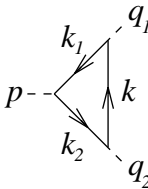
### §2.4 Summary

The way we setup minus regularization does not rely on the structure of the covariant or the time-ordered diagrams, but works on the level of the external momenta only. If an amplitude has a covariant structure before regularization, minus regularization guarantees that it remains covariant. In our implementation of BPHZ regularization, the renormalization point corresponds to all invariants connected to the external momenta being equal to zero. These conditions allow minus regularization to take on a number of forms. Of these, we shall apply MR0 and MR1. The main difference between them is that MR0 does not choose one of the momenta as a preferred direction, and therefore it explicitly maintains all symmetries in the external momenta. Furthermore, MR0 gives rise to shorter formulas for the regularized integrands.

In the next two sections both methods are being applied to the parts of two LF time-ordered triangle diagrams in the Yukawa model containing transverse divergences, viz the fermion triangle and the one-boson exchange correction.

### §3 Equivalence for the fermion triangle

In the Yukawa model there is an effective three-boson interaction, because to a fermion loop with a scalar coupling Furry's theorem does not apply. The leading order contribution to this process is the fermion triangle. A scalar boson of mass  $\mu$  and momentum  $p$  comes in and decays into two bosons of momentum  $q_1$  and  $q_2$  respectively. The fermions in the triangle have mass  $m$ . The covariant expression for the amplitude is



$$p \text{---} \begin{array}{c} \nearrow k_1 \\ \searrow k_2 \end{array} \begin{array}{c} \nearrow k \\ \searrow k \end{array} \begin{array}{c} \nearrow q_1 \\ \searrow q_2 \end{array} = \int_{\text{Min}} d^4k \frac{\text{Tr} [(k_1 + m)(k_2 + m)(k + m)]}{(k_1^2 - m^2)(k_2^2 - m^2)(k^2 - m^2)}. \quad (\text{IV-26})$$

The usual imaginary parts of the Feynman propagators are not written explicitly. We have omitted numerical factors and have set the coupling constant to unity. The momenta  $k_1$  and  $k_2$  indicated in the diagram are given by

$$k_1 = k - q_1, \quad k_2 = k + q_2. \quad (\text{IV-27})$$

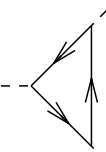
Of course, by momentum conservation we have

$$p = q_1 + q_2. \quad (\text{IV-28})$$

We evaluate the integral (IV-26) first in the usual covariant way, and subsequently carry out  $k^-$ -integration to produce the LF time-ordered diagrams. Note that integral (IV-26) is an ill-defined object. In both methods mentioned we have to define what we mean by this integral.

#### §3.1 Covariant calculation

The following method is usually applied to calculate the fermion triangle in a covariant way. First, one introduces Feynman parameters  $x_1$  and  $x_2$ , and then one shifts the loop variable  $k$  to complete the squares in the denominator. The result is



$$= 8 \int_0^1 dx_1 \int_0^{1-x_1} dx_2 \int_{\text{Min}} d^4k \frac{m^3 + m(3k^2 + \mathcal{P}^2) + \text{terms odd in } k}{(k^2 - m^2 + \mathcal{Q}^2)^3}, \quad (\text{IV-29})$$

with

$$\mathcal{Q}^2 = x_1(1-x_1) q_1^2 + x_2(1-x_2) q_2^2 + 2x_1x_2 q_1 \cdot q_2, \quad (\text{IV-30})$$

$$\mathcal{P}^2 = x_1(3x_1-2)q_1^2 + x_2(3x_2-2)q_2^2 + (2(x_1+x_2) - 6x_1x_2 - 1) q_1 \cdot q_2. \quad (\text{IV-31})$$

As a last step, we remove the terms odd in  $k$ .

### §3.2 BPHZ regularization

The regularized fermion triangle can be found by applying the BPHZ regularization scheme (IV-11) to the covariant formula (IV-29). The integral is now finite; so we can do the Wick rotation and perform the  $k$  integrations. The result is

$$\begin{array}{c} \text{R} \\ \diagup \quad \diagdown \\ \text{---} \quad \text{---} \\ \diagdown \quad \diagup \end{array} = -4\pi^2 i \int_0^1 dx_1 \int_0^{1-x_1} dx_2 \int_0^1 d\lambda \frac{m(m^2(5\mathcal{Q}^2 - \mathcal{P}^2) - 6\lambda\mathcal{Q}^4)}{(m^2 - \lambda\mathcal{Q}^2)^2}. \quad (\text{IV-32})$$

The superscript R indicates an integral regularized according to the BPHZ method.

### §3.3 Light-front calculation

Using the method given in Ref. [16] we proceed as follows. The  $k^-$  dependence of a spin projection in the numerator is removed by separating it into an on-shell spin projection and an instantaneous part:

$$\not{k}_i + m = (\not{k}_{i \text{ on}} + m) + (k^- - k_{i \text{ on}}^-)\gamma^+, \quad (\text{IV-33})$$

where the vector  $k_{i \text{ on}}^\mu$  is given by

$$\left(k_i^-, k_i^+, k_i^\perp\right)_{\text{on}} = \left(\frac{k_i^{\perp 2} + m^2}{2k_i^+}, k_i^+, k_i^\perp\right). \quad (\text{IV-34})$$

Factors like  $(k^- - k_{i \text{ on}}^-)$  can be divided out against propagators and this cancellation gives rise to instantaneous fermions. The integration over  $k^-$  is performed by contour integration. The poles of the propagators are given by

$$H^- = \frac{k^\perp{}^2 + m^2}{2k^+}, \quad (\text{IV-35})$$

$$H_1^- = q_1^- - \frac{k_1^{\perp 2} + m^2}{2k_1^+}, \quad (\text{IV-36})$$

$$H_2^- = -q_2^- + \frac{k_2^{\perp 2} + m^2}{2k_2^+}. \quad (\text{IV-37})$$

This integration gives rise to the different time-ordered diagrams, as explained in more detail in Chapter I. The result is

$$\begin{aligned} \text{Triangle Diagram} &= \text{Diagram 1} + \text{Diagram 2} + \text{Diagram 3} \\ &+ \text{Diagram 4} + \text{Diagram 5} + \text{Diagram 6}. \end{aligned} \quad (\text{IV-38})$$

The diagrams on the right-hand side are LF time-ordered diagrams. Time goes from left to right. The pictures can be recognized as time-ordered diagrams because of the time-ordering of the vertices and the occurrence of instantaneous fermions, indicated by a horizontal tag. Explicitly;

$$\text{Triangle Diagram with Tag} = 2\pi i \int d^2 k^\perp \int_0^{q_1^+} \frac{dk^+}{8k_1^+ k_2^+ k^+} \frac{\text{Tr}[(\not{k}_{1\text{on}} + m)(\not{k}_{2\text{on}} + m)(\not{k}_{\text{on}} + m)]}{(H_1^- - H_2^-)(H_1^- - H^-)}, \quad (\text{IV-39})$$

$$\text{Triangle Diagram with Tag} = 2\pi i \int d^2 k^\perp \int_0^{q_1^+} \frac{dk^+}{8k_1^+ k_2^+ k^+} \frac{\text{Tr}[(\not{k}_{1\text{on}} + m)\gamma^+(\not{k}_{\text{on}} + m)]}{H_1^- - H^-}, \quad (\text{IV-40})$$

$$\text{Triangle Diagram with Tag} = 2\pi i \int d^2 k^\perp \int_0^{q_1^+} \frac{dk^+}{8k_1^+ k_2^+ k^+} \frac{\text{Tr}[(\not{k}_{1\text{on}} + m)(\not{k}_{2\text{on}} + m)\gamma^+]}{H_1^- - H_2^-}, \quad (\text{IV-41})$$

$$\text{Triangle Diagram with Tag} = -2\pi i \int d^2 k^\perp \int_{-q_2^+}^0 \frac{dk^+}{8k_1^+ k_2^+ k^+} \frac{\text{Tr}[(\not{k}_{1\text{on}} + m)(\not{k}_{2\text{on}} + m)(\not{k}_{\text{on}} + m)]}{(H_1^- - H_2^-)(H^- - H_2^-)}, \quad (\text{IV-42})$$

$$\text{Triangle Diagram with Tag} = -2\pi i \int d^2 k^\perp \int_{-q_2^+}^0 \frac{dk^+}{8k_1^+ k_2^+ k^+} \frac{\text{Tr}[\gamma^+(\not{k}_{2\text{on}} + m)(\not{k}_{\text{on}} + m)]}{H^- - H_2^-}, \quad (\text{IV-43})$$

$$\text{Triangle Diagram with Tag} = -2\pi i \int d^2 k^\perp \int_{-q_2^+}^0 \frac{dk^+}{8k_1^+ k_2^+ k^+} \frac{\text{Tr}[(\not{k}_{1\text{on}} + m)(\not{k}_{2\text{on}} + m)\gamma^+]}{H_1^- - H_2^-}. \quad (\text{IV-44})$$

Note that the diagrams (IV-41) and (IV-44) with the instantaneous exchanged fermions have the same integrand. However, the longitudinal momentum  $k^+$  has

a different sign. We encountered such a similarity before in §4 of Chapter II for the current.

Although we could have expected diagrams with two instantaneous fermions, we see that they are not present. This is so because we use a scalar coupling and therefore two  $\gamma^+$  matrices becoming neighbors give 0. No so-called forced instantaneous loops are present. These FILs obscure the equivalence of LF and covariant perturbation theory and have been analyzed in Chapter III.

The traces can be calculated. We obtain

$$\begin{aligned} \text{Tr} & [(\not{k}_{1\text{on}} + m)(\not{k}_{2\text{on}} + m)(\not{k}_{\text{on}} + m)] \\ & = 4m(m^2 + k_{1\text{on}} \cdot k_{\text{on}} + k_{2\text{on}} \cdot k_{\text{on}} + k_{1\text{on}} \cdot k_{2\text{on}}), \end{aligned} \quad (\text{IV-45})$$

$$\text{Tr} [(\not{k}_{1\text{on}} + m)(\not{k}_{2\text{on}} + m)\gamma^+] = 4m(2k^+ - q_1^+ + q_2^+), \quad (\text{IV-46})$$

$$\text{Tr} [(\not{k}_{1\text{on}} + m)\gamma^+(\not{k}_{\text{on}} + m)] = 4m(2k^+ - q_1^+), \quad (\text{IV-47})$$

$$\text{Tr} [\gamma^+(\not{k}_{2\text{on}} + m)(\not{k}_{\text{on}} + m)] = 4m(2k^+ + q_2^+). \quad (\text{IV-48})$$

We see that the high orders in  $k^\perp$  have disappeared in the traces. However, logarithmic divergences remain in all LF time-ordered diagrams (IV-39)-(IV-44). We tackle them with minus regularization, as introduced in the previous subsection.

### §3.4 Equivalence

As the fermion triangle is a scalar amplitude, there is only one structure function present. It belongs to the third category we mentioned in §1: it is logarithmically divergent, but has no longitudinal divergences.

#### Type 3: LF structure functions with overall transverse divergences

We applied minus regularization to the integrands of the six LF time-ordered diagrams, using both the MR0 and MR1 methods. We used MATHEMATICA to do the substitution and the differentiation with respect to  $\lambda$ , given by Eq. (IV-19). However, MATHEMATICA was not able to do the integration, neither analytically nor numerically. Therefore the integrand was implemented in FORTRAN which was well capable of doing the four-dimensional integration using IMSL routines based on Gaussian integration.

Because the integrations cannot be done exactly, we saw no possibility of giving a rigorous proof of the equivalence of LF and covariant perturbation theory. Instead we make a choice for the parameters, such as the masses and the external momenta, and show that our method gives the same result as the covariant calculation with BPHZ regularization.

We calculated the decay amplitude of a scalar boson at rest, as is pictured in Fig. IV-3. From a physical point of view, there is no preferred direction, and therefore we demand that our choice of the coordinates of the light-front have

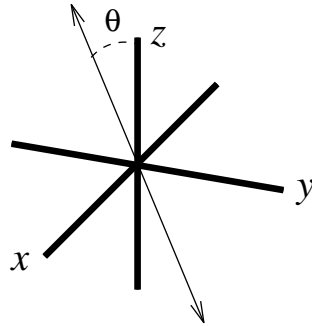


Figure IV-3: A boson is at rest and decays into two particles flying off in opposite directions. The angle  $\theta$  is the angle between the momentum of one of the fermions and the  $z$ -axis.

no influence on the outcome of the calculation. The decay amplitude, which is a scalar quantity, should give the same result for each possible direction in which the bosons can fly off.

Of the six minus-regularized LF time-ordered fermion triangle diagrams contributing to the boson decay, each one has a manifest rotational invariance in the  $x$ - $y$ -plane, and therefore we expect the same for the sum. However, since LF perturbation theory discriminates between the  $z$ -direction and the other space directions, the LF time-ordered diagrams can (and should) differ as a function of the angle,  $\theta$ , between the momentum of one of the particles flying off and the  $z$ -axis. The absolute value of the momentum is kept fixed. It is not immediately clear that the sum should be invariant. This investigation becomes more interesting since it is believed [10] that rotational invariance is broken in naive light-cone quantization of the Yukawa model.

The results are shown in Figs. IV-4-IV-6. They demonstrate that rotational invariance is not broken. Note that we have dropped the factor  $-i$  common to all diagrams. Two LF time-ordered diagrams (IV-40) and (IV-43) contributing to the boson decay and indicated by double-dashed lines are so small they can hardly be identified in Fig. IV-4. In Fig. IV-5 we depict these two on a scale that is a factor 100 larger. In the same figure we show the difference of the sum of the six LF time-ordered diagrams (using MR1 and 128 points in every integration variable) and the covariant result. It has a maximum of 0.03%. In Figs. IV-4 and IV-5 we see that interchanging the outgoing bosons is the same as replacing  $\theta$  by  $\pi - \theta$ . This property is expected because of Bose-Einstein symmetry. We verified that the individual diagrams are rotational invariant around the  $z$ -axis. We illustrate this in Fig IV-6.

Summing up, we find that the sum of the minus-regularized LF time-ordered diagrams is rotational invariant. The deviation from the covariant result is very small. We checked, by varying the number of integration points, that the deviations are due to numerical inaccuracies only. We conclude that, for the fermion

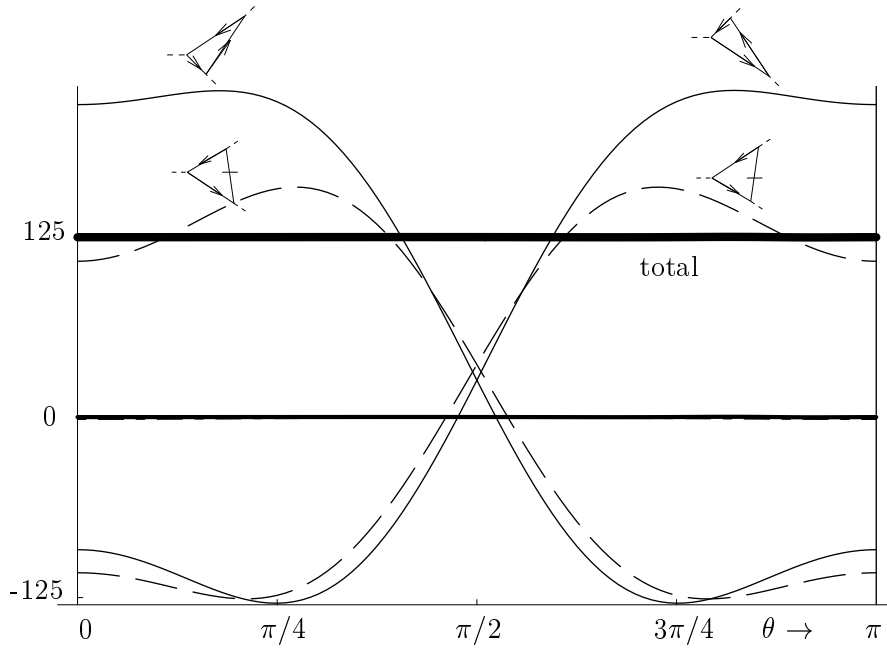


Figure IV-4: The thick line at a value of 125 represents the sum of the six LF time-ordered amplitudes. It is independent of the angle  $\theta$ , defined in Fig. IV-3. The four largest contributions come from the diagrams without instantaneous parts (solid lines) and the diagrams with an instantaneous exchanged fermion (dashed lines), as indicated by the diagrams.

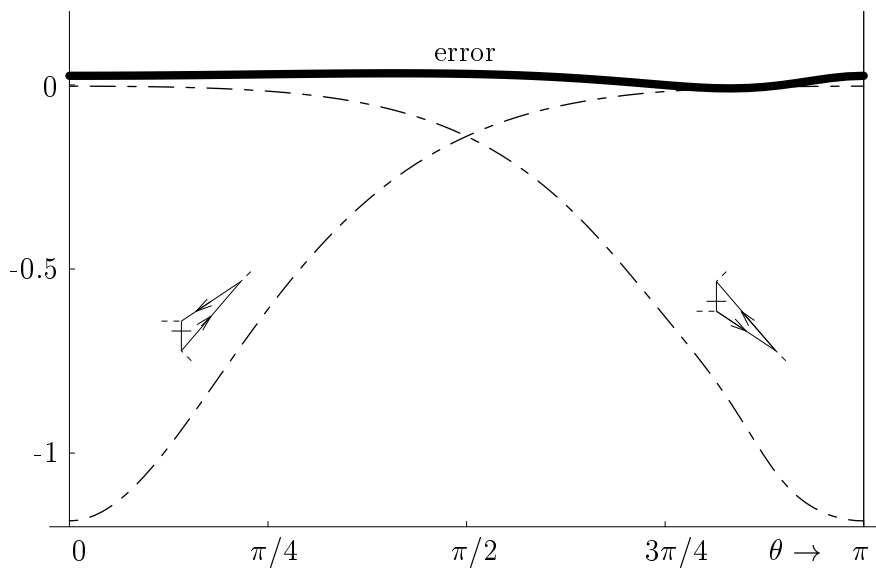


Figure IV-5: The amplitudes of the two small contributions (double-dashed lines) and the difference between the sum of the six LF time-ordered diagrams and the covariant amplitude (thick solid line).

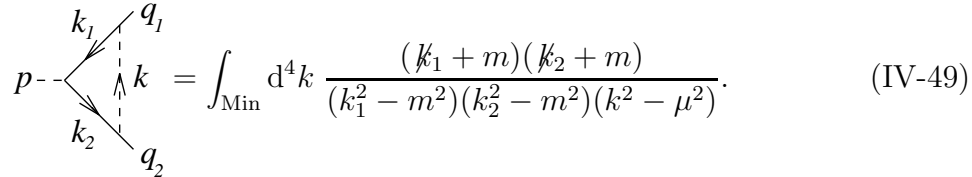
Figure IV-6: Commutative diagram of the boson decay amplitude. The boson is at rest in the origin and decays. The outgoing bosons fly off in opposite directions. Points on the surfaces have polar coordinates  $(A, \theta, \phi)$ , where  $A$  is the magnitude of the amplitude and  $\theta$  and  $\phi$  are the polar angles of the momentum of one of the outgoing particles, as defined in Fig. IV-3. Because the diagrams on the second line are very small, the scale has been enlarged by a factor of 100. For the LF time-ordered diagrams on the first three lines minus regularization (both MR0 and MR1) is used, for the covariant diagram on the last line we used BPHZ regularization.



triangle, the covariant calculation in combination with the BPHZ regularization scheme gives the same result as the LF calculation in combination with minus regularization.

### §4 Equivalence for the one-boson exchange diagram

The second process under investigation was studied before by Burkardt and Langanau [10], and in §2 of Chapter III as an example of how different LF time-orderings are constructed. A scalar boson of mass  $\mu$  and momentum  $p$  decays into two fermions of mass  $m$  and momentum  $q_1$  and  $q_2$  respectively. The lowest order correction to this process is the one-boson exchange correction. The amplitude is given by the integral

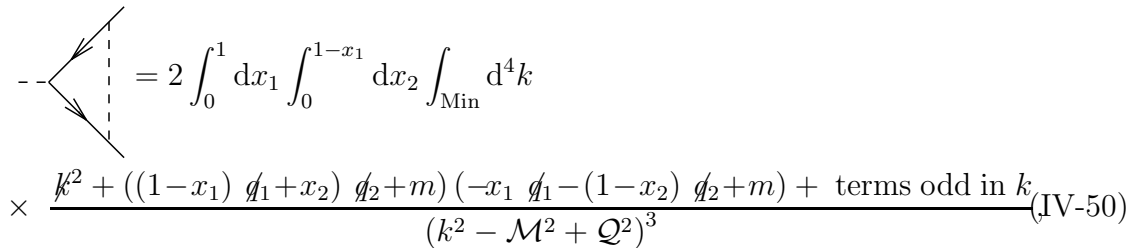


$$p \text{---} \begin{array}{l} \nearrow^{k_1} q_1 \\ \searrow_{k_2} q_2 \end{array} \text{---} \begin{array}{c} \uparrow k \\ \downarrow \end{array} = \int_{\text{Min}} d^4k \frac{(k_1+m)(k_2+m)}{(k_1^2-m^2)(k_2^2-m^2)(k^2-\mu^2)}. \quad (\text{IV-49})$$

Again, this equation is undefined as it stands. First we have to make it a well-defined object. In §4.1 we apply the covariant method and in §4.3 we use LF coordinates.

#### §4.1 Covariant calculation

Using Feynman parametrization the one-boson exchange correction can be rewritten as



$$\text{---} \begin{array}{l} \nearrow \\ \searrow \end{array} \text{---} \begin{array}{c} \uparrow \\ \downarrow \end{array} = 2 \int_0^1 dx_1 \int_0^{1-x_1} dx_2 \int_{\text{Min}} d^4k \times \frac{k^2 + ((1-x_1) \not{q}_1 + x_2) \not{q}_2 + m) (-x_1 \not{q}_1 - (1-x_2) \not{q}_2 + m) + \text{terms odd in } k}{(k^2 - \mathcal{M}^2 + \mathcal{Q}^2)^3} \quad (\text{IV-50})$$

with

$$\mathcal{M}^2 = (x_1 + x_2)m^2 + (1 - x_1 - x_2)\mu^2, \quad (\text{IV-51})$$

$$\mathcal{Q}^2 = x_1(1 - x_1)q_1^2 + x_2(1 - x_2)q_2^2 + 2x_1x_2q_1 \cdot q_2, \quad (\text{IV-52})$$

and where terms odd in  $k$  in the numerator are not specified, since they will be removed according to the covariant prescription. We also define

$$\mathcal{P}^2 = \mathcal{Q}^2 + (1 - x_1 - x_2)q_1 \cdot q_2. \quad (\text{IV-53})$$

From Eq. (IV-50) we can infer that the Dirac structure of the diagram is

$$\begin{array}{c} \diagup \\ \text{---} \\ \diagdown \end{array} = F^1 + F^{2\mu} \gamma_\mu + F^{3\mu\nu} \frac{1}{2} [\gamma_\mu, \gamma_\nu]. \quad (\text{IV-54})$$

where the vector part contains a symmetric and an anti-symmetric part,

$$F^{2\mu} = F^{2s}(q_1^\mu + q_2^\mu) + F^{2a}(q_1^\mu - q_2^\mu), \quad (\text{IV-55})$$

and the tensor part has the form

$$F^{3\mu\nu} = (q_1^\mu q_2^\nu - q_1^\nu q_2^\mu) F^3. \quad (\text{IV-56})$$

The functions  $F^i$  depend on the masses and the external momenta  $q_1^2$ ,  $q_2^2$  and  $q_1 \cdot q_2$ . If we define the integral operator

$$I[f] = 2 \int_0^1 dx_1 \int_0^{1-x_1} dx_2 \int_{\text{Min}} d^4k (k^2 - \mathcal{M}^2 + \mathcal{Q}^2)^{-3} f, \quad (\text{IV-57})$$

then we have, using  $q_1^2 = q_1^2$ , et cetera.

$$F^1 = I [k^2 + m^2 - \mathcal{P}^2], \quad (\text{IV-58})$$

$$F^{2a} = 2mI [1 - x_1 - x_2], \quad (\text{IV-59})$$

$$F^{2s} = 2mI [-x_1 + x_2], \quad (\text{IV-60})$$

$$F^3 = I [1 - x_1 - x_2]. \quad (\text{IV-61})$$

We see that the only function which needs to be regularized is  $F^1$ . The functions  $F^2$  and  $F^3$  are convergent and do not require regularization in a covariant calculation.

## §4.2 BPHZ regularization

The regularized structure function  $F^{1R}$  can be found by applying the BPHZ regularization scheme (IV-11) to the structure function (IV-58). The integral is now finite; so we can do the Wick rotation and perform the  $k$  integrations.

$$F^{1R}(q_1^2, q_2^2, q_1 \cdot q_2) = -2\pi^2 i \int_0^1 dx_1 \int_0^{1-x_1} dx_2 \int_0^1 d\lambda \left( \frac{\mathcal{Q}^2(\lambda\mathcal{P}^2 - m^2)}{2(\mathcal{M}^2 - \lambda\mathcal{Q}^2)^2} + \frac{\mathcal{Q}^2 + \frac{1}{2}\mathcal{P}^2}{\mathcal{M}^2 - \lambda\mathcal{Q}^2} \right) \quad (\text{IV-62})$$

We have not been able to do all three integrations exactly. The  $\lambda$  integration and one of the  $x$  integrations can be done analytically, and the remaining integration numerically. As  $F^{2\mu}$  and  $F^3$  do not need to be regularized, this concludes the covariant calculation of the one-boson exchange correction.

### §4.3 Light-front calculation

In the previous chapters it was shown how to derive the LF time-ordered diagrams corresponding to the covariant diagram (IV-49) using  $k^-$ -integration. One can write the time-ordered diagrams individually, or one can combine propagating and instantaneous parts into so-called blinks. Blinks have the advantage that the  $1/k^+$ -singularities cancel and the number of diagrams is reduced.

In the two triangle diagrams studied here it makes no difference whether blinks are used or not. In the case of the fermion triangle we calculated LF time-ordered diagrams. Here we use blinks, to demonstrate that our technique also works in this case. The one-boson exchange correction has two blink diagrams:

$$\text{Triangle} = \text{Blink}_1 + \text{Blink}_2 \quad (\text{IV-63})$$

The poles of the two fermion propagators in the triangle are given by Eqs. (IV-36) and (IV-37). The pole of the boson propagator is given by

$$H^- = \frac{k^\perp{}^2 + \mu^2}{2k^+}. \quad (\text{IV-64})$$

The amplitudes including blinks are

$$\text{Blink}_1 = -2\pi i \int d^2k^\perp \int_{-q_2^+}^0 \frac{dk^+}{8k_1^+ k_2^+ k^+} \frac{(\not{k}_{2\text{on}} - \not{p} + m)(\not{k}_{2\text{on}} + m)}{(H_1^- - H_2^-)(H^- - H_2^-)}, \quad (\text{IV-65})$$

$$\text{Blink}_2 = 2\pi i \int d^2k^\perp \int_0^{q_1^+} \frac{dk^+}{8k_1^+ k_2^+ k^+} \frac{(\not{k}_{1\text{on}} + m)(\not{k}_{1\text{on}} + \not{p} + m)}{(H_1^- - H_2^-)(H_1^- - H^-)}. \quad (\text{IV-66})$$

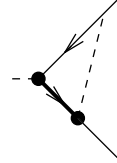
We focus on the blink in Eq. (IV-66). It simplifies because we can use

$$\not{k}_{1\text{on}} \not{k}_{1\text{on}} = k_{1\text{on}} \cdot k_{1\text{on}} = m^2. \quad (\text{IV-67})$$

Therefore we obtain

$$\text{Blink}_2 = 2\pi i \int d^2k^\perp \int_0^{q_1^+} \frac{dk^+}{8k_1^+ k_2^+ k^+} \frac{2m^2 + \not{k}_{1\text{on}}(\not{p} + 2m)}{(H_1^- - H_2^-)(H_1^- - H^-)}. \quad (\text{IV-68})$$

In the same way as we did for the covariant amplitude we can identify the different Dirac structures



$$= F_1^1 + F_1^{2\mu} \gamma_\mu + F_1^{3\mu\nu} \frac{1}{2} [\gamma_\mu, \gamma_\nu]. \quad (\text{IV-69})$$

Although at first sight it looks as if the diagram in Eq. (IV-68) has a covariant structure, covariance is spoiled by the integration boundaries for  $k^+$ . Therefore these functions are not covariant objects. We have to investigate equivalence for the structure functions separately.

The LF structure function  $F_1^1$  can be found by taking the trace of Eq. (IV-68), since all the other structures are traceless. Carrying out the traces one finds

$$F_1^1 = 2\pi i \int d^2 k^\perp \int_0^{q_1^+} \frac{dk^+}{8k_1^+ k_2^+ k^+} \frac{2m^2 + k_{1\text{on}} \cdot p}{(H_1^- - H_2^-)(H_1^- - H^-)}. \quad (\text{IV-70})$$

The other structures of the blink diagram (IV-68) are:

$$F_1^{2\mu} = 2\pi i \int d^2 k^\perp \int_0^{q_1^+} \frac{dk^+}{8k_1^+ k_2^+ k^+} \frac{2m (k_{1\text{on}})^\mu}{(H_1^- - H_2^-)(H_1^- - H^-)}, \quad (\text{IV-71})$$

$$F_1^{3\mu\nu} = 2\pi i \int d^2 k^\perp \int_0^{q_1^+} \frac{dk^+}{8k_1^+ k_2^+ k^+} \frac{(k_{1\text{on}})^\mu p^\nu}{(H_1^- - H_2^-)(H_1^- - H^-)}. \quad (\text{IV-72})$$

In a similar way we can derive the structure functions corresponding to the other blink diagram.

#### §4.4 Equivalence

We can identify the different types of divergences, as explained in §1:

##### **Type 1: LF structure functions without transverse divergences**

The parts of the blink diagrams without any ultraviolet divergences are  $F_i^{2\mu}$  and  $F_i^{3\mu\nu}$ , except for  $\mu$  being  $-$ . No cancellations need to be found and no regularization is necessary.

##### **Type 2: LF structure functions with cancelling transverse divergences**

In the last two structure functions we see something odd happening. Both  $F_i^{2\mu}$  and  $F_i^{3\mu\nu}$  are divergent for  $\mu$  being  $-$ . However, these divergences are not present in the covariant structure functions  $F^{2\mu}$  and  $F^{3\mu\nu}$ . It would be illegal to apply minus regularization, since the covariant amplitude does not need to be regularized. We found that the divergences corresponding to the first blink cancel exactly

against those of the second blink. To simplify the calculation we use internal variables  $x'$  and  $k^\perp$  and external variables  $\chi$ ,  $q_i^-$  and  $q_i^\perp$ . These are introduced in Appendix C.

We have to verify the following relation of equivalence

$$F^{2-} = F_1^{2-} + F_2^{2-}. \quad (\text{IV-73})$$

For the reasons mentioned above we have to demand that the divergent parts in the right-hand side cancel. We find that only the highest order contribution in  $k^\perp$  contributes to a divergent integral, because we can write

$$F_i^{2-} = \int d^2k^\perp \left( \frac{f_i^{2-}}{k^{\perp 2}} + g_i^{2-}(k^\perp) \right), \quad (\text{IV-74})$$

where  $g_i^{2-}(k^\perp)$  is the part of the integrand without ultraviolet divergences, and the term with  $f_i^{2-}$  gives rise to a logarithmically divergent integral. We have to check if

$$f_1^{2-} + f_2^{2-} = 0. \quad (\text{IV-75})$$

In Appendix C the full formulas for the functions  $f_i^{2-}$  are given, from which it follows that condition (IV-75) holds. For  $\mu$  being  $-$  in the structure function  $F_1^{3\mu\nu}$  one can apply the same method.

### Type 3: LF structure functions with overall transverse divergences

The structure function  $F^1$  in the covariant calculation contains an ultraviolet divergence. In the LF structure functions  $F_i^1$  these appear as divergences in the transverse direction. The equation under investigation is the following:

$$F_1^{1\text{MR}} + F_2^{1\text{MR}} = F^{1\text{R}}. \quad (\text{IV-76})$$

For the same reason as for the fermion triangle, an analytic proof of this equation is not possible. We investigated rotational invariance of the left-hand side of this equation, and furthermore we checked if it gives the same result as the covariant calculation on the right-hand side.

A boson is at rest and decays into two fermions as indicated in Fig. IV-3. The fermion mass is taken to be the same as the boson mass. Therefore there can be no on-shell singularities of intermediate states. The contributions of the two blink diagrams are given in the commutative diagram of Fig. IV-7. We made the rather arbitrary choice of applying minus regularization MR1, and used 128 points in every integration variable.

The error, i.e., the difference between the covariant calculation with BPHZ regularization and the sum of minus-regularized blink diagrams, has a maximum of 0.02%. This deviation results from numerical inaccuracies, as was checked by varying the number of integration points.

We conclude that no significant deviation from a rotational invariant amplitude is found. Moreover, we found that the sum of the LF time-ordered diagrams is the same as the covariant amplitude for the one-boson exchange correction. Again, the procedure of  $k^-$ -integration and minus regularization proved to be a valid method.

## §5 Conclusions

In the Yukawa model with a scalar coupling there are five single-loop diagrams with transverse divergences, of which two also contain longitudinal divergences. For all other one-loop diagrams and all multiple-loop diagrams that do not contain subdivergences, the proof of the equivalence of covariant and LF perturbation theory was given by Ligterink [44] upon using the  $k^-$ -integration prescription. For the two single-loop diagrams with longitudinal divergences this integration is ill-defined. This problem was dealt with in the previous chapter.

Of the three remaining diagrams two are thoroughly analyzed in this chapter. For the parts of these diagrams without transverse divergences the  $k^-$ -integration recipe applies. For the parts with transverse divergences a proof of equivalence is complicated by the fact that the amplitudes depend on three independent scalar products of the external momenta. We applied an extended version of the method of minus regularization. It is on a friendly footing with the light-front, because it can be applied to both longitudinal and transverse divergences. Moreover, it has strong similarities to BPHZ regularization, which is suitable for covariant perturbation theory. We were able to tune the regularization in such a way that minus regularization is analogous to BPHZ regularization. Therefore, we expect an exact equality between the covariant and the LF amplitudes. We showed that rotational invariance is maintained and we expect that other nonmanifest symmetries on the light-front, such as boosts in the  $x$ - $y$ -plane, are also conserved.

The final formulas obtained did not yield to analytic integration. Therefore we had to resort to multidimensional numerical integration. As rotational invariance was shown previously to be violated in naive light-cone quantization [10], we investigated rotational invariance, which is one of the nonmanifest symmetries on the light-front. Our results demonstrate, within the errors due to the numerical methods used, that covariant and LF time-ordered perturbation theory give the same physical matrix elements.

One diagram with transverse divergences is not discussed in this thesis, namely the fermion box with four external boson lines. It is a scalar object, similar to the fermion triangle. The results obtained for the latter convinced us that upon minus regularization we shall find a covariant result. As there are more time-orderings, and because one cannot test for rotational invariance as easily as for the triangle diagrams, we did not investigate this much more complicated situation.

We trust that with our elaborate discussion of divergent diagrams in the

Figure IV-7: Commutative diagram of the one-boson exchange correction. A boson decays at rest. The outgoing fermions fly off in opposite directions. As in Fig. IV-6, the radial coordinate gives the amplitude of the regularized diagram for the fermion flying off in this direction. For the LF structure functions on the first two lines, minus regularization (MR1) is used; for the covariant structure function on the last line, we used BPHZ regularization.

Yukawa model we have illustrated the power of minus regularization and taken away doubts about the covariance of LF perturbation theory.



## Entanglement of Fock-space expansion and covariance

In Chapter I we made the comparison between LF and IF quantization and we saw that LFD has a number of advantages, one being that it has the lowest number of dynamical operators, namely three. However, two of them involve rotations around the  $x$  or  $y$ -axis. Therefore LF time-ordered amplitudes are not invariant under such rotations.

The question of rotations in LFD was discussed before with the aim of constructing the angular momentum operators; see, e.g., Fuda [32] and the review by Carbonell *et al.* [12]. While these authors emphasize the algebraic properties of the generators of the Poincaré group, we stress the connection between expansions in Fock-space and covariance. It has been remarked before by Brodsky *et al.* [33] that the higher components in Fock space contribute to the difference between the Bethe-Salpeter equation and the evolution equation in LFD. These authors do not give numerical estimates of the corrections. The latter has been done by Mangin-Brinet and Carbonell [34], and by Frederico [35], who studied the same model and found the effect of higher Fock states on the binding energy to be small. In a calculation of positronium, Trittmann and Pauli [36] used an effective theory, where the effects of all Fock states are included in the interaction. They found rotational symmetry to be restored in the solution.

### §1 Formulation of the problem

In this chapter we consider first standard LF quantization and discuss the problem of noncovariance, which includes violation of rotational invariance, in the framework of LF time-ordered perturbation theory. We give numerical results for the simplified case of two heavy scalars exchanging light scalar particles. This choice is motivated by the popular meson-exchange models in nuclear physics. We do not include the internal spin degrees of freedom, as this is a complication that may obscure the main point of our investigation: the connection between the breaking of covariance and a truncation of the expansion in Fock space. In two interesting papers, Fuda [37, 38] reported on detailed calculations of realistic one-meson exchange models in both LF and IF dynamics. There the emphasis is on the comparison between the two, when in both cases the ladder approxima-

tion is made. It is the purpose of this chapter to show to what extent the ladder approximation itself may violate covariance.

### §1.1 Suppression of higher Fock states

A reason why LFD is often preferred is that higher Fock states are said to be more strongly suppressed in this form of dynamics. The reason for this suppression is believed to be the spectrum condition discussed before in §2.3 of Chapter I. As a disadvantage, the lack of manifest rotational invariance, and therefore covariance, is mentioned. We call a symmetry manifest when it is connected to a kinematical operator. Then all time-ordered diagrams exhibit this symmetry. Equal-time ordered diagrams lack boost invariance, whereas on the light-front the longitudinal boost  $P^+$  is a kinematical operator. Therefore, if one refers to a lack of manifest covariance, one should include not only rotational invariance but also other nonmanifest symmetries. One reason why scientists have rather stressed rotational invariance comes easily to mind: in many cases it is easy to convince oneself by inspection whether a matrix element is rotational invariant, viz when the amplitude can be expressed in terms of scalar products of three-vectors. On the other hand, it is not more difficult to test numerically for invariance under boost transformations than for invariance under rotations. Indeed, the method used in this chapter can easily be extended to check for boost invariance.

A way to test for covariance is to compare the LF time-ordered diagrams to the covariant amplitude, since we know that the latter is invariant under any of the Poincaré symmetry operations. For on energy-shell amplitudes ( $S$ -matrix elements), there is an exact equality, as was proved by Ligterink and Bakker [16] and which is confirmed in our results. Off energy-shell there is a breaking of Poincaré symmetry, which, however, is found to be surprisingly small in the case considered in this chapter.

So why are we using these LF time-ordered diagrams in the first place, when there is an equivalent covariant method available? We do, because we want to determine the properties of the bound state using the Hamiltonian form of dynamics. In this method, covariance can never be fully maintained. However, one may try to apply it in such a way that breaking of covariance is minimal. In many applications in nuclear physics, a one-meson exchange approximation is made for the interaction and the scattering amplitude is computed by formally iterating this interaction, leading to the Lippmann-Schwinger equation in the ladder approximation. In this approximation one retains two- and three-particle intermediate states and neglects Fock states containing four or more particles. These Fock sectors are needed to make the sum of LF time-ordered diagrams equal to the covariant amplitude, exhibiting the symmetries under all Poincaré transformations. If these contributions are large, one can expect a significant breaking of covariance, since the LF time-ordered diagrams are only invariant under application of the kinematical symmetries.

For this reason we concentrate in this article on the determination of the contributions of these higher Fock states. Our main concern shall be the box diagram, defined on page V-21. Then we label the correction as  $\mathcal{R}_{4+}$ . We shall calculate  $\mathcal{R}_{4+}$  explicitly for the box diagram with scalar particles of different masses. The box diagram can be associated with the two-meson exchange between two nucleons. If spin were included, several well-known complications would arise, the most important one being the occurrence of instantaneous propagators [16, 13]. We do not want these complications to interfere with the main point of our investigation: the connection between Fock-space truncations and lack of covariance. Therefore spin is omitted. We have not included crossed box diagrams, because they are not relevant for a discussion on covariance, since both the crossed and noncrossed box diagrams are covariant by themselves.

However, it is well-known [39] that the use of ladder diagrams alone in the Bethe-Salpeter equation does not lead to the proper one-body limit when the mass of one of the nucleons goes to infinity. Therefore, in order to use boson exchanges in bound state calculations within the framework of LFD it is probably necessary to include diagrams with crossed meson lines as well.

## §1.2 Setup

First, we explain the Lippmann-Schwinger formalism and the special role of the box diagram. In §3 we describe how to calculate both the covariant and the LF time-ordered amplitudes. After this, we are ready for our numerical experiments. In §5 the masses of the external particles are chosen in such a way that on-shell singularities of the intermediate states are avoided, and therefore it is easy to compare IF and LF Hamiltonian dynamics. In that section it is shown that  $\mathcal{R}_{4+}$  is much smaller in LFD than in IF dynamics (IFD), confirming the claim that in LFD higher Fock states are more strongly suppressed. Moreover, it tells us that covariance is more vulnerable in IFD than on the light-front!

After this exercise, we concentrate on the light-front, and in §6 we calculate the LF time-ordered diagrams for the more interesting case in which we have particles of fixed masses  $m$  (called nucleons) and  $\mu$  (called mesons). As the process we are concerned with, scattering, is above threshold, we have to deal with on-shell singularities. We show that the breaking of covariance is again small in the ladder approximation.

Although in §7, where we discuss off-shell amplitudes below threshold, no on-shell singularities are encountered, matters become more complicated because the notion of the c.m. system (c.m.s) becomes ambiguous, since the total momentum  $P^z$  is dynamical and found to be unequal to the combined momentum of the two particles,  $p^z + q^z$ . However, we are still able to relate the breaking of covariance and Fock-space truncation.

The lack of covariance of the LF time-ordered amplitudes means that the amplitude depends not only on the scalar products of the external momenta,

but on the angles between the quantization axis and the external momenta as well. Consequently, the amplitudes must have singularities as a function of these angles in addition to the familiar singularities as functions of the invariants. The positions of these singularities are found analytically in §8, in the framework of explicitly covariant LFD. This gives a qualitative understanding of the numerical results in §5 and §6. In §9 explicitly covariant LFD is applied to the off energy-shell results of §7.

## §2 The Lippmann-Schwinger formalism

The Hamiltonian method aims at the determination of stationary states, i.e., eigenstates of the Hamiltonian. Here we take the Yukawa-type model with scalar coupling

$$\mathcal{L}_{\text{int}} = g\Phi^2\phi. \quad (\text{V-1})$$

Two types of particles are considered: “nucleons” ( $N, \Phi$ ) with mass  $m$  and “mesons” ( $m, \phi$ ) with mass  $\mu$ . The Hamiltonian  $H \equiv P^-$  consists of a part  $H_0$  which describes free particles and a part  $V$  which describes the interaction:

$$H = H_0 + V. \quad (\text{V-2})$$

We shall denote the second term on the right-hand side as the potential. The problem of constructing the Hamiltonian from the underlying Lagrangian has been recently reviewed by Brodsky *et al.* [15]. Here we study two-nucleon states only. Moreover, we neglect self-energy diagrams.

We consider  $H_0$ , the kinematic part of the Hamiltonian in the two-nucleon (2N) sector. In the instant-form, quantization is carried out on planes of constant time (equal-time planes). Then we find for two particles of mass  $m$  and momenta  $p$  and  $q$ , respectively,

$$H_0^{\text{IF}} = \sqrt{\vec{p}^2 + m^2} + \sqrt{\vec{q}^2 + m^2}, \quad (\text{V-3})$$

which leads to both negative and positive energy solutions. It is well-known [40] that in this form the overall momenta and the relative momenta are difficult to separate.

In LF quantization the square root, and therefore the negative energy solutions are absent. The interaction-free part of the two-body Hamiltonian is

$$H_0^{\text{LF}} = \frac{p^{\perp 2} + m^2}{2p^+} + \frac{q^{\perp 2} + m^2}{2q^+}, \quad (\text{V-4})$$

which demonstrates that positive energies occur for positive plus-momenta. Moreover, one can easily separate the motion of a many-particle system as a whole from the internal motion of its constituents in the LF case [40].

We shall focus on light-front quantization of our model in which the interaction of the nucleons is due to meson exchange. We write the potential in the form

$$V = V_1 + V_2 + V_3 + \dots \quad (\text{V-5})$$

where the subscript denotes the number of mesons simultaneously exchanged. The potentials only contain irreducible diagrams to prevent double counting.  $V_1$  contains one-meson exchanges only:

$$V_1 = \begin{array}{c} q \text{ --- } q' \\ | \\ p \text{ --- } p' \end{array} = \begin{array}{c} \text{---} \\ / \text{---} \\ \backslash \text{---} \end{array} + \begin{array}{c} \text{---} \\ \backslash \text{---} \\ / \text{---} \end{array}. \quad (\text{V-6})$$

The irreducible diagrams contributing to  $V_1$  are depicted in Eq. (V-6). In these diagrams time goes from left to right. The nucleons are denoted by solid lines, and the mesons by dashed lines. Irreducible diagrams contributing to  $V_2$  are those diagrams of order  $g^4$  that cannot be separated into two pieces by cutting two nucleon lines or two nucleon lines and one meson line only. In terms of Fock-space sectors this means that  $V_1$  contains two-nucleon and one-meson intermediate states, and  $V_2$  contains only two-nucleon two-meson intermediate states.

The potential  $V_1$  is a covariant object in case the external lines are on shell. The meaning of the equality sign in Eq. (V-6) is that the full covariant amplitude can be written as a sum of two LF time-ordered diagrams. Whereas the Feynman diagram contains the propagator  $1/((q' - q)^2 - \mu^2)$ , the LF time-ordered diagrams contain the energy denominator  $1/(P^- - H_0)$ ,  $P^-$  being the parametric energy.  $H_0$  is the sum of the kinetic energies of the particles in the intermediate state:

$$H_0 = \sum_i \frac{k_i^{\perp 2} + m_i^2}{2k_i^+}. \quad (\text{V-7})$$

The two diagrams contain  $\theta$ -functions of the plus-component of the momentum of the exchanged meson: one has the factor  $\theta(p^+ - q^+)$ , the other  $\theta(q^+ - p^+)$ .

In a Feynman diagram the external lines are on mass-shell and the initial and final states have the same energy, which coincides with the parametric energy. Then the minus-component of the total four-momentum of a two-particle state satisfies the relation

$$P^- = p^- + q^- = p'^- + q'^- = \frac{p^{\perp 2} + m^2}{2p^+} + \frac{q^{\perp 2} + m^2}{2q^+}. \quad (\text{V-8})$$

As the minus-component of the total momentum is the only dynamical momentum operator, the other three components are conserved in any LF time-ordered diagram. For instance,  $P^+ = p^+ + q^+ = p'^+ + q'^+$ . This conservation law is very important in LF quantization. It leads immediately to the spectrum condition: in any intermediate state all massive particles have plus-momenta greater than

zero and the sum of the plus-components of the momenta of the particles in that state is equal to the total plus-momentum.

The expansion in Fock space does not coincide with an expansion in powers of the coupling constant. This can easily be seen when one considers an approach closely resembling the Lippmann-Schwinger method. The eigenstates  $|\psi\rangle$  of the Hamiltonian

$$H|\psi\rangle = P^-|\psi\rangle \quad (\text{V-9})$$

are also solutions of the Lippmann-Schwinger equation

$$|\psi\rangle = |\phi\rangle + \frac{1}{P^- - H_0}V|\psi\rangle, \quad (\text{V-10})$$

where  $|\phi\rangle$  specifies the boundary conditions. The formal solution of this equation is

$$|\psi\rangle = \sum_{i=0}^{\infty} \left( \frac{1}{P^- - H_0}V \right)^i |\phi\rangle. \quad (\text{V-11})$$

An equation similar to Eq. (V-10) exists for the scattering amplitude:

$$\boxed{T} = \bigcirc V + \bigcirc V \boxed{T}. \quad (\text{V-12})$$

If one substitutes  $V_1$  for  $V$  in these equations, one obtains the *ladder approximation*. This approximation does not generate all diagrams; so one needs to add corrections. At order  $g^4$  this correction is  $V_2$ :

$$V_2 = \begin{array}{c} \text{---} \\ \diagup \text{---} \\ \diagdown \text{---} \\ \text{---} \end{array} + \begin{array}{c} \text{---} \\ \diagdown \text{---} \\ \diagup \text{---} \\ \text{---} \end{array}. \quad (\text{V-13})$$

If one takes into account all the contributions to  $V$  from Eq. (V-5), then the full scattering amplitude is

$$\begin{array}{c} \boxed{T} \\ \text{---} \\ \text{---} \\ \text{---} \\ \text{---} \end{array} = \begin{array}{c} \text{---} \\ \diagup \text{---} \\ \diagdown \text{---} \\ \text{---} \end{array} + \begin{array}{c} \text{---} \\ \diagdown \text{---} \\ \diagup \text{---} \\ \text{---} \end{array} \\ + \begin{array}{c} \text{---} \\ \diagup \text{---} \\ \diagdown \text{---} \\ \text{---} \\ \text{---} \end{array} + \begin{array}{c} \text{---} \\ \diagdown \text{---} \\ \diagup \text{---} \\ \text{---} \\ \text{---} \end{array} + \begin{array}{c} \text{---} \\ \diagup \text{---} \\ \diagdown \text{---} \\ \text{---} \\ \text{---} \\ \text{---} \end{array} + \begin{array}{c} \text{---} \\ \diagdown \text{---} \\ \diagup \text{---} \\ \text{---} \\ \text{---} \\ \text{---} \end{array} \\ + \mathcal{O}(g^6). \quad (\text{V-14})$$

In the ladder approximation one only takes  $V_1$  into account. Effectively, one then describes the full interaction between two nucleons by

$$\begin{array}{c} \boxed{T} \\ \text{---} \\ \text{---} \\ \text{---} \\ \text{---} \end{array} = \begin{array}{c} \text{---} \\ \diagup \text{---} \\ \diagdown \text{---} \\ \text{---} \end{array} + \begin{array}{c} \text{---} \\ \diagdown \text{---} \\ \diagup \text{---} \\ \text{---} \end{array} \\ + \begin{array}{c} \text{---} \\ \diagup \text{---} \\ \diagdown \text{---} \\ \text{---} \\ \text{---} \end{array} + \begin{array}{c} \text{---} \\ \diagdown \text{---} \\ \diagup \text{---} \\ \text{---} \\ \text{---} \end{array} + \begin{array}{c} \text{---} \\ \diagup \text{---} \\ \diagdown \text{---} \\ \text{---} \\ \text{---} \\ \text{---} \end{array} + \begin{array}{c} \text{---} \\ \diagdown \text{---} \\ \diagup \text{---} \\ \text{---} \\ \text{---} \\ \text{---} \end{array} \\ + \mathcal{O}(g^6). \quad (\text{V-15})$$

In this approximation intermediate states containing more than three particles do not occur. This implies that time-ordered box diagrams with four particles in the intermediate state are neglected, as we can see if we compare the expansions in Eqs. (V-14) and (V-15). As the individual diagrams contributing to  $V_2$  are not covariant, the sum of box diagrams produced by the ladder approximation is not covariant.

Using equal-time quantization, 20 out of the 24 possible time-orderings have intermediate states containing more than three particles. On the light-front, the spectrum condition destroys many of the time-ordered diagrams. There are six nonvanishing diagrams, of which four only contain two- and three-particle intermediate states. One concludes that the one-meson exchange kernel neglects the majority of the contributing time-ordered box diagrams in equal-time quantization, whereas on the light-front most of the nonvanishing diagrams are taken into account. This does not mean necessarily that in IF dynamics the ladder approximation misses most of the amplitude, since the missing diagrams have smaller sizes. The contribution of the missing diagrams needs to be investigated in order to see how much the higher Fock sectors are suppressed.

There is one thing which seems to complicate matters on the light-front. The individual LF time-ordered diagrams are not rotational invariant. When a number of them is missing, the full amplitude will also lack rotational invariance, as is mentioned often in the literature. This feature does not occur on the equal-time plane, since there rotational invariance is a manifest symmetry. However, in other types of Hamiltonian dynamics other symmetries are nonmanifest. In IF Hamiltonian dynamics, e.g., boost invariance is not manifest. Therefore we refer to breaking of covariance, which is a general feature of any form of Hamiltonian dynamics, if one truncates the Fock-space expansion.

We would like to estimate the contribution of the missing diagrams, irrespective of the strength of the coupling. It is not possible to do this in a completely general way, so we perform our numerical calculations for the box diagram only. We assume that our results will be indicative for the higher orders too.

We define the fraction

$$\mathcal{R}_{4+}^{\text{LF}} = \frac{\text{Diagram 1} + \text{Diagram 2}}{\text{Diagram 3}}. \quad (\text{V-16})$$

The subscript 4 indicates that this variable includes all diagrams having at least four particles in some intermediate state. For  $\mathcal{R}_{4+}^{\text{IF}}$  one would have to add the diagrams containing five- and six-particle intermediate states in the numerator, as these give nonvanishing contributions in the instant-form. The diagram in the denominator is the covariant diagram.

We shall show that the correction  $V_2$  is indeed much less important numerically in LFD than in IFD. So the  $2N2m$ -state is in LFD much less important

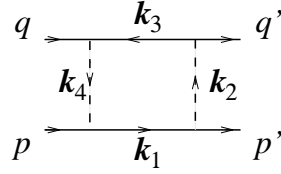


Figure V-1: Kinematics for the box diagram. The arrows denote the momentum flow.

than in IFD. We conjecture that this property of LFD—that the Fock-state expansion converges much more rapidly than in IFD—persists in higher orders in the coupling constant.

### §3 The box diagram

In the previous section we saw that the lowest level at which breaking of covariance is to be expected is the two-meson exchange diagram, also referred to as the box diagram. The discussion is limited to scalar particles. Although a bound state of scalar particles is not found in nature, we do not include spin because we want to avoid in this investigation the complications due to instantaneous terms.

We look at the process of two nucleons with momenta  $p$  and  $q$ , respectively, coming in and exchanging two meson of mass  $\mu$ . The outgoing nucleons have momenta  $p'$  and  $q'$ . The kinematics is given in Fig. V-1. The internal momenta are

$$k_1 = k, \quad (\text{V-17})$$

$$k_2 = k - p', \quad (\text{V-18})$$

$$k_3 = k - p - q, \quad (\text{V-19})$$

$$k_4 = k - p. \quad (\text{V-20})$$

We have to keep in mind that these relations only hold for those components of the momenta that are conserved.

#### §3.1 The covariant box diagram

The covariant box diagram is given by

$$\overline{\overline{\begin{array}{|c|} \hline \text{---} \\ \hline \text{---} \\ \hline \end{array}}} = \int_{\text{Min}} \frac{-i d^4k}{(k_1^2 - m^2)(k_2^2 - \mu^2)(k_3^2 - m^2)(k_4^2 - \mu^2)}, \quad (\text{V-21})$$

where the imaginary parts  $i\epsilon$  of the masses are not written explicitly. If the external states are on energy-shell, that is,

$$P^- = p^- + q^- = p'^- + q'^-, \quad (\text{V-22})$$



then the time-ordered diagrams are the same as those derived by integrating the covariant diagram over LF energy  $k^-$ . In that case we have

$$\begin{array}{c} \text{---} \\ | \quad | \\ \text{---} \\ | \quad | \\ \text{---} \end{array} = \begin{array}{c} \text{---} \\ / \quad \backslash \\ \text{---} \\ \backslash \quad / \\ \text{---} \end{array} + \begin{array}{c} \text{---} \\ \backslash \quad / \\ \text{---} \\ / \quad \backslash \\ \text{---} \end{array} + \begin{array}{c} \text{---} \\ / \quad \backslash \\ \text{---} \\ / \quad \backslash \\ \text{---} \end{array} \\ + \begin{array}{c} \text{---} \\ \backslash \quad / \\ \text{---} \\ \backslash \quad / \\ \text{---} \end{array} + \begin{array}{c} \text{---} \\ / \quad \backslash \\ \text{---} \\ \backslash \quad / \\ \text{---} \end{array} + \begin{array}{c} \text{---} \\ \backslash \quad / \\ \text{---} \\ / \quad \backslash \\ \text{---} \end{array} . \quad (\text{V-23})$$

The example of the box diagram with scalar particles of equal masses has been worked out before by Ligterink and Bakker [16].

### §3.2 The LF time-ordered diagrams

It is well-known [13, 26] how to construct the LF time-ordered diagrams. They are expressed in terms of integrals over energy denominators and phase-space factors. In the case of the box diagram, we need the ingredients given below. The phase space factor is

$$\phi = 16|k_1^+ k_2^+ k_3^+ k_4^+|. \quad (\text{V-24})$$

Without loss of generality we consider the case  $p^+ \geq p'^+$ . The internal particles are on mass-shell; however, the intermediate states are off energy-shell. A number of intermediate states occur. We label the corresponding kinetic energies according to which of the internal particles, labeled by  $k_1 \dots k_4$  in Fig. V-1, are in this state:

$$H_{14} = q^- + \frac{k_1^{\perp 2} + m^2}{2k_1^+} - \frac{k_4^{\perp 2} + \mu^2}{2k_4^+}, \quad (\text{V-25})$$

$$H_{13} = \frac{k_1^{\perp 2} + m^2}{2k_1^+} - \frac{k_3^{\perp 2} + m^2}{2k_3^+}, \quad (\text{V-26})$$

$$H_{12} = q'^- + \frac{k_1^{\perp 2} + m^2}{2k_1^+} - \frac{k_2^{\perp 2} + \mu^2}{2k_2^+}, \quad (\text{V-27})$$

$$H_{34} = p^- - \frac{k_3^{\perp 2} + m^2}{2k_3^+} + \frac{k_4^{\perp 2} + \mu^2}{2k_4^+}, \quad (\text{V-28})$$

$$H_{24} = q'^- + p^- + \frac{k_2^{\perp 2} + \mu^2}{2k_2^+} - \frac{k_4^{\perp 2} + \mu^2}{2k_4^+}, \quad (\text{V-29})$$

$$H_{23} = p'^- + \frac{k_2^{\perp 2} + \mu^2}{2k_2^+} - \frac{k_3^{\perp 2} + m^2}{2k_3^+}. \quad (\text{V-30})$$

A minus sign occurs if the particle goes in the direction opposite to the direction defined in Fig. V-1. All particles are on mass-shell, including the external ones:

$$\begin{array}{ll} q^- = \frac{q^{\perp 2} + m^2}{2q^+}, & q'^- = \frac{q'^{\perp 2} + m^2}{2q'^+}, \\ p^- = \frac{p^{\perp 2} + m^2}{2p^+}, & p'^- = \frac{p'^{\perp 2} + m^2}{2p'^+}. \end{array} \quad (\text{V-31})$$

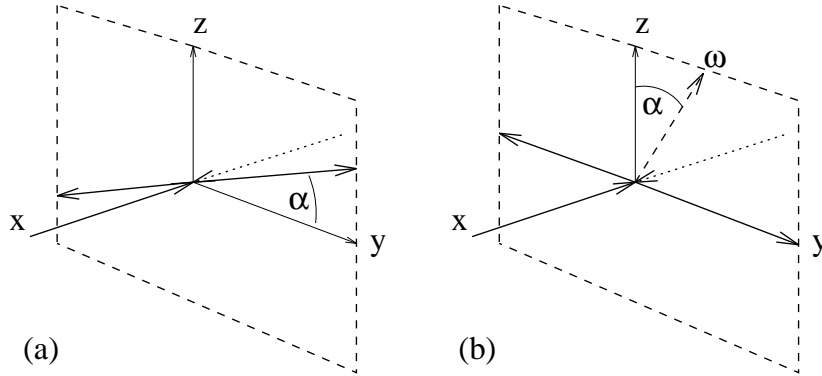


Figure V-2: (a) Two particles come in along the  $x$ -axis. They scatter into the  $y-z$  plane over an angle of  $\pi/2$ . The azimuthal angle is given by  $\alpha$ . (b) Another viewpoint. The outgoing particles go along the  $y$ -axis. The light-front vector  $\omega$  makes an angle  $\alpha$  with respect to the  $z$ -axis.

We can now construct the LF time-ordered diagrams. Diagrams (V-32) and (V-34) will be later referred to as trapezium diagrams, (V-33) as the diamond, and (V-35) as the stretched box.

$$\begin{array}{c} \text{---} \\ \text{---} \\ \text{---} \end{array} = \int d^2 k^\perp \int_0^{p'^+} \frac{-2\pi dk^+}{\phi(P^- - H_{14})(P^- - H_{13})(P^- - H_{12})}, \quad (\text{V-32})$$

$$\begin{array}{c} \text{---} \\ \text{---} \\ \text{---} \end{array} = \int d^2 k^\perp \int_{p'^+}^{p^+} \frac{-2\pi dk^+}{\phi(P^- - H_{14})(P^- - H_{13})(P^- - H_{23})}, \quad (\text{V-33})$$

$$\begin{array}{c} \text{---} \\ \text{---} \\ \text{---} \end{array} = \int d^2 k^\perp \int_{p^+}^{p^+ + q^+} \frac{-2\pi dk^+}{\phi(P^- - H_{34})(P^- - H_{13})(P^- - H_{23})}, \quad (\text{V-34})$$

$$\begin{array}{c} \text{---} \\ \text{---} \\ \text{---} \end{array} = \int d^2 k^\perp \int_{p'^+}^{p^+} \frac{-2\pi dk^+}{\phi(P^- - H_{14})(P^- - H_{24})(P^- - H_{23})}, \quad (\text{V-35})$$

$$\begin{array}{c} \text{---} \\ \text{---} \\ \text{---} \end{array} = \begin{array}{c} \text{---} \\ \text{---} \\ \text{---} \end{array} = 0. \quad (\text{V-36})$$

The factor  $2\pi$  matches the conventional factor  $i$  in Eq. (V-21). The last two diagrams are zero because we consider  $p^+ \geq p'^+$  and therefore these diagrams have an empty  $k^+$ -range. If we take  $p^+ \leq p'^+$ , which case will also occur in forthcoming sections, diagrams (V-36) have nonvanishing contributions.

## §4 A numerical experiment

We look at the scattering of two particles over an angle of  $\pi/2$ . In Fig. V-2 the process is viewed in two different ways.

Fig. V-2a pictures the situation where the scattering plane is rotated around the  $x$ -axis. The viewpoint in Fig. V-2b concentrates on the influence of the

orientation of the quantization plane and is connected to explicitly covariant LFD, as will be discussed in §8. Both viewpoints should render identical results, since all angles between the five relevant directions (the quantization axis and the four external particles) are the same. We choose for the momenta

$$p^\mu = (v^0, +v^x, 0, 0), \quad (\text{V-37})$$

$$q^\mu = (v^0, -v^x, 0, 0), \quad (\text{V-38})$$

$$p'^\mu = (v^0, 0, -v^y, -v^z), \quad (\text{V-39})$$

$$q'^\mu = (v^0, 0, +v^y, +v^z). \quad (\text{V-40})$$

indicating that we have chosen the fixed quantization plane  $x^+ = 0$  (Fig. V-2a). The incoming and outgoing particles have the same absolute values of the momenta in the c.m.s. Therefore,

$$|\vec{v}|^2 = (v^x)^2 = (v^y)^2 + (v^z)^2 = |\vec{v}'|^2. \quad (\text{V-41})$$

The Mandelstam variables are

$$s = (p + q)^2 = 4(v^0)^2, \quad (\text{V-42})$$

$$t = (p - p')^2 = -2|\vec{v}|^2, \quad (\text{V-43})$$

$$u = (p - q')^2 = -2|\vec{v}|^2. \quad (\text{V-44})$$

We are now ready to perform the numerical experiments for three cases, which are described in §5-§7. In the experiments two parameters are focused on. We shall vary the azimuthal angle  $\alpha$  in the  $y$ - $z$ -plane,

$$\alpha = \arctan \frac{v^z}{v^y}, \quad (\text{V-45})$$

and the incoming c.m.s.-momentum

$$v = v^x. \quad (\text{V-46})$$

In the remainder we will omit the units for the masses, which are  $\text{MeV}/c^2$ .

## §5 Light-front versus instant-form dynamics

One of the claims of LFD is that higher Fock states are more strongly suppressed than in IFD. We can investigate this claim for the box diagram easily in the following case.

We take the external states on energy-shell, Eq. (V-22), such that the equality (V-23) holds. At the same time we avoid on-shell singularities for the intermediate states by giving the external particles a slightly smaller mass  $m'$ ,

$$m'^2 = p^2 < m^2, \quad (\text{V-47})$$

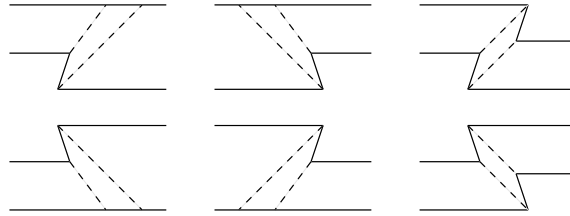


Figure V-3: Time-ordered diagrams that contribute to  $\mathcal{R}_5$ . The diagrams in the first column have five particles in the first intermediate state. The diagrams in the second column have five particles in the last intermediate state, and the diagrams on the right have five-particle intermediate states for both the first and third intermediate states.

such that we can still relate the amplitude to an  $S$ -matrix element.

The process we look at is described in the previous section and has two scalars of mass  $m'$  coming in along the  $x$ -axis, interacting, and scattered over a scattering angle of  $\pi/2$ . Stretched boxes give maximal contributions (see next section) if the quantization axis is in the scattering plane, which is the case if the azimuthal angle  $\alpha = \pi/2$ .

$\mathcal{R}_{4+}^{\text{LF}}$  is easily found by calculating the stretched box.  $\mathcal{R}_{4+}^{\text{IF}} = \mathcal{R}_4^{\text{IF}} + \mathcal{R}_5^{\text{IF}} + \mathcal{R}_6^{\text{IF}}$ , however, has 20 nonzero contributions. As an example, we show the six contributions to  $\mathcal{R}_5$  in Fig. V-3.

This illustrates why  $\mathcal{R}_5^{\text{LF}} = 0$ . All contributing diagrams contain vacuum creation or annihilation vertices, which are forbidden by the spectrum condition. There are 12 diagrams contributing to  $\mathcal{R}_6$ , and all contain vacuum creation or annihilation vertices. Therefore,  $\mathcal{R}_6^{\text{LF}}$  vanishes.

We calculated  $\mathcal{R}_{4+}^{\text{IF}}$  by subtracting the four diagrams only containing three particle intermediate states from the full sum. This sum can be obtained by doing the covariant calculation, or by adding all LF time-ordered boxes. Our results are given in Fig. V-4. We also calculated  $\mathcal{R}_{5+}^{\text{IF}}$ .

We conclude that on the light-front contributions of higher Fock states are significantly smaller than in IFD. In the limit  $v \rightarrow 0$ , the ratio  $\mathcal{R}_{4+}^{\text{LF}}$  goes to zero, because the phase space becomes empty. However, in IFD there is a finite contribution of  $\mathcal{R}_{4+}^{\text{IF}} = 4.5\%$  in this limit. Even if one includes five-particle intermediate states, the LF is the winner by far.

Note that  $m'$ , given by Eq. (V-47), varies as a function of  $p^2$ , and therefore also as a function of  $v$ , but is independent of  $\alpha$ . The deviation of  $m'$  from  $m$  is small: less than 2.3% for  $v < 200$  and less than 9% for  $v < 400$ . As the deviation of the mass  $m'$  from  $m$  is only small, we are convinced that these results are indicative for calculations above threshold. However, we do not want to do these calculations, because then one needs to subtract the on-shell singularities of the equal-time ordered boxes.

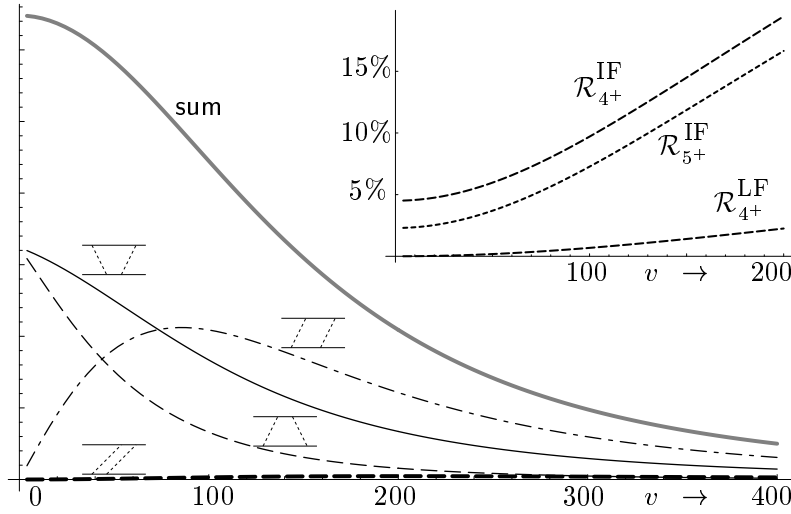


Figure V-4: LF time-ordered boxes for a scattering angle of  $\pi/2$  as a function of the incoming momentum  $v$ . We also give the ratios of boxes with at least four particles ( $\mathcal{R}_{4+}^{\text{IF}}$  and  $\mathcal{R}_{4+}^{\text{LF}}$ ) or five particles ( $\mathcal{R}_{5+}^{\text{IF}}$ ,  $\mathcal{R}_{5+}^{\text{LF}} = 0$ ) in one of the intermediate states.

## §6 Numerical results above threshold

As in §5, we look at the scattering of two particles over an angle of  $\pi/2$ . We focus on LFD, and therefore we simply write  $\mathcal{R}_4 = \mathcal{R}_{4+}^{\text{LF}}$ . We do not try to avoid on-shell singularities by taking different masses for the internal and external nucleons. Two nucleons of mass  $m = 940$  scatter via the exchange of scalar mesons of mass  $\mu = 140$ . Again, there is a scalar coupling and no spin is included.

### §6.1 Evaluation method

Contrary to the case considered in §5, now it is not straightforward to evaluate the contributions of the LF time-ordered boxes, because the nonstretched boxes contain on-shell singularities, thoroughly analyzed in §8. Here we briefly sketch how we deal numerically with the singularities. Using the analysis of §8, we identify the singularity  $I_{\text{sing}}$  and rewrite the nonstretched boxes as

$$\int d^3k I = \int d^3k (I - I_{\text{sing}}) + \int d^3k I_{\text{sing}}. \quad (\text{V-48})$$

The integrand  $I_{\text{sing}}$  has a simple algebraic form, such that the integration in one dimension over the singularity can be done analytically, and the remaining integral is regular. This integral is then done numerically by MATHEMATICA. The integral over  $(I - I_{\text{sing}})$  was implemented in FORTRAN. These two numbers are added to give the results presented in §6.2 and §6.3.

Figure V-5: Amplitudes above threshold from  $\alpha = 0$  to  $\alpha = 2\pi$ . Here  $\mathcal{R}_4$  is the maximal fraction of the stretched box to the absolute value of the sum.

## §6.2 Results as a function of $\alpha$

We shall now vary the direction of  $\vec{v}$ , given by the azimuthal angle  $\alpha$ , however not its length. Therefore the Mandelstam variables are independent of  $\alpha$ , and we expect the full amplitude to be invariant. We tested this numerically for a number of values of  $v$ . In the region  $0 \leq \alpha \leq \pi$ , we used the formulas (V-32) until (V-35). In the region  $\pi \leq \alpha \leq 2\pi$  the diagrams (V-33) and (V-35) vanish. However, then there are contributions from the diagrams in (V-36). The results are shown in Fig. V-5. The results are normalized to the value of the covariant amplitude. The contributions from the different diagrams vary strongly with the angle  $\alpha$ . Since the imaginary parts are always positive, they are necessarily in the range  $[0, 1]$  when divided by the imaginary part of the covariant amplitude. The real parts can behave much more eccentrically, especially for higher values of the incoming c.m.s.-momentum  $v$ . An analysis of the  $\alpha$ -dependence is given in §8. Clearly, the LF time-ordered diagrams add up to the covariant amplitude; so we see that in all cases we obtain covariant (in particular rotationally invariant) results for both the real and imaginary parts.

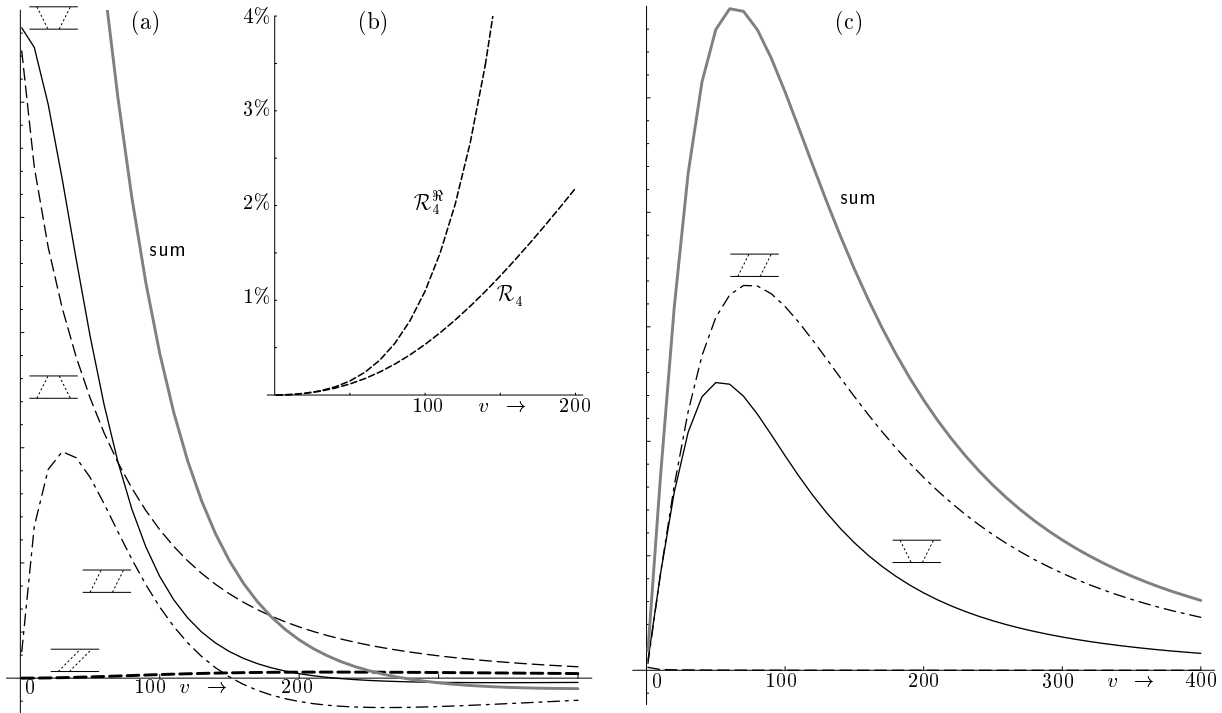


Figure V-6: Real (a) and imaginary (c) parts of the LF time-ordered boxes above threshold for  $\alpha = \pi/2$  as a function of the momentum of the incoming particles  $v$ . The inset (b) shows the ratio of the stretched box to the real part of the amplitude ( $\mathcal{R}_4^{\Re}$ ) and to the absolute value ( $\mathcal{R}_4$ ).

### §6.3 Results as a function of $v$

We look at scattering in the  $x$ - $z$ -plane ( $\alpha = \pi/2$ ), because in that case the contributions from the stretched boxes are maximized. The results are shown in Fig. V-6.

We depict the ratio of the stretched box, the diagram with two simultaneously exchanged mesons, to both the real part and to the magnitude of the total amplitude. Since the real part has a zero near  $v = 280$ , the ratio  $\mathcal{R}_4^{\Re}$  becomes infinite at that value of the incoming momentum. Therefore  $\mathcal{R}_4$  gives a better impression of the contribution of the stretched box. We conclude from our numerical results that the stretched box is relatively small at low energies, but becomes rather important at higher energies.

## §7 Numerical results off energy-shell

In the previous section, we tested covariance of the LF formalism for amplitudes with on energy-shell external particles, by using the c.m.s., where  $P^\perp = p'^\perp + q'^\perp = 0$  and  $P^z = p'^z + q'^z = 0$ . However, on the light-front the operator  $P^z$



is dynamical, and the last equality does not hold anymore off energy-shell, as one can easily verify in the following way. Consider the case of a bound state with mass  $\mathcal{M} < 2m$ , where  $\mathcal{M}$  is related to the parametric LF energy  $P^-$  by the mass-shell relation

$$P^- = \frac{\mathcal{M}^2 + P^\perp{}^2}{2P^+}. \quad (\text{V-49})$$

The bound state is off energy-shell and its mass  $\mathcal{M}$  is smaller than the sum of the constituent masses. Therefore we have

$$p'^- + q'^- > P^-. \quad (\text{V-50})$$

The plus and transverse momenta are kinematic; so

$$p'^+ + q'^+ = P^+, \quad (\text{V-51})$$

$$p'^\perp + q'^\perp = P^\perp. \quad (\text{V-52})$$

Adding Eqs. (V-50) and (V-51) gives

$$p'^z + q'^z > P^z. \quad (\text{V-53})$$

If  $P^z = 0$ , then Eq. (V-53) implies that  $p'^z + q'^z > 0$ . Therefore the two outgoing particles cannot have exactly opposite momenta as in Eqs. (V-39) and (V-40). In terms of the explicitly covariant LFD, introduced in §8, this reflects the fact that the off energy-shell relation between  $p' + q'$  and  $P$  contains an extra four-momentum like in Eq. (V-99), below. What was the reason that we chose opposite momenta in the previous sections in the first place? Our reason was that we wanted to have a manifest symmetry of the amplitude, because it is obvious that the Mandelstam variables  $s$ ,  $t$ , and  $u$  given by Eqs. (V-42)-(V-44) remain the same under the rotations we investigated.

In the present case where the states are taken off energy-shell, the full amplitude is not covariant. We can, however, study this breaking of covariance by comparing amplitudes that satisfy the conditions (V-50)-(V-53) and, at the same time, choosing the scattering angle  $\theta$ , the plus-momentum  $p'^+$  and the magnitude of  $p'^\perp$  in such a way that the Mandelstam variables  $s$ ,  $t$ , and  $u$  remain constant, while the azimuthal angle  $\alpha$  is varied. In the limiting case that  $P^-$  is equal to  $p'^- + q'^-$ , the amplitude becomes on energy-shell and the dependence on  $\alpha$  in the full amplitude drops.

The variation of the amplitude with  $\alpha$  can be compared to the relative contribution of the stretched boxes. We shall do that in what follows, but first we describe in detail the choice of momenta for the particles.

### §7.1 Determination of the momenta

As in the previous sections, we shall fix the direction of the incoming particles, as in Eqs. (V-37) and (V-38), and vary the direction of the outgoing particles.

For on energy-shell amplitudes, there are only two independent Mandelstam variables. Off energy-shell, more independent Lorentz invariant objects are found. We construct the momenta in such a way that all six inner products between them are constant. We first look at  $p \cdot q'$  and  $p \cdot p'$ , and later we verify if the conditions found ensure the invariance of the four others:

$$\begin{aligned} p \cdot q' &= p^+ q'^- + q'^+ p^- - p^\perp \cdot q'^\perp & (V-54) \\ &= x_p P^+ \frac{q'^{\perp 2} + m^2}{2(1-x_{p'}) P^+} + (1-x_{p'}) P^+ \frac{p^{\perp 2} + m^2}{2x_p P^+} - p^\perp \cdot q'^\perp, \end{aligned}$$

$$\begin{aligned} p \cdot p' &= p^+ p'^- + p'^+ p^- - p^\perp \cdot p'^\perp & (V-55) \\ &= x_p P^+ \frac{q'^{\perp 2} + m^2}{2x_{p'} P^+} + x_{p'} P^+ \frac{p^{\perp 2} + m^2}{2x_p P^+} - p^\perp \cdot p'^\perp. \end{aligned}$$

We have introduced the fractions

$$x_p = p^+ / P^+, \quad x_{p'} = p'^+ / P^+. \quad (V-56)$$

Since the perpendicular momenta are conserved, we have in the c.m.s.  $p'^\perp = -q'^\perp$ , so the inner products of the perpendicular momenta can be written as

$$p^\perp \cdot p'^\perp = |p^\perp| |p'^\perp| \cos \theta, \quad (V-57)$$

$$p^\perp \cdot q'^\perp = -|p^\perp| |p'^\perp| \cos \theta, \quad (V-58)$$

where  $\theta$  is the scattering angle. We can now solve Eqs. (V-54)-(V-57) for  $x_{p'}$ ,  $|p'^\perp|$  and  $\theta$ . There are many curves satisfying these conditions. For uniqueness, we demand that the curve go through the point in which  $x_{p'} = x_p = 1/2$ ,  $|p'^\perp| = |p^\perp|$ , and  $\theta = \pi/2$ . We find that the curve is then parametrized by

$$\theta = \pi/2, \quad (V-59)$$

$$\frac{p'^{\perp 2} + m^2}{x_{p'}(1-x_{p'})} = 4(p^{\perp 2} + m^2). \quad (V-60)$$

Writing down the other four inner products between the four-vectors of the external momenta, we checked that they are invariant if the momenta satisfy Eqs. (V-59) and (V-60). Because the particles come in along the  $x$ -axis, the above relations define an ellipse in the  $y$ - $z$ -plane. In the case of IFD these ellipses reduce to circles with their center at the origin and radius  $v$ . Our procedure to obtain numerical values for the momenta was the following. We take  $p'^x = 0$  and varied  $p'^y = |p^\perp| \cos \alpha$ . Now Eq. (V-60) gives us  $x_{p'}$ . All components of  $p'$  and  $q'$  are then easily found. In Fig. V-7 we have indicated the  $y$  and  $z$ -components of the momenta of the external particles for the two cases we investigate. The  $z$ -component, not being a LF variable, does not enter the computer code. We

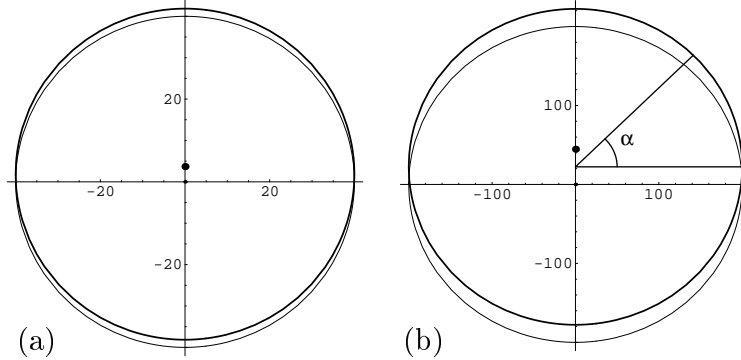


Figure V-7: Momenta  $p'$  and  $q'$  of the outgoing particles (thick line) in the scattering plane (horizontal  $p'^y$  and  $q'^y$ ; vertical:  $p'^z$  and  $q'^z$ ) for two cases: (a)  $v = 40$  and (b)  $v = 200$ . The momentum  $p' + q'$  is indicated by the dot. As a reference we have drawn the locus for on-shell external particles (thin line): a circle centered at the origin.

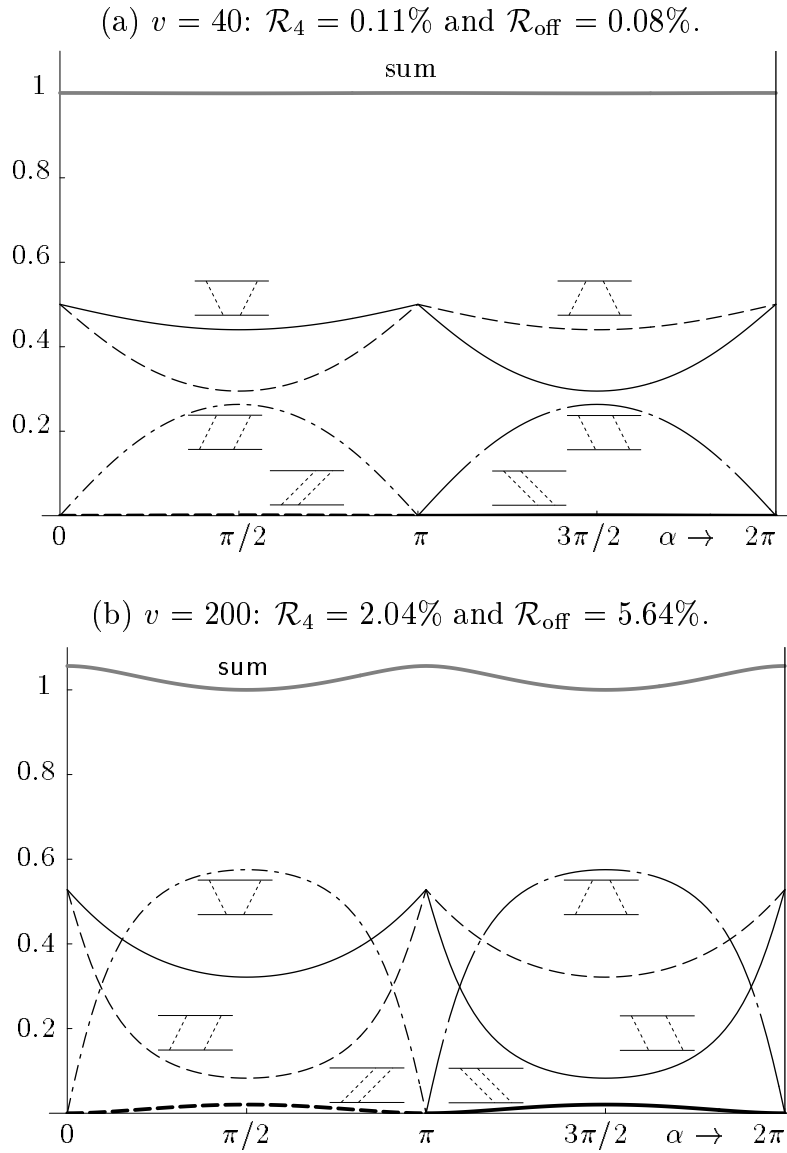
determined it from the relation  $p'^z = (p'^+ - p'^-)/\sqrt{2}$  with the purpose of showing the effect of off-shellness in this numerical experiment. We see that Eqs. (V-52) and (V-53) hold. The off energy-shell momenta form an ellipse. However, the deviation from a circle with radius  $v$  is hardly visible.

## §7.2 Calculation of the amplitude

We did numerical experiments for particles that are weakly bound:  $2m - \mathcal{M} = 2 \text{ MeV}/c^2$ . In Fig. V-8 we show the contributions of the different boxes and their sum as we vary the angle  $\alpha$ . The calculations are the same as in the previous section, using the formulas (V-32)-(V-36), except that the momenta of the outgoing particles have changed such that (V-59) and (V-60) are satisfied. As there does not exist a covariant amplitude in the off energy-shell case, we normalized the curves shown by dividing the amplitudes by their sum at  $\alpha = \pi/2$ .

In Fig. V-8 we see the consequences of the off energy-shell initial and final states. Condition (V-22) is violated; therefore, Eq. (V-23) does not hold and breaking of covariance can be expected. We see that the contributions of the higher Fock states  $\mathcal{R}_4$  are smaller than the effect of the off-shellness  $\mathcal{R}_{\text{off}}$ , defined as the largest difference between two full amplitudes at arbitrary values of  $\alpha$ . This is confirmed in Fig. V-9, in which  $\alpha$  is fixed and the incoming c.m.s-momentum  $v$  is varied.

From Fig. V-8 we infer that the full amplitude is maximal at  $\alpha = 0$  and  $\alpha = \pi$ . The minimum is reached at  $\alpha = \pi/2$  and  $\alpha = 3\pi/2$ . Therefore the maximal breaking of covariance of the amplitude can be calculated by taking the difference of the total sum at the angles  $\alpha = 0$  and  $\alpha = \pi/2$ . We see that at typical values for incoming momentum ( $v \leq 50$ )  $\mathcal{R}_{\text{off}}$  is small, even smaller than  $\mathcal{R}_4$ . However, at higher momenta it dominates over the stretched box. In this

Figure V-8: The LF time-ordered boxes as a function of  $\alpha$ .

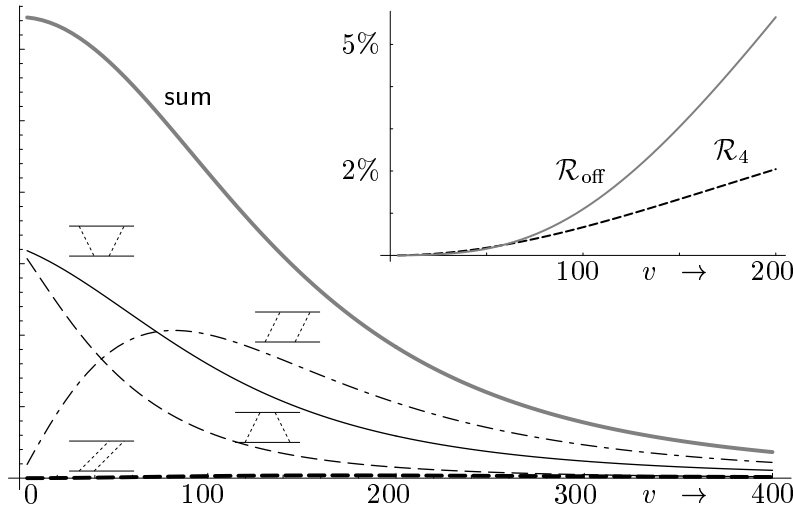


Figure V-9: LF time-ordered boxes as a function of  $v$  for  $\alpha = \pi/2$ . The inset shows the maximum contributions of the stretched box and the maximal breaking of covariance.

region we see that the stretched box contributions remain small.

A detailed explanation of the behavior of the off energy-shell amplitudes is given in §9.

## §8 Analysis of the on energy-shell results

The angle dependence of the LF time-ordered amplitudes found numerically can be understood analytically. The variation of the LF amplitudes with the angle  $\alpha$  means that they have singularities in this variable, either at finite values of  $\alpha$  or at infinity. They should disappear when they are summed to give the covariant amplitude. These singularities can be most conveniently analyzed in the explicitly covariant version of LFD (see for a review [12]). In this version the orientation of the light-front is given by the invariant equation  $\omega \cdot x = 0$ . The amplitudes are calculated by the rules of the graph technique explained in Ref. [12]. After a transformation of variables, these amplitudes coincide with those given by ordinary LFD. However, they are parametrized in a different way. The dependence of the amplitudes on the angle  $\alpha$  means, in the covariant version, that they depend on the four-vector  $\omega$  determining the orientation of the LF plane:  $M = M(p, q, p', q', \omega)$ . Hence, besides the usual Mandelstam variables  $s$  (V-42) and  $t$  (V-43) the amplitude  $M$  depends on the scalar products of  $\omega$  with the four-momenta. Since  $\omega$  determines the direction only (the theory is invariant relative to the substitution  $\omega \rightarrow a\omega$ ), an amplitude should depend on the ratios of the scalar products of the four-momenta with  $\omega$ . Hence [41]

$$M = M(s, t, x_p, x_{p'}), \quad (\text{V-61})$$

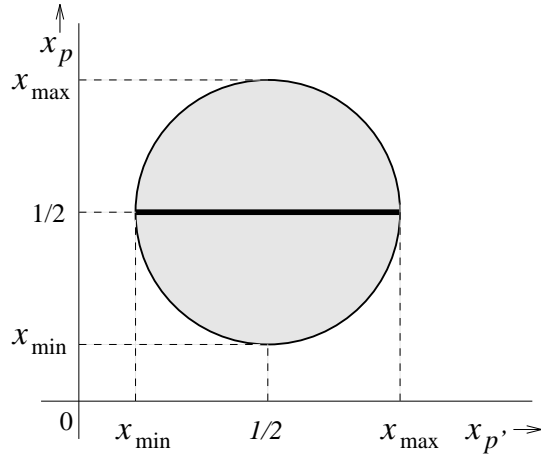


Figure V-10: Physical region in the  $x_p$ - $x_{p'}$ -plane for a scattering angle  $\theta = \pi/2$ . If the incoming particles are in the  $x$ - $y$ -plane the physical region reduces to the thick line at  $x_p = 1/2$ .

where

$$x_p = \frac{\omega \cdot p}{\omega \cdot (p + q)}, \quad x_{p'} = \frac{\omega \cdot p'}{\omega \cdot (p + q)}. \quad (\text{V-62})$$

Formulas (V-62) coincide with the definitions (V-56) if we use the  $z$ -axis as the quantization axis. The  $\omega$ -dependence is reduced to two scalar variables  $x_p$  and  $x_{p'}$ , since the direction of  $\vec{\omega}$  is determined by two angles. Hence, this amplitude should have singularities in the variables  $x_p$  and  $x_{p'}$ . Their positions will be found below. The amplitude corresponding to the sum of all time-ordered diagrams should not depend on  $x_p$  and  $x_{p'}$ .

Let us find the physical domain of the variables  $x_p$  and  $x_{p'}$ , corresponding to all possible directions of  $\vec{\omega}$  for fixed  $s, t$ . In the c.m.s., the variables Eqs. (V-62) are represented as

$$x_p = \frac{1}{2} - \frac{v}{\sqrt{s}} \hat{\omega} \cdot \hat{p}, \quad x_{p'} = \frac{1}{2} - \frac{v}{\sqrt{s}} \hat{\omega} \cdot \hat{p}', \quad (\text{V-63})$$

where, e.g.,  $\hat{\omega} \cdot \hat{p}$  is the scalar product of the unit vectors  $\hat{\omega} = \vec{\omega}/|\vec{\omega}|$  and  $\hat{p} = \vec{p}/|\vec{p}|$  in three-dimensional Euclidian space, and  $v = \sqrt{s/4 - m^2}$  is the momentum of the particle in the c.m.s. The Eqs. (V-63) determine an ellipse in the  $x_p$ - $x_{p'}$ -plane. Its boundary is obtained when  $\vec{\omega}$  is in the scattering plane, that is,  $\hat{n} \cdot \hat{p} = \cos \gamma$  or  $\hat{n} \cdot \hat{p} = \cos(\gamma - \theta)$ , where  $\gamma$  is the angle between  $\vec{p}$  and  $\vec{\omega}$  in coplanar kinematics and  $\theta$  is the scattering angle in the c.m.s. The case when  $\vec{\omega}$  is out of the scattering plane corresponds to the interior of the ellipse. For a scattering angle  $\theta = \pi/2$ , the ellipse turns into a circle, shown in Fig. V-10.

For the kinematics shown in Fig. V-2 and Eqs. (V-37)-(V-40), i.e., when  $\vec{\omega} \perp \vec{p}$ , it follows from Eqs. (V-63) that the value  $x_p$  is fixed:  $x_p = \frac{1}{2}$ , whereas for a given

$\alpha$  we obtain

$$x_{p'} = \frac{1}{2} - \frac{v}{2v_0} \sin \alpha, \quad (\text{V-64})$$

with  $v_0 = \sqrt{m^2 + v^2}$ . So  $x_{p'}$  varies along a straight line when  $\hat{\omega}$  is rotated in the  $y$ - $z$ -plane. The bounds of the physical region of  $x_{p'}$  are

$$x_{\min} = \frac{1}{2} - \frac{v}{2v_0}, \quad x_{\max} = \frac{1}{2} + \frac{v}{2v_0}. \quad (\text{V-65})$$

When  $0 \leq \alpha \leq \pi/2$ ,  $x_{p'}$  moves from  $1/2$  to  $x_{\min}$ . When  $\pi/2 \leq \alpha \leq \pi$ ,  $x_{p'}$  moves in the opposite direction in the same interval. This explains why all the curves in Figs. V-5 and V-8 in the interval  $0 \leq \alpha \leq \pi$  are symmetric relative to  $\alpha = \pi/2$ .

When  $\pi \leq \alpha \leq 3\pi/2$ ,  $x_{p'}$  moves from  $1/2$  to  $x_{\max}$  and, finally, when  $3\pi/2 \leq \alpha \leq 2\pi$ , it goes back in the same interval. As in the previous paragraph, this explains why all the curves in Figs. V-5 and V-8 in the interval  $\pi \leq \alpha \leq 2\pi$  are symmetric relative to  $\alpha = 3\pi/2$ . When  $\alpha = \pi/2$  and  $3\pi/2$ , the values of  $x_{p'}$  are on the boundary of the physical region.

Note also that the amplitudes for the trapezium (dashed and solid curves in Figs. V-5 and V-8) are evidently obtained by the replacement  $p \leftrightarrow q$ ,  $p' \leftrightarrow q'$ , which, according to the definition in Eq. (V-62), corresponds to  $x_{p'} \rightarrow 1 - x_{p'}$ . This is the same as the replacement  $\alpha \rightarrow 2\pi - \alpha$  in Eq. (V-64). Therefore the curves for the other trapezium, when  $\alpha$  goes from  $2\pi$  to  $0$ , are identical to the curves for the trapezium, when  $\alpha$  increases from  $0$  to  $2\pi$ . The same is true for the other diagrams (diamonds and stretched boxes).

### §8.1 Trapezium

The method of finding the singularities of the LF diagrams was developed in [41]. Here we restrict ourselves to the example of the diagram (V-32). Its counterpart in the explicitly covariant LFD is shown in Fig. V-11. The dotted lines in this figure are associated with fictitious particles (spurions), with four-momenta proportional to  $\omega$ . The four-momenta of the particles (the spurions not included) are not conserved in the vertices. Conservation is restored by taking into account the spurion four-momentum. In the ordinary LF approach, this corresponds to nonconservation of the minus-components of the particles. The spurions make up for the difference.

According to the rules of the graph technique [12], one should associate with a particle line with four-momentum  $p$  and mass  $m$  the factor  $\theta(\omega \cdot p) \delta(p^2 - m^2)$  and associate with the spurion line with four-momentum  $\omega \tau_i$  the factor  $1/(\tau_i - i\epsilon)$ . Then one integrates, with measure  $d^4 k_i / (2\pi)^3$ , over all the four-momenta  $k_i$  not restricted by the conservation laws in the vertices and over all  $\tau_i$ . The expression for the amplitude of Fig. V-11 is

$$\text{Diagram} = \int \theta(\omega \cdot k) \delta(k^2 - m^2) \theta(\omega \cdot (p' - k)) \delta((p' - k + \omega \tau_1)^2 - \mu^2)$$

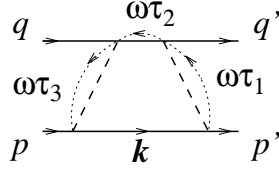


Figure V-11: Trapezium in explicitly covariant LFD.

$$\begin{aligned} & \times \theta(\omega \cdot (p + q - k)) \delta((p + q - k + \omega \tau_2)^2 - m^2) \theta(\omega \cdot (p - k)) \delta((p - k + \omega \tau_3)^2 - \mu^2) \\ & \times \frac{d\tau_1}{(\tau_1 - i\epsilon)} \frac{d\tau_2}{(\tau_2 - i\epsilon)} \frac{d\tau_3}{(\tau_3 - i\epsilon)} \frac{d^4 k}{(2\pi)^3}. \end{aligned} \quad (\text{V-66})$$

Like in Eq. (V-21), we omit the coupling constant. Performing the integrals over  $\tau_i$  and  $dk_0$  in Eq. (V-66) by means of the  $\delta$ -functions, we get

$$\overline{\text{trapezium}} = \int \frac{\theta(\omega \cdot (p' - k))}{\mu^2 - (p' - k)^2} \frac{\theta(\omega \cdot (p + q - k))}{m^2 - (p + q - k)^2} \frac{\theta(\omega \cdot (p - k))}{\mu^2 - (p - k)^2} \theta(\omega \cdot k) \frac{d^3 k}{2\varepsilon_k (2\pi)^3}. \quad (\text{V-67})$$

By transformation of variables (see for the details appendix B of Ref. [12]), expression (V-67) can be transformed such that it exactly coincides with Eq. (V-32).

For Feynman amplitudes the method to find their singularities was developed by Landau [42]. A method very similar to that one can be applied to time-ordered amplitudes. If we would omit for a moment the  $\theta$ -functions in Eq. (V-67) and would not take into account that  $k^2 = m^2$ , for finding the singularities we should construct the function  $\varphi_1 = \alpha_1(\mu^2 - (p' - k)^2) + \alpha_2(m^2 - (p + q - k)^2) + \alpha_3(m^2 - (p - k)^2)$  formed from the denominator of Eq. (V-67). The singularities of the trapezium are found by putting to zero the derivatives of  $\varphi_1$  with respect to  $\alpha_{1-3}$  and with respect to  $k$ . However, the trapezium may have singularities corresponding to a coincidence of the singularities of its integrand with the boundary of the integration domain caused by the presence of the  $\theta$ -functions. So we must find a conditional extremum. The restrictions can be taken into account using Lagrange multipliers [41]. Hence we should consider the function

$$\begin{aligned} \varphi &= \alpha_1(\mu^2 - (p' - k)^2) + \alpha_2(m^2 - (p + q - k)^2) \\ &+ \alpha_3(\mu^2 - (p - k)^2) + \alpha_4(k^2 - m^2) + \gamma_1 \omega \cdot (k - p'), \end{aligned} \quad (\text{V-68})$$

where  $\alpha_4$  and  $\gamma_1$  are the Lagrange multipliers. One should also consider the functions obtained from  $\varphi$  at  $\alpha_1 = 0$ , subsequently at  $\alpha_2 = 0$ , at  $\alpha_3 = 0$ , at  $\alpha_1 = \alpha_2 = 0$ , et cetera. One should not consider the function obtained from Eq. (V-68) by  $\alpha_4 = 0$ , since the integral (V-67) contains the three-dimensional integration volume  $d^3 k$ , and the condition  $k^2 = m^2$  cannot be removed. Therefore there is no need to introduce the term  $\gamma_2 \omega \cdot k$ , since the  $k^2 = m^2$  condition prevents



this term from being zero and, hence, does not impose any restrictions. The case  $\gamma_1 = 0$  reproduces the singularities of the Feynman graph. Therefore below we shall consider the case  $\gamma_1 \neq 0$  resulting in the singularities in the variables  $x_p$  and  $x_{p'}$ . We suppose that  $\omega \cdot p \geq \omega \cdot p'$ . This corresponds to the condition  $p^+ \geq p'^+$  of §3. In the kinematics shown in Fig. V-2 this means that  $x_{p'} \leq 1/2$  and  $0 \leq \alpha \leq \pi$ . In this case, the second and third  $\theta$ -functions in Eq. (V-67) do not give any restrictions and can be omitted. Therefore we omit also the term  $\gamma_3 \omega \cdot (p - k) + \gamma_4 \omega \cdot (p + q - k)$ .

The derivatives of  $\varphi$  with respect to  $k$ , the  $\alpha$ 's, and  $\gamma_1$  give

$$\partial\varphi/\partial k = \alpha_1 2(p' - k) + \alpha_2 2(p + q - k) + \alpha_3 2(p - k) + \alpha_4 2k + \gamma_1 \omega = 0, \quad (\text{V-69})$$

with

$$\begin{aligned} (p' - k)^2 &= \mu^2, & (p + q - k)^2 &= m^2, \\ (p - k)^2 &= \mu^2, & k^2 &= m^2, & \omega \cdot k &= \omega \cdot p'. \end{aligned} \quad (\text{V-70})$$

We multiply Eq. (V-69) in turn by  $(p' - k)$ ,  $(p + q - k)$ , et cetera, and get

$$\begin{aligned} (\text{V-69}) \times p' - k &: \alpha_1 2\mu^2 + \alpha_2 \mu^2 + \alpha_3 (2\mu^2 - t) - \alpha_4 \mu^2 = 0, \\ (\text{V-69}) \times p + q - k &: \alpha_1 \mu^2 + \alpha_2 2m^2 + \alpha_3 \mu^2 + \alpha_4 (s - 2m^2) + \gamma_1 (1 - x_{p'}) = 0, \\ (\text{V-69}) \times p - k &: \alpha_1 (2\mu^2 - t) + \alpha_2 \mu^2 + \alpha_3 2\mu^2 - \alpha_4 \mu^2 + \gamma_1 (x_p - x_{p'}) = 0, \\ (\text{V-69}) \times k &: -\alpha_1 \mu^2 + \alpha_2 (s - 2m^2) - \alpha_3 \mu^2 + 2\alpha_4 m^2 + \gamma_1 x_{p'} = 0, \\ (\text{V-69}) \times \omega &: \alpha_2 (1 - x_{p'}) + \alpha_3 (x_p - x_{p'}) + \alpha_4 x_{p'} = 0. \end{aligned} \quad (\text{V-71})$$

These equations have a nontrivial solution if and only if

$$\begin{vmatrix} 2\mu^2 & \mu^2 & (2\mu^2 - t) & -\mu^2 & 0 \\ \mu^2 & 2m^2 & \mu^2 & (s - 2m^2) & (1 - x_{p'}) \\ (2\mu^2 - t) & \mu^2 & 2\mu^2 & -\mu^2 & (x_p - x_{p'}) \\ -\mu^2 & (s - 2m^2) & -\mu^2 & 2m^2 & x_{p'} \\ 0 & (1 - x_{p'}) & (x_p - x_{p'}) & x_{p'} & 0 \end{vmatrix} = 0. \quad (\text{V-72})$$

Eq. (V-72) is quadratic in  $x_{p'}$ . Its solution is simple but lengthy. We show it for the particular case of the kinematics of Fig. V-2 supposing that the particles in the c.m.s. have momenta  $v$ . In this case  $s$  and  $t$  are given by Eqs. (V-42) and (V-43). The solution of Eq. (V-72) is

$$x_{p'}^0 = \frac{1}{2} \pm \frac{v}{2v_0} \frac{\sqrt{2\mu^4 + 8\mu^2 v^2 + 4v^4}}{\sqrt{\mu^4 + 8\mu^2 v^2 + 4v^4}}. \quad (\text{V-73})$$

The position of the singularity in the variable  $x_{p'}$  is denoted by  $x_{p'}^0$ . According to Landau [42] the behavior in the vicinity of  $x_{p'}^0$  should be either logarithmic, proportional to  $|x_{p'} - x_{p'}^0|^\beta$ , or proportional to  $|x_{p'} - x_{p'}^0|^\beta \log(x_{p'} - x_{p'}^0)$ , where  $\beta$  is a noninteger number.

When  $\mu \ll v$  we find from Eq. (V-73)

$$x_{p'} = \frac{1}{2} \pm \frac{v}{2v_0} \left(1 + \frac{\mu^4}{8v^4}\right). \quad (\text{V-74})$$

Comparing with Eq. (V-65), we see that at small  $\mu$  or at large  $v$  the singularities come closer to the physical region of  $x_{p'}$ . We will see below that this will be a property of all the singularities depending on  $\mu$  and  $v$ . This explains the numerical results, showing that with an increase of  $v$  the graphs of the amplitudes versus  $\alpha$  become more sharply peaked.

Now consider the case when one of the  $\alpha$ 's is zero. Let  $\alpha_1 = 0$ . Then Eq. (V-68) is reduced to

$$\varphi = \alpha_2(m^2 - (p+q-k)^2) + \alpha_3(\mu^2 - (p-k)^2) + \alpha_4(k^2 - m^2) + \gamma_1 \omega \cdot (k-p'). \quad (\text{V-75})$$

Similarly to the previous case, we get an equation for the singularities, which can be obtained from Eq. (V-72) by deleting the first row and column:

$$\begin{vmatrix} 2m^2 & \mu^2 & (s-2m^2) & (1-x_{p'}) \\ \mu^2 & 2\mu^2 & -\mu^2 & (x_p - x_{p'}) \\ (s-2m^2) & -\mu^2 & 2m^2 & x_{p'} \\ (1-x_{p'}) & (x_p - x_{p'}) & x_{p'} & 0 \end{vmatrix} = 0. \quad (\text{V-76})$$

Under the given kinematical conditions, its solution with respect to  $x_{p'}$  is

$$x_{p'}^0 = \frac{1}{2} \pm \frac{\mu}{4v} \sqrt{\frac{\mu^2 + 4v^2}{m^2 + v^2}}. \quad (\text{V-77})$$

In the limit  $\mu \rightarrow 0$  or  $v \rightarrow \infty$ , these singularities are again approaching the physical region.

Let  $\alpha_2 = 0$ . The singularity condition is obtained from Eq. (V-72) by deleting the second row and column:

$$\begin{vmatrix} 2\mu^2 & (2\mu^2 - t) & -\mu^2 & 0 \\ (2\mu^2 - t) & 2\mu^2 & -\mu^2 & (x_p - x_{p'}) \\ -\mu^2 & -\mu^2 & 2m^2 & x_{p'} \\ 0 & (x_p - x_{p'}) & x_{p'} & 0 \end{vmatrix} = 0. \quad (\text{V-78})$$

Its solution reads

$$x_{p'}^0 = \frac{x_p \mu (4m^2 \mu - \mu^3 - \mu t \pm 2\sqrt{t}\sqrt{tm^2 + \mu^4 - 4m^2 \mu^2})}{4m^2 \mu^2 - (t - \mu^2)^2}. \quad (\text{V-79})$$

In the limit  $v \rightarrow \infty$ , it is simplified:

$$x_{p'}^0 = -\frac{\mu^2}{4v^2} \pm \frac{\mu m}{2v^2}. \quad (\text{V-80})$$

Let  $\alpha_3 = 0$ . The singularity condition is obtained from Eq. (V-72) by deleting the third row and column:

$$\begin{vmatrix} 2\mu^2 & \mu^2 & -\mu^2 & 0 \\ \mu^2 & 2m^2 & (s - 2m^2) & (1 - x_{p'}) \\ -\mu^2 & (s - 2m^2) & 2m^2 & x_{p'} \\ 0 & (1 - x_{p'}) & x_{p'} & 0 \end{vmatrix} = 0. \quad (\text{V-81})$$

The determinant in Eq. (V-81) can be evaluated:

$$4sx_{p'}^2 - 4sx_{p'} + 4m^2 - \mu^2 = 0. \quad (\text{V-82})$$

The solutions of Eq. (V-82) are

$$x_{p'}^0 = \frac{1}{2} \pm \frac{\sqrt{v^2 + \mu^2/4}}{2v_0}. \quad (\text{V-83})$$

For  $\mu \rightarrow 0$  they also approach the boundary of the physical region of  $x_{p'}$ .

Now consider the cases when a number of coefficients are zero. Let  $\alpha_1 = \alpha_3 = 0$ . The singularity condition can be obtained from Eq. (V-72) by deleting the first and third rows and columns:

$$\begin{vmatrix} 2m^2 & (s - 2m^2) & (1 - x_{p'}) \\ (s - 2m^2) & 2m^2 & x_{p'} \\ (1 - x_{p'}) & x_{p'} & 0 \end{vmatrix} = 0. \quad (\text{V-84})$$

This equation reduces to

$$x_{p'}^2 - x_{p'} s + m^2 = 0. \quad (\text{V-85})$$

Its solutions are

$$x_{p'}^0 = \frac{1}{2} + \frac{v}{2v_0} = x_{\max}, \quad x_{p'}^0 = \frac{1}{2} - \frac{v}{2v_0} = x_{\min}. \quad (\text{V-86})$$

Since we consider the interval  $0 \leq \alpha \leq \pi$  corresponding to  $x_{\min} \leq x_{p'} \leq 1/2$ , the singularity at  $x_{p'}^0 = x_{\max}$  is beyond the physical region, whereas the singularity

at  $x_{p'}^0 = x_{\min}$  is just on the boundary of the physical region. The amplitude in this point gets an imaginary part:

$$\text{Im} \frac{\text{Im} \int_{x_{\min}}^{x_p} \frac{dx}{\sqrt{4m^2 - x^2}}}{\int_{x_{\min}}^{x_p} \frac{dx}{\sqrt{4m^2 - x^2}}} \neq 0 \text{ at } x_{p'} > x_{\min}, \quad (\text{V-87})$$

$$\text{Im} \frac{\text{Im} \int_{x_{\min}}^{x_p} \frac{dx}{\sqrt{4m^2 - x^2}}}{\int_{x_{\min}}^{x_p} \frac{dx}{\sqrt{4m^2 - x^2}}} = 0 \text{ at } x_{p'} = x_{\min}. \quad (\text{V-88})$$

Eq. (V-88) corresponds to  $\alpha = \pi/2$ . This explains why all the dashed curves of the imaginary parts in Fig. V-5 go through zero at the point  $\alpha = \pi/2$ .

Now put  $\alpha_1 = \alpha_2 = 0$ . The corresponding singularity condition is obtained from Eq. (V-72) by deleting the first and second rows and columns:

$$\begin{vmatrix} 2\mu^2 & -\mu^2 & (x_p - x_{p'}) \\ -\mu^2 & 2m^2 & x_{p'} \\ (x_p - x_{p'}) & x_{p'} & 0 \end{vmatrix} = 0. \quad (\text{V-89})$$

Eq. (V-89) reads

$$x_{p'}^2 m^2 - x_{p'} x_p (2m^2 - \mu^2) + x_p^2 m^2 = 0. \quad (\text{V-90})$$

Its solution is

$$x_{p'}^0 = \frac{x_p}{2m^2} \left( 2m^2 - \mu^2 \pm i\mu \sqrt{4m^2 - \mu^2} \right). \quad (\text{V-91})$$

These two singularities are fixed points in the complex plane. At  $x_p = 1/2$  and  $\mu \ll m$ , they are approaching the point  $x_{p'} = 1/2$  in the physical region, i.e.,  $\alpha = 0$  and  $\alpha = \pi$ .

The case  $\alpha_2 = \alpha_3 = 0$  leads to the singularity condition obtained from Eq. (V-72) by deleting the second and third rows and columns:

$$\begin{vmatrix} 2\mu^2 & -\mu^2 & 0 \\ -\mu^2 & 2m^2 & x_{p'} \\ 0 & x_{p'} & 0 \end{vmatrix} = 0. \quad (\text{V-92})$$

It gives  $x_{p'}^0 = 0$ . This is a fixed singularity in the nonphysical region.

Above, we have considered the region  $\omega \cdot p \geq \omega \cdot p'$ . In the region  $\omega \cdot p \leq \omega \cdot p'$  the integration domain is restricted by the step function  $\theta(\omega \cdot (p - k))$  instead of  $\theta(\omega \cdot (p' - k))$  in Eq. (V-67). The integrals defining these amplitudes define different analytic functions depending on the region considered. In the point  $x_{p'} = 1/2$ , i.e., at  $\alpha = 0$  and  $\alpha = \pi$ , the values of the functions coincide, but their analytic behavior is different.

This can indeed be seen in Fig. V-5. The slopes at  $\alpha = 0$  and  $\alpha = \pi$  are different.

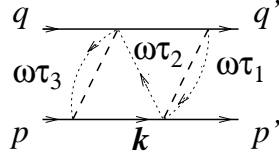


Figure V-12: Diamond in explicitly covariant LFD.

## §8.2 Diamond

The diamond corresponding to Eq. (V-33) is shown in Fig. V-12. The analytical expression is

$$\begin{aligned}
 \text{Diagram} &= \int \theta(\omega \cdot k) \delta(k^2 - m^2) \theta(\omega \cdot (k - p')) \delta((k - p' + \omega \tau_1 - \omega \tau_2)^2 - \mu^2) \\
 &\quad \times \theta(\omega \cdot (p + q - k)) \delta((p + q - k + \omega \tau_2)^2 - m^2) \theta(\omega \cdot (p - k)) \delta((p - k + \omega \tau_3)^2 - \mu^2) \\
 &\quad \times \frac{d\tau_1 d\tau_2 d\tau_3}{(\tau_1 - i\epsilon)(\tau_2 - i\epsilon)(\tau_3 - i\epsilon)} \frac{d^4 k}{(2\pi)^3}. \quad (\text{V-93})
 \end{aligned}$$

Performing the integrations in Eq. (V-93) over  $\tau_i$ , we get

$$\begin{aligned}
 \text{Diagram} &= \int \frac{\theta(\omega \cdot (k - p'))}{\mu^2 - (k - p')^2 + \frac{\omega \cdot (k - p')}{\omega \cdot (p + q - k)} [m^2 - (p + q - k)^2]} \\
 &\quad \times \frac{\theta(\omega \cdot (p + q - k))}{m^2 - (p + q - k)^2} \frac{\theta(\omega \cdot (p - k))}{\mu^2 - (p - k)^2} \theta(\omega \cdot k) \frac{d^3 k}{2\varepsilon_k (2\pi)^3}. \quad (\text{V-94})
 \end{aligned}$$

We still suppose that  $\omega \cdot p > \omega \cdot p'$ . However, now, in contrast to the trapezium,  $\omega \cdot p' \leq \omega \cdot k \leq \omega \cdot p$ , and both restrictions have to be taken into account.

In order to find the singularities, one should consider the extremum of the function:

$$\begin{aligned}
 \varphi &= \alpha_1 \left\{ \mu^2 - (k - p')^2 + \frac{\omega \cdot (k - p')}{\omega \cdot (p + q - k)} (m^2 - (p + q - k)^2) \right\} \\
 &\quad + \alpha_2 \{ m^2 - (p + q - k)^2 \} + \alpha_3 \{ \mu^2 - (p - k)^2 \} + \alpha_4 (k^2 - m^2) \\
 &\quad + \gamma_1 \omega \cdot (k - p') + \gamma_2 \omega \cdot (k - p). \quad (\text{V-95})
 \end{aligned}$$

At  $\omega \cdot p' = \omega \cdot p$ , i.e., at  $\alpha = 0$  and  $\alpha = \pi$ , the integration domain vanishes and the diamond becomes zero, as shown in Fig. V-5. It remains zero in the interval  $\pi \leq \alpha \leq 2\pi$ .

## §8.3 Stretched box

The stretched box, corresponding to Eq. (V-35), is shown in Fig. V-13. The



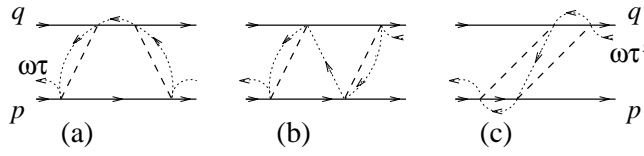


Figure V-14: Off energy-shell amplitudes in explicitly covariant LFD: (a) The trapezium. (b) The diamond. (c) The stretched box. The external momenta are the same for all diagrams.

Performing the integrations in Eq. (V-96) over  $\tau_i$ , we get

$$\begin{aligned}
 \text{---} \text{---} &= \int \frac{\theta(\omega \cdot (p + q - k))}{m^2 - (p + q - k)^2 + \frac{\omega \cdot (p + q - k)}{\omega \cdot (k - p')} [\mu^2 - (k - p')^2]} \\
 &\times \frac{\theta(\omega \cdot (k - p'))}{\mu^2 - (k - p')^2 + \frac{\omega \cdot (k - p')}{\omega \cdot (p - k)} [\mu^2 - (p - k)^2]} \frac{\theta(\omega \cdot (p - k))}{\mu^2 - (p - k)^2} \theta(\omega \cdot k) \frac{d^3 k}{2\varepsilon_k (2\pi)^3}.
 \end{aligned} \tag{V-97}$$

In order to find the singularities, one must consider the extremum of the function:

$$\begin{aligned}
 \varphi &= \alpha_1 \left\{ m^2 - (p + q - k)^2 + \frac{\omega \cdot (p + q - k)}{\omega \cdot (k - p')} (\mu^2 - (k - p')^2) \right\} \\
 &+ \alpha_2 \left\{ \mu^2 - (k - p')^2 + \frac{\omega \cdot (k - p')}{\omega \cdot (p - k)} (\mu^2 - (p - k)^2) \right\} \\
 &+ \alpha_3 \{ \mu^2 - (p - k)^2 \} + \alpha_4 (k^2 - m^2) + \gamma_1 \omega \cdot (k - p') + \gamma_2 \omega \cdot (k - p).
 \end{aligned} \tag{V-98}$$

Calculating the derivative of Eqs. (V-75), (V-95), and (V-98), for example, with respect to  $\alpha_{1-4}$ , at  $\gamma_1 = \gamma_2 = 0$ , one finds identical equations determining the singularities. These do not depend on  $x_p$  and  $x_{p'}$ , and coincide with the ones of the Feynman graph. Similarly, one can see that any singularity depending on  $x_p$  and  $x_{p'}$  cannot appear in a separate diagram only. It appears at least in two amplitudes. These singularities cancel each other in the sum of the amplitudes.

## §9 Analysis of the off energy-shell results

The off energy-shell amplitude is shown graphically in Fig. V-14. It contains incoming and outgoing spurion lines with the momenta  $\omega\tau$  and  $\omega\tau'$ , respectively. The conservation law has the form

$$p + q - \omega\tau = p' + q' - \omega\tau' = P. \tag{V-99}$$

From Eq. (V-99) one can infer that, if  $\vec{P} = 0$ , then  $\vec{p}' + \vec{q}' \neq 0$ , as was indicated for the  $z$ -components in §7. To parametrize the off energy-shell amplitude, we introduce different initial and final Mandelstam variables  $s$

$$s = (p + q)^2, \quad s' = (p' + q')^2, \tag{V-100}$$

and the total mass squared:

$$\mathcal{M}^2 = (p + q - \omega\tau)^2 = (p' + q' - \omega\tau')^2. \quad (\text{V-101})$$

So, in general, the off energy-shell amplitude is parametrized as

$$M = M(s, s', \mathcal{M}^2, t, x_p, x_{p'}). \quad (\text{V-102})$$

The on energy-shell amplitude Eq. (V-61) is obtained from Eq. (V-102) by the substitution  $s = s' = \mathcal{M}^2$ . One can also consider the half off energy-shell amplitude with one incoming or outgoing spurion line. It is obtained from Eq. (V-102) by the substitutions  $s = \mathcal{M}^2 \neq s'$  or  $s' = \mathcal{M}^2 \neq s$ .

In the case of the trapezium, Fig. V-14a, the external spurion lines enter and exit from the diagram at the same points as the momenta  $p$  and  $p'$ . So they can be incorporated by the replacement

$$p \rightarrow p - \omega\tau, \quad p' \rightarrow p' - \omega\tau'. \quad (\text{V-103})$$

This corresponds to new masses of the initial and final particles for the bottom line:

$$\begin{aligned} m_i^2 &= (p - \omega\tau)^2 = m^2 - x_p(s - \mathcal{M}^2), \\ m_f^2 &= (p' - \omega\tau')^2 = m^2 - x_{p'}(s' - \mathcal{M}^2). \end{aligned} \quad (\text{V-104})$$

With these new masses, one can repeat the calculations of §8.1 and find the singularities of the off energy-shell amplitude for the trapezium. The masses of the intermediate particles are not changed.

For other diagrams, both for the diamond and the stretched box, in contrast to the trapezium, the spurion line enters in the point where the momenta  $q'$  go out from the graph. This means that the calculation has to be done with the following external mass of this particle:

$$m'^2 = m^2 \rightarrow (q' - \omega\tau)^2 = m^2 - (1 - x_{p'})(s' - \mathcal{M}^2), \quad (\text{V-105})$$

whereas the mass of the particle with momentum  $p'$  is  $m$ .

As in the case when all masses are equal, the sum of all time-ordered graphs with masses different from the internal ones, but the same in all the time-ordered graphs, would not depend on  $\omega$ . However, now we take the sum of the graphs with different external masses in different particular graphs. This sum cannot be obtained by the time-ordering of a given Feynman graph. In this case the  $\omega$ -dependence is not eliminated in the sum of all the graphs, and the exact off energy-shell amplitude in a given order still depends on  $\omega$ . An example of this dependence is shown in Fig. V-8.

The off-shell amplitude is not a directly observable quantity. It may enter as part of a bigger diagram. Therefore, the off shell amplitude may depend on  $\omega$ . This  $\omega$ -dependence is not forbidden by covariance and, hence, does not violate it. On energy-shell, this dependence disappears.



## §10 Conclusions

If sufficient caution is exercised, invariance of  $S$ -matrix elements can be maintained in Hamiltonian formulations of field theory. A necessary condition to be fulfilled is that all Fock sectors included in the Feynman diagrams that contribute to a perturbative approximation of the  $S$ -matrix be retained. For the specific case of scalar field theory at fourth order in the coupling constant, we have determined the magnitude of the breaking of covariance if only the diagrams generated by the ladder approximation to Hamiltonian dynamics are included. The remaining terms, the stretched boxes, were found to contribute a small fraction, less than 2% for small to intermediate c.m.s. momenta, of the total amplitude. This fraction is, however, increasing with energy.

It was found, in a calculation closely approximating the first one, that the breaking of Lorentz invariance is much larger in IFD than in LFD, confirming quantitatively what has been claimed in the literature.

In both cases we determined quantitatively the dependence of the six LF time-ordered diagrams on the orientation of the light-front. We verified that, although the individual diagrams depend strongly on the orientation, their sum does not, as it should not. This dependence of individual diagrams may be interpreted as a breaking of rotational invariance.

Having established numerically that invariance of the  $S$ -matrix elements is obtained only if all Fock sectors relevant to a certain order in perturbation theory are included, we extended our investigation to amplitudes that are off energy-shell. Such amplitudes are not  $S$ -matrix elements, calculated between asymptotic states, from  $-\infty$  to  $+\infty$  in time. They are elements of an  $S$ -matrix calculated for finite light-front time, i.e., defined on a light-front in the interaction region, not moved to  $\pm\infty$  [12]. Therefore they depend on the orientation of this light-front. They either occur as parts of larger diagrams that are invariant, or in the calculation of LF wave functions. Not being invariant, the sum of the six LF time-ordered diagrams corresponding to the box is expected to depend on the orientation of the light-front. We found the variation of the sum of these six diagrams to grow more strongly with increasing relative momentum than the fraction carried by the stretched boxes.

All these results point to the conclusion that for low and intermediate momenta, e.g., those relevant for the bulk of the deuteron wave function, the higher Fock components are very small and are expected to play a minor role in LFD. We conjecture that this conclusion remains essentially valid for higher orders in perturbation theory.

Two remarks are in order here. First, if bound or scattering states at high values of the relative momentum are to be calculated, the higher Fock states will become much more important. Second, in the present work we neglected spin. It remains to be seen to what extent the special effects of spin, notably instantaneous propagators, will influence our conclusions.

A final point concerns the dependence of the individual diagrams on the orientation of the light-front. By an analysis very close to the Landau method for Feynman diagrams, we were able to explain all the peculiarities of the angular dependence in terms of the occurrence and position of singularities of the time-ordered diagrams as a function of the angles and their locations. In particular, the symmetries of the angular dependence and the cusps showing up at specific orientations could be explained fully.

# VI

## Summary and conclusions

*I often use the analogy of a chess game: one can learn all the rules of chess, but one doesn't know how to play well. The present situation in physics is as if we know chess, but we don't know one or two rules. But in this part of the board where things are in operation, those one or two rules are not operating much and we can get along pretty well without understanding those rules. That's the way it is, I would say, regarding the phenomena of life, consciousness and so forth.*

Richard Feynman [43]

With this thesis we hope to bring the light-front formulation of Hamiltonian dynamics closer to its final goal; the calculation of the spectrum of bound states such as small nuclei and hadrons. In particular, we hope to contribute to this advance by supplying a better understanding of the basics of LFD.

In Chapter I we have explained some of the pros and cons of the use of LFD. A Hamiltonian method is intuitively appealing. However, a general feature of Hamiltonian methods is that manifest covariance is lost. Our work deals with two topics in LFD, both concerning covariance: equivalence of light-front and covariant perturbation theory, and the entanglement of Fock-space expansion and covariance.

### **Equivalence of light-front and covariant perturbation theory**

The first part of this thesis is devoted to the proof of equivalence between covariant perturbation theory and LFD in the Yukawa model. The Yukawa model is explained in Chapter II, where also its longitudinal and transverse divergences are classified. The proof takes place at the diagrammatic level; following Kogut and Soper [13] a covariant diagram is integrated over the LF energy component  $k^-$ . For convergent diagrams a rigorous proof of the construction of all LF time-orderings is given by Ligterink [16, 44]. In the case of longitudinal divergences, i.e., when the integration over  $k^-$  is divergent, this proof needs to be extended. This is done in Chapter III where also the concept of minus regularization is introduced. In analogy to the well-known BPHZ regularization method, minus regularization was developed by Ligterink [19, 44]. It is formulated in terms of LF coordinates and we find that minus regularization exactly kills the part of

the amplitude that is ill-defined, the so-called forced instantaneous loop (FIL). The FIL is a diagram with so many instantaneous fermions that no energy denominators remain. Therefore it is *not* considered as a proper LF time-ordered diagram.

Other advantages of minus regularization are that it deals with longitudinal and transverse divergences in the same way, and that it can be easily implemented numerically. We encounter these properties in Chapter IV where we deal with diagrams in the Yukawa model that suffer from transverse divergences. The formulas of the one-boson exchange correction and the fermion triangle are too complicated for us to be able to give an algebraic proof of equivalence, and therefore we limit ourselves to a numerical check of equivalence.

*We conclude that the combined use of  $k^-$ -integration and minus regularization provides all the ingredients for the proof of equivalence between covariant and LF perturbation theory in the Yukawa model.*

Therefore, there is no need to add noncovariant counterterms to the Lagrangian of the Yukawa model as claimed by Burkardt and Langnau [10]. After our proof of equivalence for the Yukawa model it is still an open question whether our method is applicable to models such as QCD and QED. The propagator for a spin-1 particle is more complicated than those for spin-0 and spin-1/2 particles, which makes the decomposition into propagating and instantaneous parts more elaborate. An additional complication is that in models with a vector coupling two instantaneous particles can become neighbors, leading to an effective five-point interaction. It is also unclear how we should handle models with an effective coupling. A similar problem concerns the use of form factors in nuclear physics. It would be interesting to find out how they can be incorporated in a light-front formulation.

### **Entanglement of Fock-space expansion and covariance**

Confident about the usefulness of the LF time-ordered diagrams as tools in LFD, in Chapter V we make another step towards the calculation of the bound state. One has to solve the problem of diagonalizing an infinitely dimensional Hamiltonian. An approximate solution for this is provided by the use of an effective interaction. This method truncates the expansion of the interaction in higher Fock states. The splitting of the covariant box diagram into LF time-ordered diagrams with intermediate states containing at most three or four particles (the latter are referred to as stretched boxes) shows that in LFD these higher Fock states are heavily suppressed, not only because the spectrum condition allows for few diagrams, but also because the diagrams themselves are small. In addition, we find that in LFD the relative size of the diagrams containing higher Fock states is much smaller than in the instant-form of Hamiltonian dynamics.

*We conclude that the Fock-state expansion of LFD converges fast, and therefore the combined use of LFD and the ladder approximation offers good possibilities for an accurate calculation of the spectrum of bound states.*

Based on these results, we conjecture that the inclusion of stretched boxes in the kernel will not lead to a great change of the spectrum. This explains why bound-state calculations done in the past in LFD using the ladder approximation have given accurate results [45]. Note that the stretched boxes are not covariant by themselves, as they should not be. Therefore their omission leads to a breaking of covariance. Recently, Ji *et al.* [46] made an attempt to solve the problem by averaging over all directions of the orientation of the light-front. However, the stretched boxes have the same sign for all angles, and averaging over them cannot give a vanishing contribution. Therefore, upon angular averaging a small part of the amplitude will still be missing.

We have to remind the reader that our calculations were done for scalar particles. To analyze the influence of spin one can apply the same method. It may be very interesting to also investigate the contributions of crossed boxes, because it was shown by Gross [39] that in the heavy-mass limit they are necessary to retain the proper one-body equation. However, we would like to stress that for a discussion on the entanglement of covariance and the Fock-space expansion one can look at the properties of box and crossed box separately, as both are covariant objects. For a discussion on the validity of the ladder approximation one should both discuss stretched and crossed boxes.

We are confident that our investigations have contributed to an improved understanding of LF Hamiltonian field theory, fifty years after it was given birth to by Dirac. Its usefulness to solve the bound state can be considered millennium-proof.

# Appendix A

## Relations between Euclidian integrals

The two basic formulas that are used in Chapter III to compare LF time-ordered and covariant diagrams in  $d$  space-time dimensions are

$$\int d^d k f(k^2) = \frac{2\pi^{d/2}}{\Gamma(d/2)} \int_0^\infty dk k^{d-1} f(k^2), \quad (\text{A-1})$$

$$\int_0^\infty dk \frac{k^{d-1}}{(k^2 + C^2)^m} = \frac{\Gamma(d/2)\Gamma(m-d/2)}{2\Gamma(m)} (C^2)^{d/2-m}, \quad (\text{A-2})$$

with  $d \geq 1$  and  $m > 0$ . If we take  $d \geq 2$  and  $m > 1$  the following manipulations are valid. Formulas (A-1) and (A-2) can be combined to give

$$\int d^d k \frac{1}{(k^2 + C^2)^m} = \pi^{d/2} \frac{\Gamma(m-d/2)}{\Gamma(m)} (C^2)^{d/2-m}, \quad (\text{A-3})$$

$$\begin{aligned} \int d^d k \frac{A + Bk^2}{(k^2 + C^2)^m} &= \pi^{d/2} \frac{\Gamma(m-1-d/2)}{\Gamma(m)} (C^2)^{d/2-m} \\ &\times \left( (m-1-d/2)A + dBC^2/2 \right). \end{aligned} \quad (\text{A-4})$$

We can formulate the same equation for  $d-2$  dimensions and  $m-1$  as the power in the denominator. We find that the right-hand sides differ only slightly

$$\begin{aligned} \int d^{d-2} k \frac{A + Bk^2}{(k^2 + C^2)^{m-1}} &= \frac{\pi^{d/2}}{\pi} \frac{\Gamma(m-1-d/2)}{\Gamma(m-1)} (C^2)^{d/2-m} \\ &\times \left( (m-1-d/2)A + (d-2)BC^2/2 \right). \end{aligned} \quad (\text{A-5})$$

A comparison of these formulas gives

$$\int d^d k \frac{A + Bk^2}{(k^2 + C^2)^m} = \frac{\pi}{m-1} \int d^{d-2} k \frac{A + B\frac{d}{d-2}k^2}{(k^2 + C^2)^{m-1}}, \quad (\text{A-6})$$

provided we have  $d > 2$  and  $m > 1$ .

# Appendix B

## The fermion self-energy in closed form

Here we give the results for the integral (III-40) in closed form. We write for the renormalized self-energy

$$\text{---} \overset{\text{r}}{\text{---}} = \not{q} F_1(q^2) + m F_2(q^2). \quad (\text{B-1})$$

Then the two functions  $F_{1,2}$  are found to be

$$\frac{F_1(q^2)}{\pi^2 i} = - \int_0^1 dx x \log \left( 1 - \frac{x(1-x)q^2}{(1-x)m^2 + x\mu^2} \right), \quad (\text{B-2})$$

and

$$\frac{F_2(q^2)}{\pi^2 i} = - \int_0^1 dx \log \left( 1 - \frac{x(1-x)q^2}{(1-x)m^2 + x\mu^2} \right). \quad (\text{B-3})$$

For  $\mu = 0$  we find the result to be in agreement with the formula given by Ligterink and Bakker [19] and by Bjorken and Drell [25]. They use the vector coupling appropriate for the photon and therefore overall numerical factors are different.

$$\frac{F_1(q^2)}{\pi^2 i} = \frac{1}{4} + \frac{m^2}{2q^2} - \left( \frac{1}{2} - \frac{m^4}{2q^4} \right) \log \frac{m^2 - q^2}{m^2}, \quad (\text{B-4})$$

$$\frac{F_2(q^2)}{\pi^2 i} = 1 - \left( 1 - \frac{m^2}{q^2} \right) \log \frac{m^2 - q^2}{m^2}. \quad (\text{B-5})$$

For  $\mu > 0$  we have

$$\begin{aligned} \frac{F_1(q^2)}{\pi^2 i} &= \frac{1}{4} + \frac{(\mu^2 - m^2)^2 - \mu^2 q^2}{2(m^2 - \mu^2)q^2} + \left( \frac{(m^2 - \mu^2 + q^2)^2 - 2m^2 q^2}{4q^4} - \frac{m^4}{2(m^2 - \mu^2)^2} \right) \log \frac{\mu^2}{m^2} \\ &+ \left( \log \frac{D^{\frac{1}{2}} + m^2 - \mu^2 - q^2}{D^{\frac{1}{2}} - m^2 + \mu^2 + q^2} - \log \frac{D^{\frac{1}{2}} + m^2 - \mu^2 + q^2}{D^{\frac{1}{2}} - m^2 + \mu^2 - q^2} \right) \frac{D^{\frac{1}{2}}(m^2 - \mu^2 + q^2)}{4q^4}, \end{aligned} \quad (\text{B-6})$$

and

$$\begin{aligned} \frac{F_2(q^2)}{\pi^2 i} &= 1 + \left( \frac{m^2}{\mu^2 - m^2} + \frac{m^2 - \mu^2 + q^2}{2q^2} \right) \log \frac{\mu^2}{m^2} \\ &+ \frac{D^{\frac{1}{2}}}{2q^2} \left( \log \frac{D^{\frac{1}{2}} + m^2 - \mu^2 - q^2}{D^{\frac{1}{2}} - m^2 + \mu^2 + q^2} - \log \frac{D^{\frac{1}{2}} + m^2 - \mu^2 + q^2}{D^{\frac{1}{2}} - m^2 + \mu^2 - q^2} \right), \end{aligned} \quad (\text{B-7})$$

where the variable  $D$  contains the threshold behavior

$$D = (q^2 - (m + \mu)^2) (q^2 - (m - \mu)^2). \quad (\text{B-8})$$

We checked that the limit  $\mu \rightarrow 0$  of Eqs. (B-6) and (B-7) exists and is equal to Eqs. (B-4) and (B-5) respectively.



# Appendix C

## Internal and external variables

We get more insight into the properties of the structure functions used in Chapter IV if we rewrite them in terms of internal and external variables. This can be done by defining

$$x' = \frac{k^+}{q_1^+} = (x-1)\chi, \quad (\text{C-1})$$

$$x = \frac{k^+ + q_2^+}{q_2^+} = \frac{x' + \chi}{\chi}. \quad (\text{C-2})$$

Or, equivalently,

$$k^+ = x'q_1^+ = (x-1)q_2^+, \quad (\text{C-3})$$

$$k_1^+ = (x'-1)q_1^+, \quad (\text{C-4})$$

$$k_2^+ = xq_2^+. \quad (\text{C-5})$$

In the numerator of the integrals defining LF structure functions we encounter on-shell spin projections. They can be rewritten in terms of internal variables using

$$k_{1\text{on}}^- = \frac{k_1^{\perp 2} + m^2}{2(x'-1)q_1^+}, \quad (\text{C-6})$$

$$k_{2\text{on}}^- = \frac{k_2^{\perp 2} + m^2}{2xq_2^+}. \quad (\text{C-7})$$

The energy denominators can also be written in terms of internal and external variables. The poles are given by Eqs. (IV-36), (IV-37) and (IV-64):

$$\begin{aligned} 2q_1^+(H_1^- - H_2^-) &= 2q_1^+ \left( p^- + \frac{k_1^{\perp 2} + m^2}{2k_1^+} - \frac{k_2^{\perp 2} + m^2}{2k_2^+} \right) \\ &= (p^2 + p^{\perp 2}) \frac{1 + \chi}{\chi} - \frac{k_1^{\perp 2} + m^2}{1 - x'} - \frac{k_2^{\perp 2} + m^2}{x\chi}, \end{aligned} \quad (\text{C-8})$$

$$2q_1^+(H_1^- - H^-) = 2q_1^+ \left( q_1^- - \frac{k^{\perp 2} + \mu^2}{2k^+} + \frac{k_1^{\perp 2} + m^2}{2k_1^+} \right)$$

$$= q_1^2 + q_1^{\perp 2} - \frac{k^{\perp 2} + \mu^2}{x'} - \frac{k_1^{\perp 2} + m^2}{1 - x'}, \quad (\text{C-9})$$

$$\begin{aligned} 2q_2^+(H^- - H_2^-) &= 2q_2^+ \left( q_2^- + \frac{k^{\perp 2} + \mu^2}{2k^+} - \frac{k_2^{\perp 2} + m^2}{2k_2^+} \right) \\ &= q_2^2 + q_2^{\perp 2} - \frac{k^{\perp 2} + \mu^2}{1 - x} - \frac{k_2^{\perp 2} + m^2}{x}. \end{aligned} \quad (\text{C-10})$$

The integration measures can be rewritten as follows:

$$2\pi i \int_0^{q_1^+} \frac{dk^+ 4q_1^+ q_2^+}{8k_1^+ k_2^+ k^+}, = -\pi i \int_0^1 \frac{dx'}{(1-x')xx'}, \quad (\text{C-11})$$

$$-2\pi i \int_{-q_2^+}^0 \frac{dk^+ 4q_1^+ q_2^+}{8k_1^+ k_2^+ k^+} = -\pi i \int_0^1 \frac{dx}{(1-x)x(1-x)}. \quad (\text{C-12})$$

We conclude that it is possible to write the structure functions in terms of the external variables  $q_1^-$ ,  $q_2^-$ ,  $q_1^\perp$ ,  $q_2^\perp$  and  $\chi$  and integrals over the internal variables  $x$  or  $x'$  and  $k^\perp$ . The divergent parts of the structure functions  $F_i^2$  can now be written as

$$f_1^{2-} = -\pi i \int_0^1 \frac{dx'}{(1-x')xx'} \frac{m}{(x'-1)q_1^+} \frac{q_1^+}{q_2^+} \left( \frac{1}{1-x'} + \frac{1}{x\chi} \right)^{-1} \left( \frac{1}{x'} + \frac{1}{1-x'} \right)^{-1} \quad (\text{C-13})$$

$$f_2^{2-} = -\pi i \int_0^1 \frac{dx}{(1-x)x(1-x)} \frac{m}{xq_2^+} \left( \frac{1}{1-x'} + \frac{1}{x\chi} \right)^{-1} \left( \frac{1}{x} + \frac{1}{1-x} \right)^{-1}. \quad (\text{C-14})$$

Upon cancelling common factors, and using Eq. (C-2), we can evaluate the integrals and obtain

$$f_1^{2-} = -f_2^{2-} = \pi i \frac{\chi}{1+\chi} \frac{m}{q_2^+} = \pi i \frac{m}{p^+}. \quad (\text{C-15})$$

Therefore condition (IV-75) is verified.

# Samenvatting

## Lichtfront Hamiltoniaanse veldentheorie Naar een relativistische beschrijving van gebonden toestanden

Ik zal eerst de plaats van mijn onderzoek binnen de natuurkunde aangeven, en daarna op het onderzoek zelf ingaan. Het veelomvattende terrein waarop het onderzoek zich bevindt heet hoge-energiefysica, vanwege het feit dat de bij de botsingsexperimenten betrokken deeltjes dermate hoge energieën hebben dat ze bijna met de lichtsnelheid voortbewegen. Het doel van dit onderzoek is om de structuur van de materie, met name op de allerkleinste schaal, te begrijpen.

Het atoom, waar we op de middelbare school vertrouwd mee zijn geraakt, bestaat uit een kern die is omgeven door een wolk van elektronen. De kern, op haar beurt, bestaat uit protonen en neutronen. Al geruime tijd is bekend dat deze *hadronen* uit twee of drie *quarks* bestaan, en deze blijven bij elkaar door de uitwisseling van lijmdeeltjes, veelal *gluonen* genoemd. De massa van het hadron is groter dan de optelsom van de massa's van de quarks. Eén van de vragen in de hoge-energiefysica is of wij de massa van het hadron kunnen bepalen als we de wijze waarop quarks gluonen uitwisselen kennen.

Hadronen zijn voorbeelden van *gebonden toestanden*. In dit proefschrift beschrijven we een wiskundige formulering waarmee wordt geprobeerd een relativistische beschrijving te geven van gebonden toestanden, die goed aansluit bij de *Hamiltoniaanse* technieken die bekend zijn uit de quantummechanica. Zij heet *lichtfront Hamiltoniaanse veldentheorie*, een formulering waarbij als het ware met het licht wordt 'meegereisd', en daarom kan men zich voorstellen dat het geschikt is om hoog-energetische deeltjes en hun gebonden toestanden te beschrijven. Bedenk wel dat reizen met de lichtsnelheid niet mogelijk is, en dat deze beschrijving dus abstract is.

De eerste die deze aanpak voorstelde was Dirac [8] in 1949. Aangezien mijn promotie bijna vijftig jaar na het verschijnen van dit baanbrekende werk plaatsvindt, is dit een toepasselijke gelegenheid om hier bij stil te staan. Helaas duurde het tot de jaren zeventig voordat wetenschappers die geïnteresseerd zijn in gebonden toestanden het belang van Diracs werk inzagen. Het moet dan ook wel gezegd worden dat er aan deze lichtfrontdynamica (LFD) enige moeilijkheden zijn verbonden. Zo is rotatiesymmetrie niet vanzelfsprekend in deze theorie, wat ongeveer betekent dat de berekening van een meetbare grootte, zoals de massa van een samengesteld deeltje, niet noodzakelijkerwijze tot hetzelfde antwoord leidt als je het van een andere kant beschouwt. Alle symmetrieën die samenhangen met Einsteins relativiteitstheorie, waaronder rotatiesymmetrie, worden in

de natuurkunde wel samengevat onder de noemer *Lorentz-covariantie*. Natuurkundige theorieën die deze Lorentz-covariantie schenden worden, met recht, ernstig gewantrouwd.

Het doel van dit proefschrift is tweeledig. Ten eerste willen we laten zien dat de bouwstenen van LFD, de *lichtfront-tijdgeordende diagrammen* in principe tot Lorentz-covariante resultaten leiden. Vervolgens willen we laten zien dat de LFD, meer dan andere methodes, geschikt is het voor het doen van zo nauwkeurig mogelijke berekeningen aan gebonden toestanden. Hieronder zullen we per hoofdstuk op de details ingaan.

### Hoofdstuk I    **Introductie van lichtfront Hamiltoniaanse dynamica**

We beginnen met uit te leggen hoe een Hamiltoniaanse theorie moet worden opgezet en vergelijken de twee belangrijkste mogelijkheden: *quantisatie* op een vlak met gelijke tijd (de wijze die bekend is uit de niet-relativistische quantummechanica) en de methode die wij adverteren: *quantisatie* op een vlak dat raakt aan de *lichtkegel*: het lichtfront. Om een aantal problemen die bij *quantisatie* optreden te omzeilen introduceren we een methode die vanuit covariante veldentheorie tot diagrammatische regels voor LFD leidt: de  $k^-$ -integratie, dat wil zeggen de integratie over de energiecomponent van de interne impuls. Deze methode zullen we veelvuldig toepassen in de volgende hoofdstukken.

### Hoofdstuk II    **Het Yukawa-model**

Wij gebruiken het Yukawa-model om twee redenen. Het is het meest eenvoudige model dat een beschrijving geeft van de interactie tussen fermionen met spin  $1/2$  via bosonen (in ons geval zonder spin). Bovendien werd onze aandacht getrokken door een artikel van Burkardt en Langnau [10] die beweerden dat in het Yukawa-model Lorentz-covariantie gebroken wordt. Wij zullen laten zien dat als de *divergenties* op de juiste wijze behandeld worden Lorentz-covariantie niet in gevaar komt.

### Hoofdstuk III    **Longitudinale divergenties in het Yukawa-model**

Het eerste gedeelte van het bewijs van Lorentz-covariantie van LFD is reeds geleverd door Ligterink in zijn proefschrift [44]. Hij liet door een ingewikkeld wiskundig hercomberingsschema zien hoe uit een covariant diagram alle bijbehorende lichtfront-tijdgeordende diagrammen volgen door integratie over  $k^-$ . Dit bewijs is niet geldig wanneer de integraal over  $k^-$  divergent is. Dit type divergenties worden longitudinale divergenties genoemd. We laten zien dat met de *minus-regularisatiemethode* de divergenties kunnen worden verwijderd en dat Lorentz-covariantie gewaarborgd is. Minusregularisatie is door Ligterink opgezet en door ons uitgebreid. Het is een in lichtfrontcoördinaten geformuleerde reg-

ularisatiemethode analoog aan de BPHZ-methode die bekend is in covariante veldentheorie.

#### Hoofdstuk IV    Transversale divergenties in het Yukawa-model

Een tweede complicatie is de aanwezigheid in diagrammen van divergenties in de transversale componenten  $k^\perp$  van de impuls. We laten zien dat deze transversale divergenties ook met minusregularisatie kunnen worden aangepakt. Omdat de diagrammen waar deze divergenties optreden ingewikkelder zijn dan in hoofdstuk III is het niet mogelijk in alle gevallen een wiskundig bewijs te geven. Wij laten echter in een numerieke berekening zien dat ook in deze gevallen Lorentz-covariantie gehandhaafd is. Opnieuw is het toverwoord hierbij minusregularisatie.

#### Hoofdstuk V    Verstrengeling van de Fock-ruimteontwikkeling en covariantie

De volgende stap die men neemt op weg naar de berekening van de gebonden toestand is het oplossen van de *Hamiltoniaanse eigenwaardevergelijking*. Dit exact doen is schier onmogelijk, omdat de Hamiltoniaan een oneindig grote matrix is. Om toch het massaspectrum te kunnen uitrekenen maakt men meestal de *ladderbenadering*. Deze gaat er vanuit dat bij de berekening van de gebonden toestand van twee deeltjes, die via de uitwisseling van bosonen verbonden zijn, nooit twee of meer bosonen op hetzelfde moment worden uitgewisseld. Dat houdt in dat *Fock-toestanden* met vier of meer deeltjes worden genegeerd.

Echter, als men covariante storingsrekening tot in de vierde orde in de koppelingsconstante uitvoert, dan zullen er zowel diagrammen met maximaal drie deeltjes als diagrammen met maximaal vier deeltjes in een intermediaire Fock-toestand voorkomen. De laatste categorie wordt echter genegeerd in de ladderbenadering. Hierdoor gaat een gedeelte van de amplitude verloren. Bovendien wordt Lorentz-covariantie gebroken, omdat de diagrammen die weggelaten zijn op zich niet covariant zijn in LFD, een eigenschap die wordt gedeeld met elke andere Hamiltoniaanse theorie.

Wij laten zien in een numerieke berekening dat de ladderbenadering toch redelijk goed is, omdat in gevallen met waarden van massa's en snelheden die typisch zijn voor realistische gebonden toestanden (in ons geval het deutron) uitwisseling van meerdere deeltjes tegelijkertijd maximaal tot 2% bijdraagt tot het resultaat. In andere typen Hamiltoniaanse theorieën zijn deze bijdragen veel groter, en wordt de ladderbenadering dus veel slechter. Dit verklaart ook waarom berekeningen die in het verleden zijn gedaan met de ladderbenadering in LFD goede resultaten hebben gegeven.

**Hoofdstuk VI    Samenvatting en conclusies**

In de voetsporen tredend van Feynman (zie citaat op bladzijde 99) wil ik besluiten met een vergelijking tussen de natuurkunde en het schaakspel. Het doel van mijn onderzoek is niet zo zeer om de regels waarmee de schaakstukken (de deeltjes, zoals het pion) zich bewegen te ontdekken, maar om de wijze waarop zij een eenheid vormen beter te begrijpen [47].

## Scientific publications

- [1] N. C. J. Schoonderwoerd, “Charged black holes in Maxwell-scalar-Einstein theory,” undergraduate thesis, Rijksuniversiteit Groningen, RuG internal report 272, 1994.
- [2] N. C. J. Schoonderwoerd and B. L. G. Bakker, “Equivalence of covariant and light-front perturbation theory.,” in *Proceedings of the 12th International Symposium on High-Energy Spin Physics*, C. W. de Jager, T. J. Ketel, P. J. Mulders, J. E. J. Oberski, and M. Oskam-Tamboezer, eds., p. 546. World Scientific, 1997. [hep-ph/9610361](#).
- [3] N. C. J. Schoonderwoerd and B. L. G. Bakker, “Equivalence of renormalized covariant light-front perturbation theory. I. Longitudinal divergences in the Yukawa model,” *Phys. Rev.* **D57** (1998) 4965, [hep-ph/9702311](#). This article forms the basis of Chapter III.
- [4] N. C. J. Schoonderwoerd and B. L. G. Bakker, “Equivalence of renormalized covariant light-front perturbation theory. II. Transverse divergences in the Yukawa model,” *Phys. Rev.* **D58** (1998) 025013, [hep-ph/9801433](#). This article forms the basis of Chapter IV.
- [5] N. C. J. Schoonderwoerd, B. L. G. Bakker, and V. A. Karmanov, “Entanglement of Fock-space expansion and covariance in light-front Hamiltonian dynamics,” accepted for publication in *Phys. Rev.* **C** (1998), [hep-ph/9806365](#). This article forms the basis of Chapter V.
- [6] B. L. G. Bakker and N. C. J. Schoonderwoerd, “Entanglement of Fock-space expansion and covariance in light-front dynamics,” in *Proceedings of the Few Body Conference 1998*. Springer-Verlag. To be published.
- [7] Electronic version of this thesis including possible errata. [hep-ph/9811xxx](#).

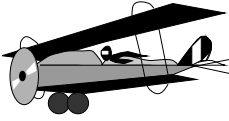
## Bibliography

- [8] P. A. M. Dirac, “Forms of relativistic dynamics,” *Rev. Mod. Phys.* **21** (1949) 392.
- [9] S. Weinberg, “Dynamics at infinite momentum,” *Phys. Rev.* **150** (1966) 1313.
- [10] M. Burkardt and A. Langnau, “Rotational invariance in light-cone quantization,” *Phys. Rev.* **D44** (1991) 3857.
- [11] H. Leutwyler and J. Stern, “Relativistic dynamics on a null plane,” *Ann. Phys.* **112** (1978) 94.
- [12] J. Carbonell, B. Desplanques, V. A. Karmanov, and J. F. Mathiot, “Explicitly covariant light front dynamics and relativistic few body systems,” *Phys. Rept.* **300** (1998) 215, [nucl-th/9804029](#).
- [13] J. B. Kogut and D. E. Soper, “Quantum electrodynamics in the infinite-momentum frame,” *Phys. Rev.* **D1** (1970) 2901.
- [14] S. J. Chang and S. K. Ma, “Feynman rules and quantum electrodynamics at infinite momentum,” *Phys. Rev.* **180** (1969) 1506.
- [15] S. J. Brodsky, H.-C. Pauli, and S. S. Pinsky, “Quantum chromodynamics and other field theories on the light cone,” *Phys. Rept.* **301** (1998) 299, [hep-ph/9705477](#).
- [16] N. E. Ligterink and B. L. G. Bakker, “Equivalence of light-front and covariant field theory,” *Phys. Rev.* **D52** (1995) 5954, [hep-ph/9412315](#).
- [17] M. Sawicki, “Light front limit in a rest frame,” *Phys. Rev.* **D44** (1991) 433.
- [18] J. P. B. C. de Melo, J. H. O. Sales, T. Frederico, and P. U. Sauer, “Pairs in the light front and covariance,” *Nucl. Phys.* **A631** (1998) 574C, [hep-ph/9802325](#).
- [19] N. E. Ligterink and B. L. G. Bakker, “Renormalization of light-front Hamiltonian field theory,” *Phys. Rev.* **D52** (1995) 5917.
- [20] C. Itzykson and J.-B. Zuber, *Quantum Field Theory*. McGraw-Hill, New York, 1985.



- 
- [21] H.-M. Choi and C.-R. Ji, “Nonvanishing zero-modes in the light-front current,” [hep-ph/9805438](#).
- [22] L. H. Ryder, *Quantum Field Theory*. Cambridge University Press, Cambridge, 1985.
- [23] D. Mustaki, S. Pinsky, J. Shigemitsu, and K. Wilson, “Perturbative renormalization of null-plane QED,” *Phys. Rev.* **D43** (1991) 3411.
- [24] J. C. Collins, *Renormalization*. Cambridge University Press, Cambridge, 1984.
- [25] J. D. Bjorken and S. D. Drell, *Relativistic Quantum Mechanics*. McGraw-Hill, 1964.
- [26] G. P. Lepage and S. J. Brodsky, “Exclusive processes in perturbative quantum chromodynamics,” *Phys. Rev.* **D22** (1980) 2157.
- [27] K. Hepp, “Proof of the Bogoliubov-Parasiuk theorem on renormalization,” *Commun. math. Phys.* **2** (1966) 301.
- [28] Y. Hahn and W. Zimmermann, “An elementary proof of Dyson’s power counting theorem,” *Commun. math. Phys.* **10** (1968) 330.
- [29] W. Zimmermann, “The power counting theorem for Minkowski metric,” *Commun. math. Phys.* **11** (1968) 1.
- [30] W. Zimmermann, “Convergence of Bogoliubov’s method of renormalization in momentum space,” *Commun. math. Phys.* **15** (1969) 208.
- [31] W. E. Caswell and A. D. Kennedy, “A simple approach to renormalization theory,” *Phys. Rev.* **D25** (1982) 392.
- [32] M. G. Fuda, “Angular momentum and light front scattering theory,” *Phys. Rev.* **D44** (1991) 1880.
- [33] S. J. Brodsky, C.-R. Ji, and M. Sawicki, “Evolution equation and relativistic bound state wave functions for scalar field models in four and six- dimensions,” *Phys. Rev.* **D32** (1985) 1530.
- [34] M. Mangin-Brinet and J. Carbonell, “Solution numerique du modele de Wick-Cutkosky dans le cadre de la light front dynamics,” Rapport de Stage ISN/ECP.
- [35] T. Frederico. Private communication.
- [36] U. Trittmann and H.-C. Pauli, “On rotational invariance in front form dynamics,” [hep-th/9705021](#).

- 
- [37] M. G. Fuda and Y. Zhang, “Light front dynamics of one boson exchange models of the two-nucleon system,” *Phys. Rev.* **C51** (1995) 23.
- [38] M. G. Fuda, “Instant form dynamics of one particle exchange models,” *Phys. Rev.* **C52** (1995) 1260.
- [39] F. Gross, “Relativistic few-body problem. I. Two-body equation,” *Phys. Rev.* **C26** (1982) 2203.
- [40] B. L. G. Bakker, L. A. Kondratyuk, and M. V. Terent’ev, “On the formulation of two body and three body relativistic equations employing light front dynamics,” *Nucl. Phys.* **B158** (1979) 497.
- [41] V. A. Karmanov, “Expression for relativistic amplitudes in terms of wave functions,” *JETP* **48** (1978) 598.
- [42] L. D. Landau, “On the analytic properties of vertex parts in quantum field theory,” *JETP* **10** (1960) 45.
- [43] P. C. W. Davies and J. Brown, *Superstrings: A theory of Everything*. Cambridge University Press, Cambridge, 1988.
- [44] N. E. Ligterink, “Light-front Hamiltonian field theory; covariance and renormalization,” Ph.D. thesis, Vrije Universiteit, Amsterdam, 1996.
- [45] V. A. Karmanov. Private communication.
- [46] C.-R. Ji, G.-H. Kim, and D.-P. Min, “The rotation average in lightcone time-ordered perturbation theory,” [hep-ph/9809232](https://arxiv.org/abs/hep-ph/9809232).
- [47] Nico Schoonderwoerd, “Stellingen”, 1998. Deze geeft commentaar bij en stellingen van een schaakpartij die in mijn persoonlijke visie een illustratie geeft van het motto van de gebonden toestand: de eenheid is meer dan de optelsom der delen.  
[www.nikhef.nl/user/schoon/stellingen.pdf](http://www.nikhef.nl/user/schoon/stellingen.pdf).



Alex, Ali, Anita & Maurits, Annet, Bernd & Hinke, Bert, Bibiana, Claudia, Claudiu, Emanuela, Esther, Evelien,

Wouter, Vibeke, Vanja, Ulrika, Tulay, Sid, Saskia, Rutger, Roland, Roelof, Robert, Rik, Rainer, Pieter, Patricia, Norbert, Nog veel

$\infty$

dank, Danke, gracias, grazie, kiitää, köszönöm, mamnoon, multumire,

Eveliëne, Ferry, Gerard, Gloria, HansD, HansK, Hassan, Henk, fam. Hoekman, Jaap,  
veel meer, Martine, Marc, Marianne, Manuel, Koen, Guido, Joukje, JeroenW, Jeroen & Margot,

